Computational Methods for Elastoplasticity: An Overview of Conventional and Less-Conventional *Approaches*

Giulia Scalet & Ferdinando Auricchio

Archives of Computational Methods in Engineering
State of the Art Reviews

ISSN 1134-3060

Arch Computat Methods Eng
DOI 10.1007/s11831-016-9208-x

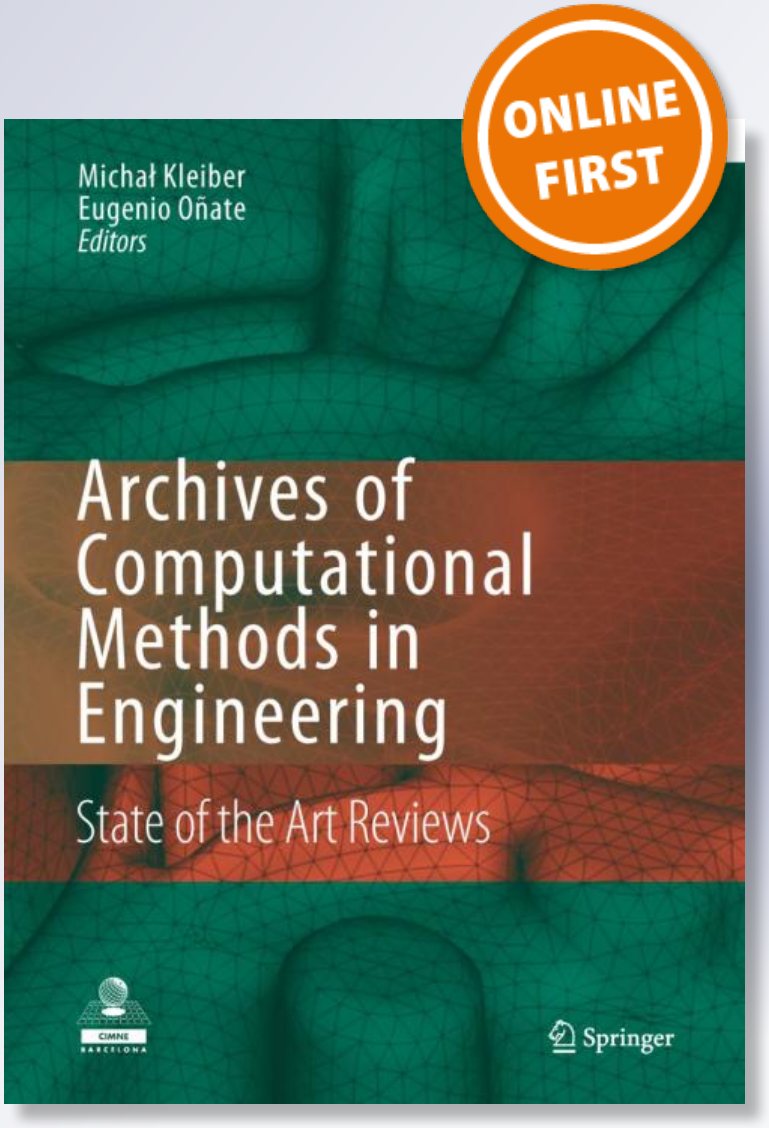

Springer

Arch Computat Methods Eng
DOI 10.1007/s11831-016-9208-x

ORIGINAL PAPER

Computational Methods for Elastoplasticity: An Overview of Conventional and *Less-Conventional* Approaches

Giulia Scalet [1] · **Ferdinando Auricchio**[1]

Received: 12 November 2016 / Accepted: 31 December 2016

Abstract The need of accurately reproducing the behaviour of elastoplastic materials in computational environments for the solution of engineering problems motivates the development of efficient and robust numerical schemes. These engineering problems often involve complex designs and/or conditions and are further complicated by the necessity of employing highly nonlinear and nonsmooth elastoplastic constitutive equations and constraints to describe material behaviour. Therefore, the numerical solution of such problems is not trivial and requires careful analyses to guarantee algorithm robustness, accuracy, and convergence in a reasonable amount of time. The aim of the present paper is to provide the reader with both an analysis and discussion, helpful in choosing the suitable numerical scheme when considering the implementation of a plasticity model. After a brief overview of the fundamental concepts for classical plasticity theory, we revise the state-of-the-art of computational methods by discussing conventional and *less-conventional* algorithms, formulated in a unified setting to allow for a comparison. Several approaches are implemented and discussed in representative numerical simulations.

1 Introduction

The origin of plasticity dates back to the mid-nineteenth century with the work published by Tresca [1]. Later, around the first half of the twentieth century, contributions to the classical *theory of plasticity* started to appear [2–5]. At first, the application of the plasticity theory to engineering problems required simplifying assumptions to derive a solution [6]. Then, thanks to the availability of powerful computers and the development of the finite element (FE) method between the nineteen-seventies and nineteen-nineties, the number of contributions to the theory of plasticity increased considerably and introduced the need for considering computational aspects to treat the governing equations. Several numerical methods [7, 8] have been proposed as a generalization of the well-known elastic predictor-radial corrector algorithm and, to date, the problem has been addressed by a large number of research papers[1] [9, 10]. Nowadays, the theory of plasticity is one of the most successful branch of Mechanics and it is based on rigorous thermodynamics principles. It provides a general framework for the continuum description of the constitutive behaviour of *plastic materials*, i.e., solids that show permanent (or plastic) deformations after being first loaded and then unloaded [9, 11]. The theory is often referred to as *rate-independent* plasticity, since it is restricted to conditions for which permanent deformations do not depend on the loading rate [9].

The mathematical (analytical or computational) modeling of elastoplastic problems is essential for a wide range of fields, including scientific research, structural design, manufacturing processes, and technological production. Several material types, such as metals, concrete, rocks, clays, and soils, may be in fact considered as plastic under specific conditions and practical applications cover industrial sectors as mechanical, civil and earth engineering, biomedical, and aerospace [12]. This highlights the

✉ Giulia Scalet
giulia.scalet@unipv.it

[1] Department of Civil Engineering and Architecture, University of Pavia, via Ferrata 3, 27100 Pavia, Italy

[1] As an example, if we type the keyword 'computational rate-independent plasticity' in ScienceDirect, we get 13, 843 papers.

Published online: 21 February 2017

importance of the mathematical modeling in the prediction of material behaviour.

Computational modeling represents a topic of significant interest due to the need of accurately describing the behaviour of real materials in numerical environments (e.g., commercial FE codes). Several engineering problems, e.g., metal forming or crash analyses of vehicles, are impossible to solve due to the involved complex designs and boundary conditions, highly non-linearity and non-smoothness of the governing constitutive equations, and/or the presence of constraints on variables. Therefore, algorithmic schemes associated to plastic constitutive equations should guarantee accuracy, robustness, convergence, and stability of the solution as well as should reduce the computational cost and CPU time as much as possible.

The objective of the present paper is to give a useful insight into the numerical treatment of plasticity equations, which can support both engineers and researchers interfacing with complex simulations. To this purpose, we aim to perform a methodological analysis, and not only a comprehensive review, of classical and *less-classical* algorithmic schemes. With the term '*less-classical*' (or '*less-conventional*') we refer to algorithms that have been rarely or recently addressed in the literature or that lack detailed analyses, despite their potential. To the authors' knowledge, the literature is very rich on classical algorithms, but no works propose an analysis and comparison of all the algorithms considered in the present paper in a unified context.

In the following, we first provide a brief overview of the continuum mechanics theory for plasticity in a unified mathematical setting. Then, we address the computational issues involved in the solution of the resulting constitutive initial value problem. To perform the analysis, we present a detailed discussion on several numerical state-update procedures for plasticity. The discussion starts with an overview of the integration schemes proposed in the literature and, then, it focuses on the solution schemes, ranging from conventional to *less-conventional* algorithms. The formulation is performed in a unified context to allow for a comparison. The analysis includes mainstream algorithms (e.g., return-map schemes) and recent and potential numerical solutions (e.g., mathematical programming, incremental energy minimization). The properties, advantages, and weaknesses of each approach are highlighted. Finally, we complete the discussion by presenting the results of several numerical simulations.

Given our purpose, we focus on a simplified plasticity problem by making the following assumptions: we concentrate on three-dimensional bodies made of isotropic elastoplastic materials within the small strain framework and we limit the discussion to bodies undergoing sufficiently slow processes such that we take the rate-independent material response as a good approximation of the real behaviour. Moreover, we restrict the implemented schemes to the case of associative plasticity.

The paper is organized as follows. Section 2 provides the theoretical formulation of plasticity. We place the attention on the constitutive initial value problem suitable for the subsequent algorithmic treatment. Section 3 addresses the main topic of this paper, namely, the overview and analysis of computational approaches to plasticity. A discussion on the treatment of the incremental initial boundary-value problem is provided. Section 4 focuses on the integration schemes typically applied to the rate equations, while Sect. 5 addresses the solution schemes. Section 6 presents and discusses representative numerical simulations to illustrate the effectiveness and performance of some numerical schemes in a wide class of problems. Finally, we conclude with Sect. 7.

Remark 1 (Notation) In the following sections, we denote *scalars* with italic letters (e.g., a, α, A, Σ), *vectors* and *second-order tensors* with boldface letters (e.g., $\mathbf{a}$, $\boldsymbol{\alpha}$, $\mathbf{A}$, $\boldsymbol{\Sigma}$), and *fourth-order tensors* with uppercase bold blackboard letters (e.g., $\mathbb{A}$, $\mathbb{G}$). We make use of the notations $||\bullet||$ and $|\bullet|$ to indicate the Euclidean norm and the absolute value function, respectively. The notations $(\bullet \cdot \bullet)$, $(\bullet : \bullet)$, and $(\bullet \otimes \bullet)$ denote, respectively, the inner (or dot), double contraction, and tensor product. The product between fourth-order and second-order tensors is indicated without any symbol. Notations $(\dot{\bullet})$, $\mathrm{tr}\,(\bullet)$, and $(\bullet)^{-1}$ denote, respectively, the time derivative, the trace, and the inverse of $\bullet$.

2 Continuum Formulation

This section reviews the mathematical problem that describes the strain and stress state of an isotropic elastoplastic continuum body under assigned external actions within the three-dimensional framework of infinitesimal deformation. The formulation is limited to *isothermal* static processes. A detailed review on the physical and mathematical background is beyond the scope of the present paper and the reader is referred to comprehensive papers and textbooks [3, 10–15].

2.1 Kinematics and Equilibrium Equations

We consider an isotropic elastoplastic body under prescribed body forces, boundary tractions and displacements, given as functions of time $t \in I \subset \mathfrak{R}^+$. The body occupies an open and bounded domain $\Omega \subset \mathfrak{R}^3$ with smooth boundary $\Gamma = \partial\Omega$. The boundary is split into a Dirichlet and a Neumann boundary, respectively Γ_D and Γ_N, such that $\overline{\Gamma} = \overline{\Gamma_D \cup \Gamma_N}$ and $\Gamma_D \cap \Gamma_N = \emptyset$. Accordingly, any material

point in the body can be associated to a point $\mathbf{x} \in \Omega$ in order to treat the body as a *continuum*.

Every material point moves with respect to its position by a *displacement* $\mathbf{u}$. Body deformation is characterized for infinitesimal deformations through the linearized Green *strain* tensor $\boldsymbol{\varepsilon}$, defined as:

$$\boldsymbol{\varepsilon} = \frac{1}{2}\left[\nabla \mathbf{u} + (\nabla \mathbf{u})^T\right] \tag{1}$$

where $\nabla(\cdot)$ denotes the gradient.

The interaction between the external world and the body can be described through *body* and *surface force* fields, which cause internal stresses, modeled by the *Cauchy stress* tensor $\boldsymbol{\sigma}$. The equilibrium between the applied external body force per unit mass $\mathbf{b}$ and the internal stresses is expressed by the *local momentum balance equation*:

$$\mathrm{div}\boldsymbol{\sigma} + \rho \mathbf{b} = \dot{\mathbf{v}} \quad \text{in } \Omega \times I \tag{2}$$

where ρ denotes the mass density, $\mathbf{v}$ the *velocity* field, and $\mathrm{div}\boldsymbol{\sigma}$ the divergence of $\boldsymbol{\sigma}$.

The *boundary conditions* are written as follows:

$$\begin{cases} \mathbf{u} = \bar{\mathbf{u}} & \text{on } \Gamma_D \times I \\ \boldsymbol{\sigma} \cdot \mathbf{n} = \bar{\mathbf{t}} & \text{on } \Gamma_N \times I \end{cases} \tag{3}$$

where $\bar{\mathbf{u}}$ and $\bar{\mathbf{t}}$ are a displacement and a surface force field assigned on Γ_D and Γ_N, respectively; $\mathbf{n}$ is the outward unit vector normal to Γ_N.

The *initial conditions* are written as follows:

$$\begin{cases} \mathbf{u}(0) = \mathbf{u}_0 & \text{in } \Omega \\ \dot{\mathbf{u}}(0) = \mathbf{v}_0 & \text{in } \Omega \end{cases} \tag{4}$$

where $\mathbf{u}_0$ and $\mathbf{v}_0$ are the initial values for the displacement and velocity fields, respectively.

The formulation is completed by the *constitutive equations* described in the following.

2.2 Constitutive Equations

In the framework of macroscopic phenomenological modeling, we adopt the *continuum thermodynamic theory with internal variables* [16], limiting the discussion to the case of *rate-independent* material response. Such an approach presents several advantages for engineering simulations, as modeling simplicity, easier numerical implementation, and lower computational times, compared to the other approaches (e.g., microscopic approaches).

2.2.1 Internal Variables

To identify the variables describing material behaviour, we consider the plastic flow as an irreversible process characterized in terms of the history of the total strain tensor $\boldsymbol{\varepsilon}$ and two kinematic variables: the *plastic strain* tensor $\boldsymbol{\varepsilon}^p$ and a set of *strain-like internal variables* $\boldsymbol{\xi}$. Such a set can be composed of second-order tensors and/or scalars, which describe internal irreversible phenomena (e.g., material hardening) and are often referred to as *hardening parameters*.

Following standard arguments, the thermodynamically conjugates to the kinematic variables are, respectively, the stress tensor $\boldsymbol{\sigma}$ and a set of *stress-like internal variables* or *thermodynamic forces* $\boldsymbol{\chi}$.

Accordingly, following [10], we may distinguish between a *strain-space* and a *stress-space* formulation of plasticity. In the strain-space formulation, which is in general adopted in a computational framework, the plastic flow is described in terms of the strain-like variables $(\boldsymbol{\varepsilon}, \boldsymbol{\varepsilon}^p, \boldsymbol{\xi})$, while the stress-like variables $(\boldsymbol{\sigma}, \boldsymbol{\chi})$ are assumed as dependent functions. However, the response functions, i.e, the yield condition and the flow rule, are formulated in stress-space in terms of $(\boldsymbol{\sigma}, \boldsymbol{\chi})$, as discussed in the following sections. Here, we focus on a strain-space formulation.

2.2.2 Additive Decomposition of the Strain

We assume that the total strain $\boldsymbol{\varepsilon}$ can be decomposed into the elastic strain $\boldsymbol{\varepsilon}^e$ and the plastic strain $\boldsymbol{\varepsilon}^p$. Accordingly:

$$\boldsymbol{\varepsilon} = \boldsymbol{\varepsilon}^e + \boldsymbol{\varepsilon}^p \tag{5}$$

Recalling the split of a second-order tensor into its volumetric and deviatoric components [16], we may write $\boldsymbol{\varepsilon}$ as follows:

$$\boldsymbol{\varepsilon} = \frac{1}{3}\,\theta \mathbf{I} + \mathbf{e} \tag{6}$$

where $\mathbf{I}$ is the second-order identity tensor, while $\theta = \mathrm{tr}\,(\boldsymbol{\varepsilon})$ and $\mathbf{e}$ are, respectively, the volumetric and deviatoric components of $\boldsymbol{\varepsilon}$.

Similarly, we may write $\boldsymbol{\varepsilon}^e$ and $\boldsymbol{\varepsilon}^p$, as follows:

$$\boldsymbol{\varepsilon}^e = \frac{1}{3}\,\theta^e \mathbf{I} + \mathbf{e}^e \tag{7}$$

$$\boldsymbol{\varepsilon}^p = \frac{1}{3}\,\theta^p \mathbf{I} + \mathbf{e}^p \tag{8}$$

where $\theta^i = \mathrm{tr}\,(\boldsymbol{\varepsilon}^i)$ and $\mathbf{e}^i$ $(i = e,\ p)$ are, respectively, the volumetric and deviatoric components of $\boldsymbol{\varepsilon}^e$ and $\boldsymbol{\varepsilon}^p$. Recall that physical evidences have shown that volume changes are almost exclusively a consequence of elastic deformation in case of metals [12]; therefore, in such a case, plastic deformation is assumed to be only of deviatoric or shearing type, i.e., $\theta^p = 0$, and thus:

$$\boldsymbol{\varepsilon}^p = \mathbf{e}^p \tag{9}$$

Therefore, we obtain:

$$\begin{cases} \mathbf{e} = \mathbf{e}^e + \mathbf{e}^p \\ \theta = \theta^e \end{cases} \tag{10}$$

2.2.3 Free-Energy

The *Helmholtz free-energy* is assumed to be a function of the total strain, plastic strain, and strain-like internal variables, i.e.,

$$\Psi = \Psi(\boldsymbol{\varepsilon}, \boldsymbol{\varepsilon}^p, \boldsymbol{\xi}) = \Psi(\boldsymbol{\varepsilon}^e, \boldsymbol{\xi}) \tag{11}$$

or, adopting an additive decomposition, it can be written as:

$$\Psi(\boldsymbol{\varepsilon}^e, \boldsymbol{\xi}) = \Psi^e(\boldsymbol{\varepsilon}^e) + \Psi^p(\boldsymbol{\xi}) \tag{12}$$

The *Gibbs free-energy* is defined through a Legendre transformation of the Helmholtz free-energy, as:

$$G = \boldsymbol{\sigma}{:}\boldsymbol{\varepsilon} - \Psi \tag{13}$$

We define the *elastic tangent* as:

$$\mathbb{C} = \frac{\partial^2 \Psi^e}{\partial (\boldsymbol{\varepsilon}^e)^2} \tag{14}$$

In case of isotropic linearized elasticity, both Ψ and G are quadratic forms, respectively, as:

$$\Psi = \frac{1}{2}\,\boldsymbol{\varepsilon}^e{:}\mathbb{C}\,\boldsymbol{\varepsilon}^e + \frac{1}{2}\,\boldsymbol{\xi} * \mathbb{D} * \boldsymbol{\xi} \tag{15}$$

$$G = \frac{1}{2}\,\boldsymbol{\sigma}{:}\mathbb{C}^{-1}\boldsymbol{\sigma} + \frac{1}{2}\,\boldsymbol{\chi} * \mathbb{D}^{-1} * \boldsymbol{\chi} \tag{16}$$

Here, the symbol $*$ indicates the appropriate product between $\boldsymbol{\chi}$, $\mathbb{D}$, and $\boldsymbol{\xi}$; $\mathbb{D}$ is the matrix of generalized plastic moduli; the elastic tangent $\mathbb{C}$ admits the following representation:

$$\mathbb{C} = 3K\,\mathbb{I}_{vol} + 2\mu\,\mathbb{I}_{dev} \tag{17}$$

where $\mathbb{I}_{vol}$ and $\mathbb{I}_{dev}$ are the volumetric and deviatoric components of the fourth-order identity tensor $\mathbb{I}$. Material parameters μ and K are referred to as the shear and bulk modulus, respectively.

2.2.4 Conjugate Variables

As a consequence of the second law of thermodynamics [10], the stress $\boldsymbol{\sigma}$ is expressed through the Helmholtz free-energy, as follows:

$$\boldsymbol{\sigma} = \frac{\partial \Psi}{\partial \boldsymbol{\varepsilon}^e} \tag{18}$$

and, recalling the split of a second-order tensor into its volumetric and deviatoric components, as:

$$\boldsymbol{\sigma} = p\mathbf{I} + \mathbf{s} \tag{19}$$

where $p = 1/3\ \mathrm{tr}\,(\boldsymbol{\sigma})$ and $\mathbf{s}$ are, respectively, the pressure and the stress deviator.

In case of isotropic linearized elasticity, the following relationship holds from Eq. (15):

$$\boldsymbol{\sigma} = \mathbb{C}\boldsymbol{\varepsilon}^e \tag{20}$$

and using Eqs. (5), (10), and (17), p and $\mathbf{s}$ are expressed as follows:

$$\begin{cases} p = K\theta \\ \mathbf{s} = 2\mu(\mathbf{e} - \mathbf{e}^p) = 2\mu\mathbf{e}^e \end{cases} \tag{21}$$

Similarly, the thermodynamic forces $\boldsymbol{\chi}$ associated to $\boldsymbol{\xi}$ are expressed through the Helmholtz free-energy, as follows:

$$\boldsymbol{\chi} = -\frac{\partial \Psi}{\partial \boldsymbol{\xi}} = -\frac{\partial \Psi^p}{\partial \boldsymbol{\xi}} \tag{22}$$

The relation conjugate to Eq. (18) is:

$$\boldsymbol{\varepsilon}^e = \frac{\partial G}{\partial \boldsymbol{\sigma}} \tag{23}$$

2.2.5 Yield criterion

The constrained evolution of stresses and thermodynamic forces is conveniently described by a convex scalar function f, called *yield criterion*. At each time, the state $(\boldsymbol{\sigma}, \boldsymbol{\chi})$ must lie in the closed connected set $E_{\boldsymbol{\sigma}}$, called *admissible region*, defined as:

$$E_{\boldsymbol{\sigma}} = \{(\boldsymbol{\sigma}, \boldsymbol{\chi}) : f(\boldsymbol{\sigma}, \boldsymbol{\chi}) \leq 0\} \tag{24}$$

A purely elastic behaviour takes place if $(\boldsymbol{\sigma}, \boldsymbol{\chi})$ lies within the interior of $E_{\boldsymbol{\sigma}}$, called *elastic region*, expressed as:

$$\mathrm{int}\big(E_{\boldsymbol{\sigma}}\big) = \{(\boldsymbol{\sigma}, \boldsymbol{\chi}) : f(\boldsymbol{\sigma}, \boldsymbol{\chi}) < 0\} \tag{25}$$

while plastic behaviour is observed if $(\boldsymbol{\sigma}, \boldsymbol{\chi})$ evolves on the boundary of $E_{\boldsymbol{\sigma}}$, called *yield surface*, defined as:

$$\partial E_{\boldsymbol{\sigma}} = \{(\boldsymbol{\sigma}, \boldsymbol{\chi}) : f(\boldsymbol{\sigma}, \boldsymbol{\chi}) = 0\} \tag{26}$$

The complement of $E_{\boldsymbol{\sigma}}$ is not attainable.

The yield criterion f can be defined in terms of the hydrostatic pressure; in such a case, f is *pressure-sensitive* and suitable for the description of materials as soils, rocks, and concrete; otherwise, the criterion is *pressure-insensitive* and suitable to describe materials as metals. We now recall some criteria generally used in engineering simulations.

Tresca yield criterion The criterion proposed by Tresca [1] is represented as:

$$f = \tau_{max} - \tau_y \tag{27}$$

or equivalently:

$$f = \big(\sigma_{max} - \sigma_{min}\big) - \sigma_y \tag{28}$$

where τ_y is the shear yield stress representing the yield limit under a state of pure shear, while $\sigma_y = 2\tau_y$ is the uniaxial yield stress; $\tau_{max} = 1/2\big(\sigma_{max} - \sigma_{min}\big)$ is the maximum shear stress, where $\sigma_{max} = \max\big(\sigma_I, \sigma_{II}, \sigma_{III}\big)$ and $\sigma_{min} = \min\big(\sigma_I, \sigma_{II}, \sigma_{III}\big)$, σ_I, σ_{II}, and σ_{III} being the principal stresses. Due to its definition in terms of the only shear stress, the Tresca criterion is pressure-insensitive.

von Mises yield criterion The criterion proposed by von Mises [2] is represented as:

$$f = \sqrt{3J_2} - \sigma_y \tag{29}$$

where σ_y is the uniaxial yield stress and $\sqrt{3J_2}$ is the von Mises effective or equivalent stress, J_2 being the second scalar invariant of the stress deviator, defined as:

$$J_2 = \frac{1}{2}\,\mathbf{s}{:}\mathbf{s} \tag{30}$$

Due to its definition in terms of the only stress deviator, the von Mises criterion is pressure-insensitive.

Mohr–Coulomb yield criterion The criterion proposed by Mohr and Coulomb [17] is expressed as:

$$f = \tau - c + \sigma_n \tan\phi \tag{31}$$

or equivalently:

$$f = \left(\sigma_{max} - \sigma_{min}\right) + \left(\sigma_{max} + \sigma_{min}\right)\sin\phi - 2c\cos\phi \tag{32}$$

where τ is the shear stress, c is the cohesion, ϕ is the angle of internal friction or frictional angle, and σ_n is the normal stress. Plastic yielding is now considered as the result of frictional sliding between material particles. Due to its definition, the Mohr–Coulomb criterion is pressure-sensitive.

Drucker–Prager yield criterion The criterion proposed by Drucker and Prager [18] consists of a modification of the von Mises criterion in which a term is added to include pressure-sensitivity. The yield function is expressed as:

$$f = \sqrt{J2} + \eta\, p - \bar{c} \tag{33}$$

where parameters η and $\bar{c}$ are material parameters.

Bigoni–Piccolroaz yield criterion The criterion proposed by Bigoni and Piccolroaz [19] considers all the three stress invariants. The yield function takes the following form:

$$f = F(p) + \frac{q}{g(\theta^*)} \tag{34}$$

where $q = \sqrt{3J_2}$ and $F(p)$ is the meridian function which determines the shape of the yield surface along the hydrostatic pressure axis[2]. It is defined as:

$$F = \left\{ \begin{array}{c} -Mp_c\sqrt{(\Phi - \Phi^m)[2(1-\alpha)\Phi + \alpha]} \text{ for } \Phi \in I_\Phi \\ +\infty \text{ for } \Phi \notin I_\Phi \end{array} \right\} \tag{35}$$

where Φ is a function of stress, defined as:

$$\Phi = \frac{-p + c}{p_c + c} \tag{36}$$

while I_Φ is defined as follows:

$$I_\Phi = \left[\frac{-p_c + c}{p_c + c}, \frac{2c}{p_c + c}\right] \tag{37}$$

[2] We adopt the definition of p reported in Eq. (19), though Bigoni and Piccolroaz [19] used the definition $p = -1/3\ \mathrm{tr}\,(\boldsymbol{\sigma})$.

M, p_c, c, m, α are material constants with the following properties:

$$M > 0, \quad p_c > 0, \quad c \geq 0, \quad m > 1, \quad 0 < \alpha < 2 \tag{38}$$

In particular, pressure-dependency is controlled by M; c and p_c denote the yield stresses in tension and compression, respectively; α and m regulate the shape of the yield surface in the meridian section.

The term $g(\theta^*)$ in Eq. (34) is a deviatoric function, defined as follows:

$$g = \frac{1}{\cos\left[\frac{\pi}{6}\beta - \frac{1}{3}\cos^{-1}\left(\eta\cos 3\theta^*\right)\right]} \quad \text{with} \quad 0 \leq \theta^* \leq \frac{\pi}{3} \tag{39}$$

where β and η are material constants determining the shape of the yield surface in the deviatoric plane, with the following properties:

$$0 \leq \beta \leq 2, \quad 0 \leq \eta < 1 \tag{40}$$

The Lode angle θ^* is a function of the second and third stress invariants characterizing the location of the stress in the deviatoric stress space and it is defined as:

$$\theta^* = \frac{1}{3}\cos^{-1}\left(\frac{3\sqrt{3}}{2}\frac{J_3}{J_2^{3/2}}\right) \tag{41}$$

with

$$J_3 = \frac{1}{3}\,\mathrm{tr}\,(\mathbf{s}^3) \tag{42}$$

In conclusion, the Bigoni–Piccolroaz criterion is based on a seven-parameter function which can be used for simulating the elastoplastic behaviour of several materials (ductile, pressure-sensitive, frictional, and quasi-brittle). Moreover, it presents features desirable for computational implementation and modeling, e.g., smoothness of the yield surface, ability of being calibrated for a large number of materials, general noncircular surface in the deviatoric plane, and possibility of being converted into classical yield criteria under limit conditions.

2.2.6 Evolution Laws

The plasticity model is defined through the definition of proper *evolution laws* for the plastic strain and strain-like internal variables (denoted, respectively, as *plastic flow rule* and *hardening law*), in the following form:

$$\left\{ \begin{array}{l} \dot{\boldsymbol{\varepsilon}}^p = \dot{\gamma}\mathbf{n} \\ \dot{\boldsymbol{\xi}} = \dot{\gamma}\mathbf{h} \end{array} \right. \tag{43}$$

where $\dot{\gamma}$ is the non-negative *consistency parameter*, $\mathbf{n} = \mathbf{n}(\boldsymbol{\sigma}, \boldsymbol{\chi})$ is the *flow vector* prescribing the direction of the plastic flow, and $\mathbf{h} = \mathbf{h}(\boldsymbol{\sigma}, \boldsymbol{\chi})$ is the *generalized hardening modulus* prescribing the type of hardening. The flow

rule $(43)_1$ can be equivalently rewritten by exploiting Eq. (5), as:

$$\dot{\boldsymbol{\varepsilon}}^e = \dot{\boldsymbol{\varepsilon}} - \dot{\gamma}\mathbf{n} \tag{44}$$

The evolution laws are often defined in terms of a *flow* (or *plastic*) *potential* $\Upsilon = \Upsilon(\boldsymbol{\sigma}, \boldsymbol{\chi})$ such that:

$$\begin{cases} \mathbf{n} = \dfrac{\partial \Upsilon}{\partial \boldsymbol{\sigma}} \\ \mathbf{h} = \dfrac{\partial \Upsilon}{\partial \boldsymbol{\chi}} \end{cases} \tag{45}$$

In such a case, Υ is a non-negative convex function of $\boldsymbol{\sigma}$ and $\boldsymbol{\chi}$ and zero-valued at the origin. When the yield function coincides with the flow potential, i.e., $\Upsilon = f$, plasticity is *associative*. In such a case, the evolution laws are called *normality rules* and the plastic strain rate is a tensor normal to the yield surface in the space of stresses. Experimental results showed that associative plasticity can be adopted to describe the behavior of metals, but not of materials as concrete and soils [9].

Equation (45) require that Υ is differentiable, despite many plasticity models are based on a non-differentiable Υ , e.g., Tresca, Mohr–Coulomb, and Drucker–Prager models. In such cases, Υ is called *pseudo-potential* or *generalized potential* and the evolution laws can be treated with the introduction of the concept of subdifferential sets [15, 20, 21]. The generalization of Eq. (43) is obtained by assuming $\mathbf{n}$ and $\mathbf{h}$ to be subgradients of Υ, i.e.,

$$\begin{cases} \mathbf{n} \in \partial_{\sigma} \Upsilon \\ \mathbf{h} \in \partial_{\chi} \Upsilon \end{cases} \tag{46}$$

An alternative approach to nonsmooth potentials was proposed by Koiter [5]. It first assumes that a finite number n of normals $\left(\mathbf{n}_1, ..., \mathbf{n}_n\right)$ is defined at a generic singular point of an isosurface of Υ. Any subgradient of Υ can be thus written as a linear combination $c_1\mathbf{n}_1 + ... + c_n\mathbf{n}_n$, with non-negative coefficients $c_1, ..., c_n$. The flow rule follows:

$$\dot{\boldsymbol{\varepsilon}}^p = \sum_{i=1}^{n} \dot{\gamma}_i \mathbf{n}_i \tag{47}$$

where $\dot{\gamma}_i$ $(i = 1, .., n)$ are the non-negative consistency parameters. This approach is applicable when a corner appears as the result of the intersection of a number of regular surfaces (e.g., cap-cone models for geomaterials, single crystal plasticity models) [9].

In the following, some evolution laws used in engineering practice are briefly recalled, for further details refer to [9]. We highlight that a flow rule associated with a pressure-insensitive yield condition results into purely deviatoric plastic flow.

Associative Tresca law The associative Tresca plasticity law takes the Tresca yield function (28) as flow potential, which is differentiable when the three principal stresses are distinct and non-differentiable when two principal stresses coincide. Therefore, the flow vector is defined as a subgradient of the Tresca function or the approach by Koiter [5] is generally adopted [9].

Associative von Mises law The associative von Mises plasticity law, also referred to as Prandtl-Reuss equation, takes the von Mises yield function (29) as flow potential. The corresponding flow vector is given by:

$$\mathbf{n} = \sqrt{\frac{3}{2}} \frac{\mathbf{s}}{||\mathbf{s}||} \tag{48}$$

and is deviatoric due to the pressure-insensitivity of the yield function.

Associative and non-associative Mohr–Coulomb law The associative Mohr–Coulomb plasticity law takes the Mohr–Coulomb yield function (31) as flow potential and the approach by Koiter [5] is generally adopted. The non-associative Mohr–Coulomb law takes, as flow potential, a Mohr–Coulomb yield function with the frictional angle ϕ replaced by a different angle $\varphi < \phi$, called dilatancy angle. For $\varphi = 0$, the plastic flow becomes deviatoric and the flow rule reduces to the associative Tresca law. For details, see also [9].

Associative and non-associative Drucker–Prager law The associative Drucker–Prager model takes as flow potential the Drucker–Prager yield function (33) which is singular at the apex of the yield surface and smooth elsewhere. At the apex singularity, the flow vector is defined as a subgradient of the yield function [9]. The non-associative Drucker–Prager law is obtained by taking, as flow potential, a Drucker–Prager yield function with the frictional angle ϕ replaced by a dilatancy angle $\varphi < \phi$, i.e.,

$$f = \sqrt{J_2} + \overline{\eta}\, p \tag{49}$$

where $\overline{\eta}$ is obtained by replacing ϕ with φ in the definition of η.

Associative and non-associative Bigoni–Piccolroaz law The associative Bigoni–Piccolroaz model takes as flow potential the Bigoni–Piccolroaz yield function (34). The non-associative Bigoni–Piccolroaz takes as flow potential the function $\Upsilon = ||\mathbf{s}||$ [22].

2.2.7 Types of Plastic Behaviour

Material behaviour may exhibit *hardening* during plastic deformation. This means that the yield surface may change in shape and size during plastic loading and the set $\boldsymbol{\xi}$ may contain strain-like internal variables which describe the hardening process (see Sect. 2.2.1). In the following, we briefly describe some classical model with or without hardening.

Perfect plasticity A model is *perfectly plastic* if no hardening is allowed, i.e., the yield level does not depend on the degree of plastification and the yield surface remains fixed. The description of such a mechanism implies a single internal variable, taken to be $\boldsymbol{\varepsilon}^p$. As an example, perfect plasticity corresponds to a constant uniaxial yield stress σ_y or constant cohesion c in Eqs. (28), (29), (31), and (33). Perfectly plastic models are suitable for the stability analysis of structures and soils and are widely employed for the determination of limit loads and safety factors.

Isotropic hardening The *isotropic hardening* mechanism produces a uniform (isotropic) expansion of the initial yield surface, without shifting. The set $\boldsymbol{\xi}$ contains a scalar variable which determines the size of the yield surface. Two approaches, known as *strain-hardening* and *work-hardening*, are generally adopted [9].

Strain-hardening is characterized by a scalar strain-like internal variable representing a measure of the accumulated plastic deformation. An example is the von Mises effective plastic strain, defined as:

$$\bar{e}^p = \int_0^t \sqrt{\frac{2}{3}} \|\dot{\boldsymbol{\varepsilon}}^p(\tau)\| d\tau \tag{50}$$

which represents the total plastic strain accumulated from the beginning of the loading history. Its rate evolution equation reads:

$$\dot{\bar{e}}^p = \sqrt{\frac{2}{3}} \|\dot{\boldsymbol{\varepsilon}}^p(t)\| \tag{51}$$

or, equivalently, using Eq. $(43)_1$ and the condition that $\|\mathbf{n}\| = 1$:

$$\dot{\bar{e}}^p = \dot{\gamma} \tag{52}$$

Accordingly, the uniaxial yield stress in Eq. (29) is a function of the accumulated plastic strain, i.e., $\sigma_y = \sigma_y(\bar{e}^p)$. The model is said to be *linear hardening* if:

$$\sigma_y = \sigma_{y,0} + H_{iso}\bar{e}^p \tag{53}$$

otherwise *nonlinear hardening*. Here, $\sigma_{y,0}$ is the uniaxial initial yield stress and H_{iso} is the linear isotropic hardening modulus.

Work-hardening is characterized by a scalar variable defining the state of hardening and represented by the dissipated plastic work W^p whose evolution is:

$$\dot{W}^p = \boldsymbol{\sigma} : \dot{\boldsymbol{\varepsilon}}^p \tag{54}$$

Accordingly, the uniaxial yield stress in Eq. (29) is a function of the dissipated plastic work, i.e., $\sigma_y = \sigma_y(W^p)$.

Kinematic hardening The *kinematic hardening* mechanism produces a shifting of the initial yield surface, without expansion. The description of such a mechanism implies a single internal variable, usually taken to be the plastic strain $\boldsymbol{\varepsilon}^p$. As an example, the von Mises yield function is given by:

$$f = \sqrt{3J_2(\mathbf{s} - \boldsymbol{\alpha})} - \sigma_y \tag{55}$$

where $\boldsymbol{\sigma} - \boldsymbol{\alpha}$ is the relative stress tensor, $\boldsymbol{\alpha}$ being the symmetric back-stress tensor. The latter is the thermodynamic force associated with kinematic hardening and represents the translation of the yield surface in the space of stresses. To complete the formulation, the simplest evolution law for $\boldsymbol{\alpha}$ is the linear kinematic (or Prager's) hardening rule:

$$\dot{\boldsymbol{\alpha}} = c_{kin}\dot{\boldsymbol{\varepsilon}}^p \tag{56}$$

where c_{kin} is a material parameter. Refinements with respect to the linear kinematic hardening law (56) have been proposed in [23]; see [12] for details.

Combined isotropic and kinematic hardening Other models can be obtained by combining the above laws for isotropic and kinematic hardening. For example, a relatively simple model with combined isotropic and kinematic hardening can be formulated by adopting the yield function (55) and allowing σ_y to be a function of $\bar{e}^p$.

2.2.8 Kuhn–Tucker Complementary Conditions

The model is completed giving the conditions on the consistency parameter $\dot{\gamma}$ and the yield criterion f. Specifically, $\dot{\gamma}$ is assumed to obey the *Kuhn–Tucker* (KT) *complementary inequality conditions* [24, 25]:

$$\dot{\gamma} \geq 0,\ f \leq 0,\ \dot{\gamma} f = 0 \tag{57}$$

In addition to conditions (57), $\dot{\gamma}$ satisfies the *consistency* (or *persistency*) *condition*:

$$\dot{\gamma}\dot{f} = 0 \tag{58}$$

which corresponds to the requirement that, for $\dot{\boldsymbol{\varepsilon}}^p$ and $\dot{\boldsymbol{\xi}}$ to be non-zero (i.e., $\dot{\gamma} > 0$), the state $(\boldsymbol{\sigma}, \boldsymbol{\chi})$ must move on $\partial E_{\boldsymbol{\sigma}}$, so that $\dot{f} = 0$. Conditions (57) and (58) are also known as loading/unloading and consistency conditions. The KT conditions reflect the multi-value nature of the evolution laws: zero rates for $\dot{\boldsymbol{\varepsilon}}^p$ and $\dot{\boldsymbol{\xi}}$ are related to an infinite number of stress-like variable states, which corresponds to the whole elastic domain [26].

Remark 2 (Interpretation of the Kuhn–Tucker complementary conditions [10]). Following [10], these situations may occur:

1. $(\boldsymbol{\sigma}, \boldsymbol{\chi}) \in \text{int}(E_{\boldsymbol{\sigma}}) \Rightarrow f < 0$. From conditions (57) we have:

$$\begin{aligned} &\dot{\gamma} f = 0 \quad \text{and} \quad f < 0 \\ &\Rightarrow \quad \dot{\gamma} = 0 \quad \Rightarrow \quad \dot{\boldsymbol{\varepsilon}}^p = \mathbf{0} \quad \text{and} \quad \dot{\boldsymbol{\chi}} = \mathbf{0} \end{aligned} \tag{59}$$

Thus, the rate form of Eq. (20) leads to:

$$\dot{\boldsymbol{\sigma}} = \mathbb{C}\,\dot{\boldsymbol{\varepsilon}} \equiv \mathbb{C}\,\dot{\boldsymbol{\varepsilon}}^e \tag{60}$$

The response is *instantaneously elastic*.

2. $(\boldsymbol{\sigma}, \boldsymbol{\chi}) \in \partial E_\sigma \Rightarrow f = 0$. Conditions (57) are automatically satisfied even if $\dot{\gamma} > 0$ and two situations can occur:

– If $\dot{f} < 0$, from condition (58) we have:

$$\begin{aligned} &\dot{\gamma} \dot{f} = 0 \quad \text{and} \quad \dot{f} < 0 \\ &\Rightarrow \quad \dot{\gamma} = 0 \quad \Rightarrow \quad \dot{\boldsymbol{\varepsilon}}^p = \mathbf{0} \quad \text{and} \quad \dot{\boldsymbol{\chi}} = \mathbf{0} \end{aligned} \tag{61}$$

Since Eq. (60) holds and $(\boldsymbol{\sigma}, \boldsymbol{\chi}) \in \partial E_\sigma$, the response is called *unloading from a plastic state*.

– If $\dot{f} = 0$, condition (58) is automatically satisfied. If $\dot{\gamma} > 0$, then $\dot{\boldsymbol{\varepsilon}}^p \neq \mathbf{0}$ and $\dot{\boldsymbol{\chi}} \neq \mathbf{0}$ and the response is *plastic loading*; if $\dot{\gamma} = 0$ is *neutral loading*.

2.2.9 Consistency Condition and Elastoplastic Tangent Modulus

To provide an interpretation of the consistency condition and the expression for the elastoplastic tangent modulus, we briefly summarize the results reported in [10]. We first consider the situation: $(\boldsymbol{\sigma}, \boldsymbol{\chi})(t) \in \partial E_\sigma \;\Leftrightarrow\; f(t) = 0$ at time $t > 0$. If $\dot{f} > 0$, then $f(t + \Delta t) > 0$ for some $\Delta t > 0$, which violates condition $f \leq 0$. Therefore, $\dot{f} \leq 0$. Then, we specify that:

$$\begin{cases} \dot{\gamma} > 0 \;\Rightarrow\; \dot{f} = 0 \\ \dot{f} < 0 \;\Rightarrow\; \dot{\gamma} = 0 \end{cases} \tag{62}$$

Therefore, condition (58) corresponds to the requirement previously reported, that is, for $\dot{\boldsymbol{\varepsilon}}^p$ and $\dot{\boldsymbol{\chi}}$ to be non-zero (i.e., $\dot{\gamma} > 0$), $(\boldsymbol{\sigma}, \boldsymbol{\chi})(t) \in \partial E_\sigma$ must move on ∂E_σ, so that $\dot{f} = 0$.

To exploit condition (58), we derive the following time derivative of f at $(\boldsymbol{\sigma}, \boldsymbol{\chi}) \in E_\sigma$:

$$\begin{aligned} \dot{f} = \;& \partial_\sigma f{:}\dot{\boldsymbol{\sigma}} + \partial_\chi f * \dot{\boldsymbol{\chi}} = \partial_\sigma f{:}\mathbb{C}(\dot{\boldsymbol{\varepsilon}} - \dot{\boldsymbol{\varepsilon}}^p) + \partial_\chi f * \dot{\boldsymbol{\chi}} = \\ &= \partial_\sigma f{:}\mathbb{C}\,\dot{\boldsymbol{\varepsilon}} - \dot{\gamma}\left(\partial_\sigma f{:}\mathbb{C}\,\mathbf{n} + \partial_\chi f * \mathbb{D} * \mathbf{h}\right) \leq 0 \end{aligned} \tag{63}$$

Then, the following assumption, reported in [10], always holds for associative perfect plasticity.

Assumption 1 [10] The flow rule, hardening law, and yield condition in stress-space are such that the following inequality holds:

$$\partial_\sigma f{:}\mathbb{C}\,\mathbf{n} + \partial_\chi f * \mathbb{D} * \mathbf{h} > 0 \tag{64}$$

for all admissible states $(\boldsymbol{\sigma}, \boldsymbol{\chi}) \in \partial E_\sigma$.

For proof, refer to [10].

It follows from Eq. (58) that:

$$\dot{f} = 0 \;\Leftrightarrow\; \dot{\gamma} = \frac{\langle \partial_\sigma f{:}\mathbb{C}\,\dot{\boldsymbol{\varepsilon}} \rangle}{\partial_\sigma f{:}\mathbb{C}\,\mathbf{n} + \partial_\chi f * \mathbb{D} * \mathbf{h}} \tag{65}$$

where $\langle \cdot \rangle = \max(0, \cdot)$. Therefore, the consistency parameter is a function of time. In view of Eqs. (63) and (64), we conclude that[3]:

$$\text{for } f = 0 \text{ and } \dot{f} = 0, \;\; \dot{\gamma} \geq 0 \;\Leftrightarrow\; \partial_\sigma f{:}\mathbb{C}\dot{\boldsymbol{\varepsilon}} \geq 0 \tag{66}$$

Finally, we have:

$$\dot{\boldsymbol{\sigma}} = \mathbb{C}(\dot{\boldsymbol{\varepsilon}} - \dot{\boldsymbol{\varepsilon}}^p) = \mathbb{C}(\dot{\boldsymbol{\varepsilon}} - \dot{\gamma}\mathbf{n}) = \mathbb{C}^{ep}\dot{\boldsymbol{\varepsilon}} \tag{67}$$

where $\mathbb{C}^{ep}$ is the *tangent elastoplastic modulus* given by:

$$\mathbb{C}^{ep} = \begin{cases} \mathbb{C} & \text{if } \dot{\gamma} = 0 \\ \mathbb{C} - \dfrac{\mathbb{C}\,\mathbf{n} \otimes \mathbb{C}\,\partial_\sigma f}{\partial_\sigma f{:}\mathbb{C}\,\mathbf{n} + \partial_\chi f * \mathbb{D} * \mathbf{h}} & \text{if } \dot{\gamma} > 0 \end{cases} \tag{68}$$

We remark that $\mathbb{C}^{ep}$ is generally non-symmetric for arbitrary $\mathbf{n}$, except in the case of associative flow rule.

2.2.10 Equivalent Formulation of the Kuhn–Tucker Complementary Conditions

We now reformulate the KT complementary inequality conditions (57) as a nonsmooth (non-differentiable) equation and, then, we construct parametric smooth (continuously differentiable) functions. The advantages are twofold: (i) we have to deal with only one scalar nonlinear equation, instead of the KT complementary inequality conditions; (ii) a smoothing function can be easier treated in numerical simulations.

Complementarity functions The KT complementarity inequality conditions (57) can be equivalently rewritten by using a *complementarity function* $\Phi{:}\mathfrak{R}^2 \to \mathfrak{R}$, such that:

$$\Phi(\dot{\gamma}, f) = 0 \;\Leftrightarrow\; \dot{\gamma} \geq 0,\; f \leq 0,\; \dot{\gamma} f = 0 \tag{69}$$

Complementarity problems and functions have been largely treated in the literature (see [27–30] and references therein). Among the others, widely used functions are the *Fischer–Burmeister* and the *min* function, as detailed in the following.

The *Fischer–Burmeister* (FB) *complementarity function* Φ^{FB} is defined as follows [31]:

$$\Phi^{FB}(\dot{\gamma}, f) = \sqrt{\dot{\gamma}^2 + f^2} - \dot{\gamma} + f \tag{70}$$

[3] Note that plastic or neutral loading takes place at $(\boldsymbol{\sigma}, \boldsymbol{\chi}) \in \partial E_\sigma$ if the angle in the inner product defined by $\mathbb{C}$ between $\partial_\sigma f$ (i.e., the normal to ∂E_σ at $\boldsymbol{\sigma}$) and $\dot{\boldsymbol{\varepsilon}}$ is less or equal than $\pi/2$ [10].

such that condition (68) holds.

Proof We start by proving:

$$\Phi^{FB}(\dot{\gamma},f)=0 \;\Rightarrow\; \dot{\gamma}\geq 0,\, f\leq 0,\, \dot{\gamma}f=0 \tag{71}$$

By defining $\Phi^{FB}=\sqrt{\dot{\gamma}^2+f^2}-\dot{\gamma}+f=0$, we have:

$$\sqrt{\dot{\gamma}^2+f^2}=\dot{\gamma}-f,\quad \dot{\gamma}\geq f \tag{72}$$

Squaring both members:

$$\dot{\gamma}^2+f^2=f^2+\dot{\gamma}^2-2f\dot{\gamma} \tag{73}$$

and simplifying, we obtain $f\dot{\gamma}=0$. If $f\leq 0, \dot{\gamma}\geq 0$ for (71). Thus, condition (70) is verified.

Now, we prove:

$$\dot{\gamma}\geq 0,\, f\leq 0,\, \dot{\gamma}f=0 \;\Rightarrow\; \Phi^{FB}(\dot{\gamma},f)=0 \tag{74}$$

We impose the following equality:

$$\sqrt{\dot{\gamma}^2+f^2}=\dot{\gamma}-f,\quad \dot{\gamma}\geq f \tag{75}$$

Then, squaring both members:

$$\dot{\gamma}^2+f^2=f^2+\dot{\gamma}^2-2f\dot{\gamma} \tag{76}$$

and simplifying, we obtain $f\dot{\gamma}=0$, that is verified by hypothesis. Therefore, we have $\sqrt{f^2+\dot{\gamma}^2}+f-\dot{\gamma}=0=\Phi^{FB}$ and condition (73) is verified. □

The first derivatives of the FB function are:

$$\begin{cases}\dfrac{\partial\Phi^{FB}}{\partial\dot{\gamma}}=\dfrac{\dot{\gamma}}{\sqrt{\dot{\gamma}^2+f^2}}-1\\[2ex] \dfrac{\partial\Phi^{FB}}{\partial f}=\dfrac{f}{\sqrt{\dot{\gamma}^2+f^2}}+1\end{cases} \tag{77}$$

while the second derivatives are:

$$\begin{cases}\dfrac{\partial^2\Phi^{FB}}{\partial\dot{\gamma}^2}=\dfrac{1}{\sqrt{\dot{\gamma}^2+f^2}}-\dfrac{\dot{\gamma}^2}{\left(\dot{\gamma}^2+f^2\right)^{3/2}}\\[2ex] \dfrac{\partial^2\Phi^{FB}}{\partial f^2}=\dfrac{1}{\sqrt{\dot{\gamma}^2+f^2}}-\dfrac{f^2}{\left(\dot{\gamma}^2+f^2\right)^{3/2}}\\[2ex] \dfrac{\partial^2\Phi^{FB}}{\partial\dot{\gamma}\partial f}=\dfrac{\partial^2\Phi^{FB}}{\partial f\partial\dot{\gamma}}=-\dfrac{f\dot{\gamma}}{\left(\dot{\gamma}^2+f^2\right)^{3/2}}\end{cases} \tag{78}$$

As it can be observed, the FB function is differentiable everywhere except at $(\dot{\gamma},f)=(0,0)$.

The *min complementarity function* $\Phi^{MIN}:\mathfrak{R}^2\rightarrow\mathfrak{R}$ is defined as follows:

$$\Phi^{MIN}(\dot{\gamma},f)=\min\left[\dot{\gamma},-f\right] \tag{79}$$

such that condition (68) holds. The min function can be rewritten in the following equivalent form:

$$\min\left[\dot{\gamma},-f\right]=\dot{\gamma}-\langle\dot{\gamma}+f\rangle \tag{80}$$

Proof We start by proving:

$$\Phi^{MIN}(\dot{\gamma},f)=0 \;\Rightarrow\; \dot{\gamma}\geq 0,\, f\leq 0,\, \dot{\gamma}f=0 \tag{81}$$

If $\Phi^{MIN}=\dot{\gamma}-\langle\dot{\gamma}+f\rangle=0$ holds, only one of the two following cases occurs:

$$\begin{cases}\dot{\gamma}+f\geq 0\\ \dot{\gamma}-\langle\dot{\gamma}+f\rangle=0\end{cases}\Rightarrow\; f=0,\, \dot{\gamma}\geq 0 \tag{82}$$

and

$$\begin{cases}\dot{\gamma}+f<0\\ \dot{\gamma}-\langle\dot{\gamma}+f\rangle=0\end{cases}\Rightarrow\; \dot{\gamma}=0,\, f<0 \tag{83}$$

Thus, condition (80) is verified.

Now, we prove:

$$\dot{\gamma}\geq 0,\, f\leq 0,\, \dot{\gamma}f=0 \;\Rightarrow\; \Phi^{MIN}(\dot{\gamma},f)=0 \tag{84}$$

We impose the following equality:

$$\dot{\gamma}-\langle\dot{\gamma}+f\rangle=0 \tag{85}$$

Again, only one of the two following cases occurs for f:

$$\begin{cases}\dot{\gamma}+f\geq 0\\ \dot{\gamma}-\langle\dot{\gamma}+f\rangle=0\end{cases}\Rightarrow\; f=0,\, \dot{\gamma}\geq 0 \tag{86}$$

and

$$\begin{cases}\dot{\gamma}+f<0\\ \dot{\gamma}-\langle\dot{\gamma}+f\rangle=0\end{cases}\Rightarrow\; \dot{\gamma}=0,\, f<0 \tag{87}$$

that are both verified by hypothesis in (83). Therefore, condition (83) is verified. □

The min function is a piecewise smooth function, whose non-differentiable points form the line $\{(\dot{\gamma},f)\in\mathfrak{R}^2\mid\dot{\gamma}=-f\}$.

Smoothing functions Different approaches to overcome the non-smoothness of the complementarity functions or to handle systems of nonsmooth equations have been developed (see [27] and references therein). Here, we consider smooth approximations for the complementarity

functions, restricting our attention to the FB and min functions defined above. Particularly, we approximate the complementarity function $\Phi{:}\mathfrak{R}^2 \rightarrow \mathfrak{R}$, defined in Eq. (68), with a *smoothed function* $\Phi_\delta{:}\mathfrak{R}^2 \rightarrow \mathfrak{R}$, with δ a positive smoothing parameter.

We start by introducing an approximation for the FB function in Eq. (69), called *smoothed FB function* Φ_δ^{FB} and defined as [32]:

$$\Phi_\delta^{FB}(\dot{\gamma},f,\delta) = \sqrt{\dot{\gamma}^2+f^2+2\delta} - \dot{\gamma} + f \tag{88}$$

such that:

$$\Phi_\delta^{FB}(\dot{\gamma},f,\delta) = 0 \quad \Leftrightarrow \quad \dot{\gamma} \geq 0,\ f \leq 0,\ \dot{\gamma} f = -\delta \tag{89}$$

Proof We start by proving:

$$\Phi_\delta^{FB}(\dot{\gamma},f,\delta) = 0 \quad \Rightarrow \quad \dot{\gamma} \geq 0,\ f \leq 0,\ \dot{\gamma} f = -\delta \tag{90}$$

By defining $\Phi_\delta^{FB} = \sqrt{\dot{\gamma}^2+f^2+2\delta} - \dot{\gamma} + f = 0$, we have:

$$\sqrt{\dot{\gamma}^2+f^2+2\delta} = \dot{\gamma} - f, \quad \dot{\gamma} > f \tag{91}$$

Squaring both members, we obtain:

$$\dot{\gamma}^2+f^2+2\delta = \dot{\gamma}^2+f^2-2\dot{\gamma} f \tag{92}$$

and simplifying, we have $\dot{\gamma} f = -\delta$. If $f \leq 0$, $\dot{\gamma} \geq 0$ for (90). Thus, condition (89) is verified.

Now, we prove:

$$\dot{\gamma} \geq 0,\ f \leq 0,\ \dot{\gamma} f = -\delta \quad \Rightarrow \quad \Phi_\delta^{FB} = 0 \tag{93}$$

We impose the following equality:

$$\sqrt{\dot{\gamma}^2+f^2+2\delta} = \dot{\gamma} - f, \quad \dot{\gamma} \geq f \tag{94}$$

Squaring both members:

$$\dot{\gamma}^2+f^2+2\delta = \dot{\gamma}^2+f^2-2f\dot{\gamma} \tag{95}$$

and simplifying, we have $f\dot{\gamma} = -\delta$, that is verified by hypothesis (92). Thus, $\sqrt{\dot{\gamma}^2+f^2+2\delta} - \dot{\gamma} + f = 0 = \Phi_\delta^{FB}$ and condition (92) is verified. □

The first derivatives of Φ_δ^{FB} are the following:

$$\begin{cases} \dfrac{\partial \Phi_\delta^{FB}}{\partial \dot{\gamma}} = \dfrac{\dot{\gamma}}{\sqrt{\dot{\gamma}^2+f^2+2\delta}} - 1 \\ \dfrac{\partial \Phi_\delta^{FB}}{\partial f} = \dfrac{f}{\sqrt{\dot{\gamma}^2+f^2+2\delta}} + 1 \end{cases} \tag{96}$$

while the second derivatives are given by:

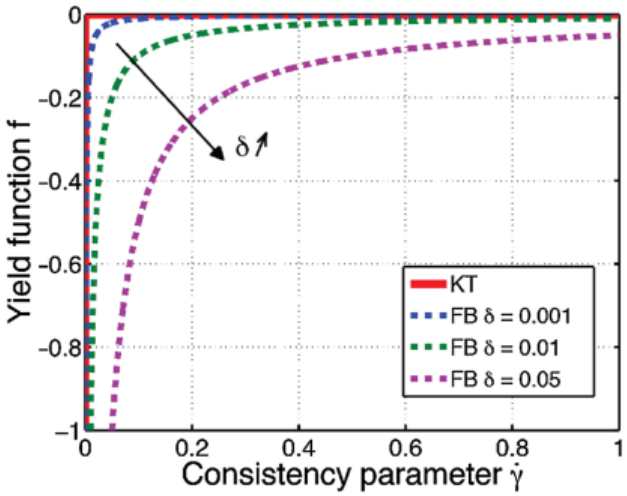

Fig. 1 Approximation of the Kuhn–Tucker (KT) conditions (57) through the smoothed Fischer–Burmeister (FB) function defined in Eq. (87), varying δ

$$\begin{cases} \dfrac{\partial^2 \Phi_\delta^{FB}}{\partial \dot{\gamma}^2} = \dfrac{1}{\sqrt{\dot{\gamma}^2+f^2+2\delta}} - \dfrac{\dot{\gamma}^2}{\left(\dot{\gamma}^2+f^2+2\delta\right)^{3/2}} \\ \dfrac{\partial^2 \Phi_\delta^{FB}}{\partial f^2} = \dfrac{1}{\sqrt{\dot{\gamma}^2+f^2+2\delta}} - \dfrac{f^2}{\left(\dot{\gamma}^2+f^2+2\delta\right)^{3/2}} \\ \dfrac{\partial^2 \Phi_\delta^{FB}}{\partial \dot{\gamma} \partial f} = \dfrac{\partial^2 \Phi_\delta^{FB}}{\partial f \partial \dot{\gamma}} = -\dfrac{f\dot{\gamma}}{\left(\dot{\gamma}^2+f^2+2\delta\right)^{3/2}} \end{cases} \tag{97}$$

Now, we may observe that for any $\delta > 0$, the function Φ_δ^{FB} is smooth everywhere and differentiable at $(\dot{\gamma},f) = (0,0)$.

Figure 1 shows the effect of the replacement of the KT complementary conditions (57) with the smoothed FB function defined in Eq. (87), varying δ. As it can be observed, Φ_δ converges to the KT complementary conditions as δ decreases.

Several smoothing functions to the min function have been proposed in the literature. The common idea is to approximate, first, the max function in Eq. (79) and, then, to derive an approximation for Φ^{MIN} defined in Eq. (78). Along this line, Chen and Mangasarian [33] introduced a family of smoothing functions, where the generic *Chen–Mangasarian* (CM) *smoothing function* to the min function is defined by:

$$\Phi_\delta^{CM}(\dot{\gamma},f,\delta) = \dot{\gamma} - \int_{-\infty}^{+\infty} \max\left[0, \dot{\gamma}+f-\delta s\right] \rho(s) ds \tag{98}$$

where $\rho{:}\mathfrak{R} \rightarrow [0,+\infty)$ is a piecewise continuous density function satisfying:

$$\int_{-\infty}^{+\infty} \rho(s) ds = 1 \tag{99}$$

and

$$k_1 := \int_{-\infty}^{+\infty} |s|\rho(s)ds < +\infty \tag{100}$$

Depending on the definition of ρ, several Φ_δ^{CM} can be derived [33].

Here, we consider the following CM function, known as *Neural Networks* (NN) smoothing function [33]:

$$\Phi_\delta^{NN}(\dot\gamma, f, \delta) = -f - \delta \ln\left[1 + \exp^{-\frac{\dot\gamma + f}{\delta}}\right] \tag{101}$$

Such a function is now differentiable. Figure 2a represents the effect of the replacement of the KT complementary conditions (57) with the NN smoothing function defined in Eq. (100), varying δ.

Another CM function, known as *Chen–Harker–Kanzow–Smale* (CHKS) smoothing function, is defined as [33]:

$$\Phi_\delta^{CHKS}(\dot\gamma, f, \delta) = \frac{\dot\gamma - f}{2} - \frac{\sqrt{(\dot\gamma + f)^2 + 4\delta^2}}{2} \tag{102}$$

Such a function is differentiable. Figure 3a represents the effect of the replacement of the KT complementary conditions (57) with the CHKS function defined in Eq. (101), varying δ.

Through the discussed smoothed complementarity functions, the KT conditions (57) are converted into a smooth unconstrained problem, whose solution approximates the solution of the original problem to a degree of accuracy depending on δ [34]. Figure 4 presents a comparison between the approaches based on the FB, NN, and CHKS smoothing functions for $\delta = 0.1$. The formulations based on the FB and CHKS lead to equivalent approximations of the KT conditions; the difference lies in the smoothing parameter, which is assumed to be δ for the FB function and δ^2 for the CHKS function. Therefore, it can be observed in Fig. 4 that the FB function requires lower values of the parameter δ to better approximate the KT conditions.

Remark 3 (Derivation of the NN function) The procedure to derive the NN function (100) consists in the introduction of the sigmoid function or *s*-function, defined as:

$$S(x, \delta) = \frac{1}{1 + \exp^{-\frac{x}{\delta}}}, \quad x \in \Re \tag{103}$$

and of its integral, known as *p*-function:

$$P(x, \delta) = \int_{-\infty}^{x} S(y, \delta)dy = x + \delta \ln\left[1 + \exp^{-\frac{x}{\delta}}\right] \tag{104}$$

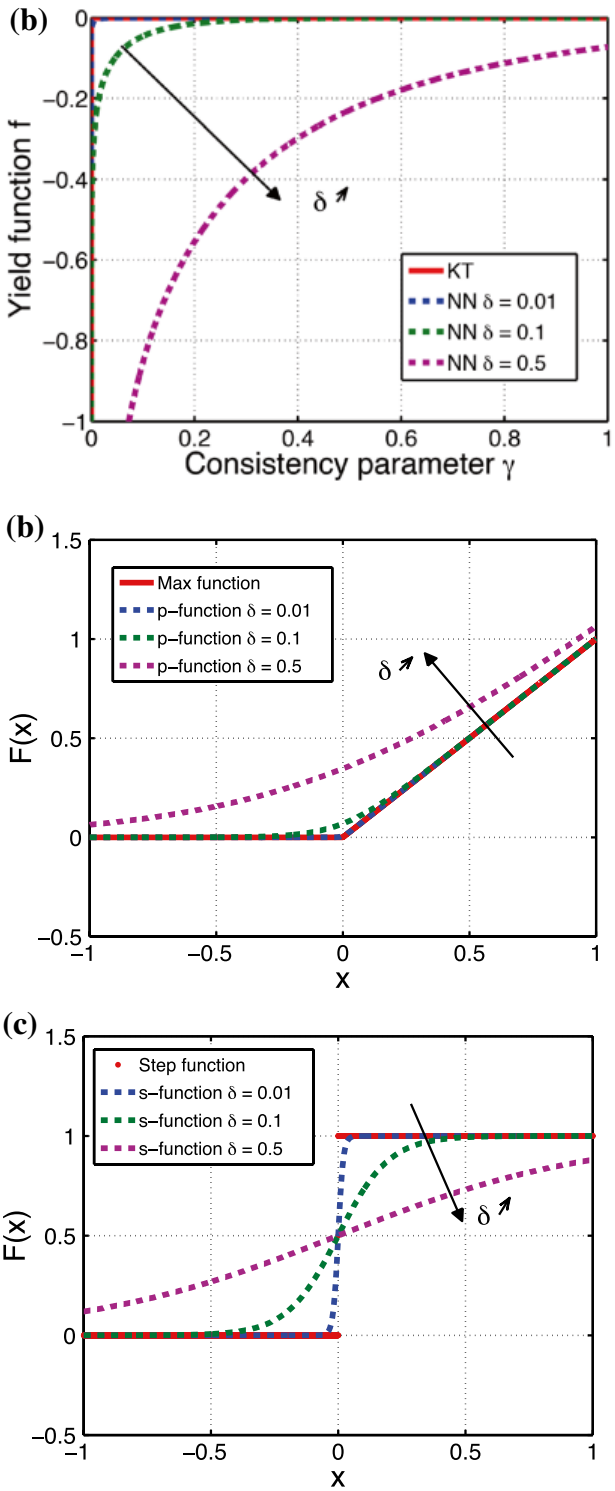

Fig. 2 Approximation of: **a** the KT complementary conditions (57) through the Neural Networks (NN) smoothing function defined in (100), varying δ; **b** the max function through the *p*-function; **c** the Heaviside step function through the *s*-function

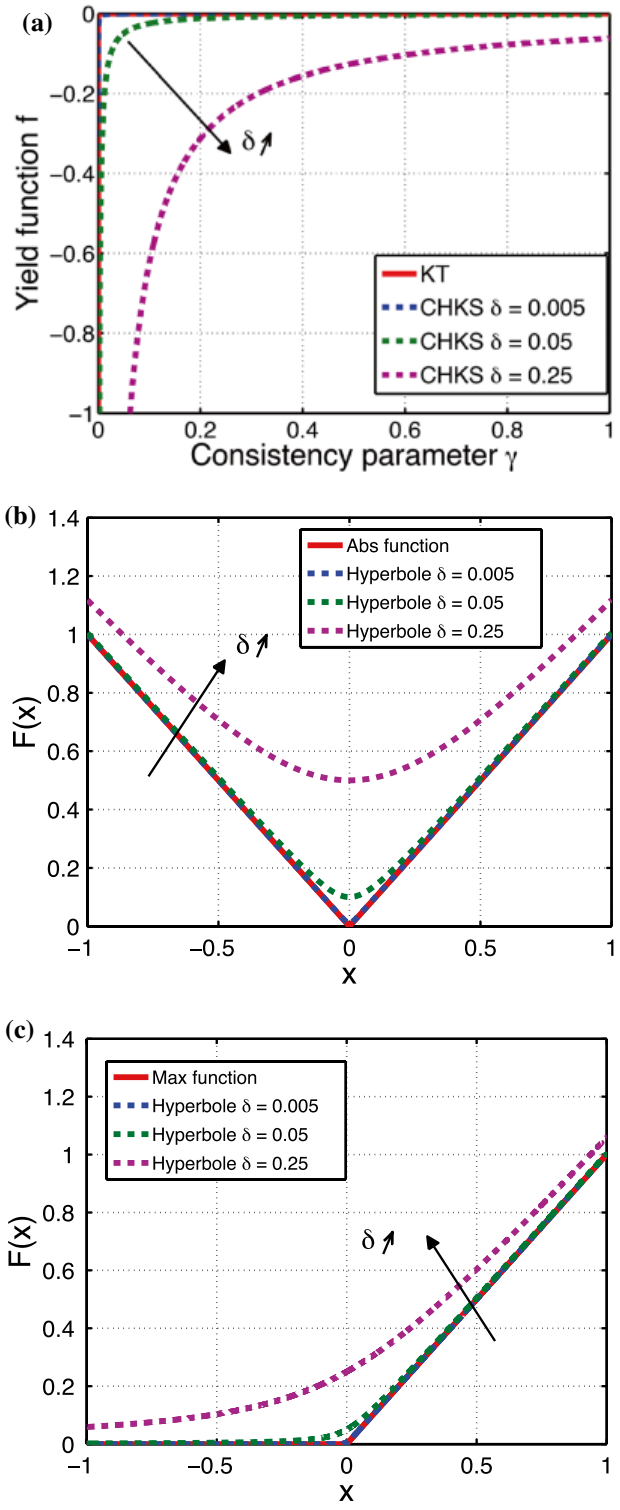

Fig. 3 Approximation of: **a** the KT complementary conditions (57) through the Chen–Harker–Kanzow–Smale (CHKS) smoothing function defined in Eq. (101), varying δ; **b** the absolute value function through a hyperbole; **c** the max function through a hyperbole

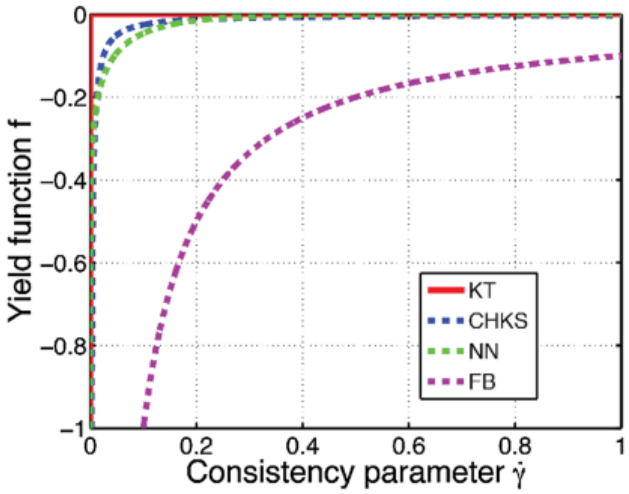

Fig. 4 Comparison between the approaches based on the Fischer–Burmeister (FB), Neural Networks (NN), and Chen-Harker-Kanzow-Smale (CHKS) smoothing functions

The s- and p-function can be treated, respectively, as an approximation of the Heaviside or unit step function (see Fig. 2c):

$$H(x) = \begin{cases} 0 & \text{if } x < 0 \\ 0.5 & \text{if } x = 0 \\ 1 & \text{if } x > 0 \end{cases} \approx S(x, \delta) \tag{105}$$

and of its integral, i.e., the max function (see Fig. 2b):

$$\langle x \rangle = \max[0, x] \approx P(x, \delta) \tag{106}$$

Remark 4 (Derivation of the CHKS function) The procedure to derive the CHKS function consists in rewriting the max function, as follows:

$$\langle x \rangle = \max[0, x] = \frac{x}{2} + \frac{|x|}{2} \tag{107}$$

Then, if we approximate the absolute-value function $|x|$ with an hyperbole (see Fig. 3b):

$$|x| \approx \sqrt{x^2 + 4\delta^2} \tag{108}$$

the approximation of the max function in (106) follows (see Fig. 3c):

$$\langle x \rangle = \max[0, x] \approx \frac{x}{2} + \frac{\sqrt{x^2 + 4\delta^2}}{2} \tag{109}$$

2.2.11 The Principle of Maximum Plastic Dissipation

We now provide an alternative formulation to the theory for associative plasticity by reporting the *principle of maximum plastic dissipation*. Such a principle plays an important role in the *variational formulation* of plasticity. It is often credited to von Mises [3] and has been studied in several works [35–37].

We define the *plastic dissipation* $D^p = D^p\left(\boldsymbol{\sigma}, \chi; \dot{\boldsymbol{\varepsilon}}^p, \dot{\xi}\right)$, as follows:

$$D^p = \boldsymbol{\sigma} : \dot{\boldsymbol{\varepsilon}}^p + \chi * \dot{\xi} \tag{110}$$

that represents the rate of work done or the dissipation due to plastic deformation.

The principle of maximum plastic dissipation states that, among all the admissible states $(\boldsymbol{\sigma}^*, \chi^*)$, the actual state $(\boldsymbol{\sigma}, \chi)$ maximizes the plastic dissipation (109), for a given state $\left(\dot{\boldsymbol{\varepsilon}}^p, \dot{\xi}\right)$. Therefore, the following inequality yields:

$$\begin{aligned} &(\boldsymbol{\sigma}, \chi) \in E_\sigma \\ &D^p\left(\boldsymbol{\sigma}, \chi; \dot{\boldsymbol{\varepsilon}}^p, \dot{\xi}\right) \geq D^p\left(\boldsymbol{\sigma}^*, \chi^*; \dot{\boldsymbol{\varepsilon}}^p, \dot{\xi}\right) \quad \forall (\boldsymbol{\sigma}^*, \chi^*) \in E_\sigma \end{aligned} \tag{111}$$

or, equivalently:

$$\begin{aligned} &(\boldsymbol{\sigma}, \chi) \in E_\sigma \\ &(\boldsymbol{\sigma} - \boldsymbol{\sigma}^*) : \left[\dot{\boldsymbol{\varepsilon}} - \mathbb{C}^{-1} \dot{\boldsymbol{\sigma}}\right] - (\chi - \chi^*) * \mathbb{D}^{-1} * \dot{\chi} \geq 0 \\ &\forall (\boldsymbol{\sigma}^*, \chi^*) \in E_\sigma \end{aligned} \tag{112}$$

Therefore, the actual state $(\boldsymbol{\sigma}, \chi)$ is solution to the following *constrained optimization problem*:

$$\max_{(\boldsymbol{\sigma}^*, \chi^*) \in E_\sigma} D^p\left(\boldsymbol{\sigma}^*, \chi^*; \dot{\boldsymbol{\varepsilon}}^p, \dot{\xi}\right) \tag{113}$$

The maximum plastic dissipation principle has the advantage of implying [10]:

i. associative evolution laws in stress-space;
ii. loading/unloading conditions in the KT complementary form (57);
iii. convexity of the elastic domain E_σ.

For the proof, refer to [10].

Inequality (110) and the weak formulation of the rate form of the momentum balance equation provide a variational formulation of plasticity (see [10] for details). Moreover, inequality (110) is valid also in cases for which the formulation no longer holds, e.g., in the case of elastic domains with a nonsmooth boundary [10].

2.2.12 Convex Analysis Setting

We now examine the elastoplastic theory by adopting the tools of convex analysis and subdifferential calculus [38] in order to deal with convex non-differentiable functions and multivalued operators [20, 39–41]. This allows to derive an alternative form for the evolution laws from a non-differential potential, which has a rigorous mathematical basis and becomes important for the analysis of the *variational problem* of elastoplasticity [39, 41].

We now transform inequality (110) to obtain the set-valued mapping relating the states $(\boldsymbol{\sigma}, \chi)$ and $\left(\dot{\boldsymbol{\varepsilon}}^p, \dot{\xi}\right)$. Following [39], we make use of the indicator function of the closed convex set E_σ:

$$I_{E_\sigma}(\boldsymbol{\sigma}, \chi) = \begin{cases} 0 & \text{if} (\boldsymbol{\sigma}, \chi) \in E_\sigma \\ +\infty & \text{otherwise} \end{cases} \tag{114}$$

which is called *complementary pseudo-potential of dissipation* and is denoted by D^{p*}. The function is convex because of the convexity of the elastic domain, but non-differentiable in the classical sense. We can thus rewrite inequality (110) in the equivalent form:

$$D^p\left(\boldsymbol{\sigma}, \chi; \dot{\boldsymbol{\varepsilon}}^p, \dot{\xi}\right) - I_{E_\sigma}(\boldsymbol{\sigma}, \chi) \geq D^p\left(\boldsymbol{\sigma}^*, \chi^*; \dot{\boldsymbol{\varepsilon}}^p, \dot{\xi}\right) - I_{E_\sigma}(\boldsymbol{\sigma}^*, \chi^*) \tag{115}$$

Since it can be demonstrated that inequality (114) corresponds to the convex inequality applied to a non-differential function [42], the states $(\boldsymbol{\sigma}, \chi)$ and $\left(\dot{\boldsymbol{\varepsilon}}^p, \dot{\xi}\right)$ are related by the following subdifferential relations:

$$\begin{cases} \dot{\boldsymbol{\varepsilon}}^p \in \partial_\sigma I_{E_\sigma} \\ \dot{\xi} \in \partial_\chi I_{E_\sigma} \end{cases} \tag{116}$$

which are equivalent to the evolution laws (43) and complementarity conditions (57). Inequality conditions are no more present. It is noted that the evolution rules take the form of a differential inclusion where the rate of both plastic strain and strain-like internal variables is expressed as the subgradient of the convex complementary pseudo-potential.

The inverse relation of the evolution rules (115) is obtained straightforwardly by using the Fenchel transform [38]:

$$\begin{aligned} D^p\left(\dot{\boldsymbol{\varepsilon}}^p, \dot{\xi}\right) &= \sup_{\sigma, \chi} \left[\boldsymbol{\sigma} : \dot{\boldsymbol{\varepsilon}}^p + \chi * \dot{\xi} - I_{E_\sigma}(\boldsymbol{\sigma}, \chi)\right] \\ &= \sup_{(\sigma, \chi) \in E_\sigma} \left[\boldsymbol{\sigma} : \dot{\boldsymbol{\varepsilon}}^p + \chi * \dot{\xi}\right] \end{aligned} \tag{117}$$

where D^p is the *pseudo-potential of dissipation*. This function is convex, non-negative, zero only at the origin, and non-differentiable at the origin, where its sub-differential set coincides with the elastic domain [15]. The fact that the pseudo-potential is homogeneous of degree one implies a rate-independent behaviour.

The inverse evolution laws are then:

$$\begin{cases} \boldsymbol{\sigma} \in \partial_{\dot{\boldsymbol{\varepsilon}}^p} D^p\left(\dot{\boldsymbol{\varepsilon}}^p, \dot{\xi}\right) \\ \chi \in \partial_{\dot{\xi}} D^p\left(\dot{\boldsymbol{\varepsilon}}^p, \dot{\xi}\right) \end{cases} \tag{118}$$

Both functions are convex and related by the Fenchel inequality.

Table 1 Initial boundary-value problem (IBVP) for a three-dimensional isotropic elastoplastic body

For any $\mathbf{x} \in \Omega$ and any $t \in I \subset \Re^+$, find the displacement field $\mathbf{u}(\mathbf{x}, t)$ which solves the following governing equations:

1. static equilibrium:

$$\text{div}\boldsymbol{\sigma} + \rho\mathbf{b} = \dot{\mathbf{v}} \quad \text{in } \Omega \times I \tag{120}$$

2. kinematic relation:

$$\boldsymbol{\varepsilon} = \frac{1}{2}\left[\nabla\mathbf{u} + (\nabla\mathbf{u})^T\right] \quad \text{in } \Omega \times I \tag{121}$$

3. constitutive equation: (see Table 2)

$$\boldsymbol{\sigma} = \boldsymbol{\sigma}(\boldsymbol{\varepsilon}^e) \quad \text{in } \Omega \times I \tag{122}$$

and satisfies the:

1. boundary conditions:

$$\begin{cases} \mathbf{u} = \overline{\mathbf{u}} & \text{on } \Gamma_D \times I \\ \boldsymbol{\sigma}\cdot\mathbf{n} = \overline{\mathbf{t}} & \text{on } \Gamma_N \times I \end{cases} \tag{123}$$

2. initial conditions:

$$\begin{cases} \mathbf{u}(0) = \mathbf{u}_0 & \text{in } \Omega \\ \dot{\mathbf{u}}(0) = \mathbf{v}_0 & \text{in } \Omega \end{cases} \tag{124}$$

Substituting the strain decomposition (5) in the constitutive laws (18) and (22), we obtain the following constitutive differential equations from Eq. (118):

$$\begin{cases} \partial_{\boldsymbol{\varepsilon}^p}\Psi(\boldsymbol{\varepsilon} - \boldsymbol{\varepsilon}^p, \xi) + \partial_{\dot{\boldsymbol{\varepsilon}}^p} D^p\left(\dot{\boldsymbol{\varepsilon}}^p, \dot{\xi}\right) \ni \mathbf{0} \\ \partial_{\xi}\Psi(\boldsymbol{\varepsilon} - \boldsymbol{\varepsilon}^p, \xi) + \partial_{\dot{\xi}} D^p\left(\dot{\boldsymbol{\varepsilon}}^p, \dot{\xi}\right) \ni \mathbf{0} \end{cases} \tag{119}$$

which are also known as *Biot's equations* of standard dissipative system [43].

Recall that, for non-associated models, the maximum dissipation inequality (110) does not hold and appropriate extensions must be sought. The generalization proposed in [26] allows for an implicit relation between the plastic strain rate and the stress. As a result, it is possible to extend the normality rule to a larger class of models including non-associated flow rule. The pseudo-potential is replaced by the *bi-potential*, which depends on both the stress and the plastic strain rate [26]. The bi-potential is bi-convex, i.e., convex with respect to the stress and the plastic strain rate when considered separately. The partial sub-derivatives of the bi-potential yield the flow rule and its inverse.

2.3 Initial Boundary-Value Problem

We are now able to formulate the local form of the *initial boundary-value problem* (IBVP) for a three-dimensional isotropic elastoplastic body, as reported in Table 1.

The local form of the *elastoplastic constitutive initial value problem* (IVP) takes the form reported in Table 2. As it can be observed, system (133) consists of first-order ordinary differential equations (ODEs), i.e., Eqs. $(133)_1$ and $(133)_2$, constrained by algebraic equations and inequalities, i.e., Eq. $(133)_3$. Under plastic loading, system (133) forms a semi-explicit system of *differential algebraic equations* (DAE) of index two[4] [44]:

$$\begin{cases} \dot{\boldsymbol{\varepsilon}}^p = \dot{\gamma}\mathbf{n}(\boldsymbol{\sigma}, \boldsymbol{\chi}) \\ \dot{\xi} = \dot{\gamma}\mathbf{h}(\boldsymbol{\sigma}, \boldsymbol{\chi}) \\ f(\boldsymbol{\sigma}, \boldsymbol{\chi}) = 0 \end{cases} \tag{128}$$

provided that $\dot{\gamma} > 0$. Moreover, the elastoplastic IVP is highly nonlinear for two main reasons: (i) the time-integration of the rate constitutive equations $(133)_1$ and $(133)_2$ requires careful consideration of the KT complementary conditions $(133)_3$; (ii) the state $(\boldsymbol{\sigma}, \boldsymbol{\chi})$ is constrained to lie inside or on the yield surface which is either fixed or evolving. The object of next sections is concerned with the numerical solution of the stated IVP.

Table 2 Initial value problem (IVP) for the elastoplastic constitutive equations of Table 1

For any $\mathbf{x} \in \Omega$ and any $t \in I \subset \Re^+$, find $\boldsymbol{\varepsilon}^p(\mathbf{x}, t)$, $\xi(\mathbf{x}, t)$, and $\dot{\gamma}(\mathbf{x}, t)$ which solve the following elastoplastic constitutive equations:

$$\begin{cases} \dot{\boldsymbol{\varepsilon}}^p = \dot{\gamma}\mathbf{n}(\boldsymbol{\sigma}, \boldsymbol{\chi}) \\ \dot{\xi} = \dot{\gamma}\mathbf{h}(\boldsymbol{\sigma}, \boldsymbol{\chi}) \\ \dot{\gamma} \geq 0,\ f(\boldsymbol{\sigma}, \boldsymbol{\chi}) \leq 0,\ \dot{\gamma} f(\boldsymbol{\sigma}, \boldsymbol{\chi}) = 0 \end{cases} \quad \text{in } \Omega \times I \tag{125}$$

where:

$$\begin{cases} \boldsymbol{\sigma} = \dfrac{\partial\Psi}{\partial\boldsymbol{\varepsilon}^e} \\ \boldsymbol{\chi} = -\dfrac{\partial\Psi}{\partial\xi} \end{cases} \tag{126}$$

and satisfy the initial conditions:

$$\begin{cases} \boldsymbol{\varepsilon}^p(0) = \boldsymbol{\varepsilon}_0^p & \text{in } \Omega \\ \xi(0) = \xi_0 & \text{in } \Omega \end{cases} \tag{127}$$

3 Computational Approach to the Elastoplastic Initial Value Problem

Due to the mathematical complexity of the elastoplastic equations in Table 2, the derivation of analytical solutions is limited to simplified situations, e.g., in case of perfect plasticity or when limit loads and steady plastic flows need

[4] The global index of a solvable differential algebraic system is the smallest positive integer *m* such that all equations are brought to the standard first-order differential form after *m* differentiations [44].

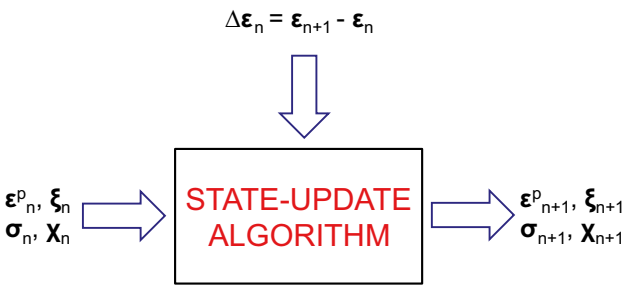

Fig. 5 State-update procedure for the numerical solution of the elastoplastic constitutive IVP of Table 2 [10]

to be computed for bodies with simple geometries [3, 9, 11]. Therefore, computational approaches are a standard practice to solve problems involving elastoplastic theories. Research studies along this line began around the nineteen-seventies with the work by Wilkins [7] and have been continued to the present. The investigations have been mostly conducted for well-known yield criteria such as the von Mises, Tresca, Drucker–Prager, and Mohr–Coulomb criteria, while few attempts have been made for the criterion by Bigoni and Piccolroaz [19], which demands more research.

The implementation of plasticity models in FE programs is generally carried out at two levels of computation, respectively the *global* and the *local* [45–51]. At the global level, the system of discrete nonlinear equations for the entire domain (see Table 1) is solved using, for example, nodal degrees of freedom such that forces and displacements are computed iteratively. For each global iteration, the discrete constitutive equations (see Table 2) are solved at the local level (generally at each quadrature point). The iterative process is continued until the fulfillment of the global system of equations and the solution is calculated for each step of the analysis.

In the present paper, we focus on the local level of computation. It consists in the solution of the elastoplastic IVP through a *state-update* procedure which first requires the *numerical integration* of the constitutive equations. The time-continuum constitutive equations are therefore transformed into incremental (or time-discrete) counterparts to obtain the *incremental elastoplastic constitutive problem*. The solution of this incremental problem is necessary for solving the global system and influences its robustness, convergence, efficiency, and accuracy.

In a classical displacement-based formulation, the state-update procedure is strain-driven (see Fig. 5): within a time increment $\Delta t_n = t_{n+1} - t_n$ (t_{n+1} and t_n being the current and previous time, respectively), the variables at the current time, $\left(\boldsymbol{\varepsilon}^p_{n+1}, \boldsymbol{\xi}_{n+1}, \boldsymbol{\sigma}_{n+1}, \boldsymbol{\chi}_{n+1}\right)$, are given as functions of the variables at the previous time, $\left(\boldsymbol{\varepsilon}^p_n, \boldsymbol{\xi}_n, \boldsymbol{\sigma}_n, \boldsymbol{\chi}_n\right)$, and of the incremental strain $\Delta\boldsymbol{\varepsilon}_n = \boldsymbol{\varepsilon}_{n+1} - \boldsymbol{\varepsilon}_n$. Here and in the following, we make use of subscript n for all the variables evaluated at previous time t_n, while we adopt subscript $n+1$ for all the variables computed at current time t_{n+1}.

In the following sections, we first focus on the time-integration of the constitutive equations presented in Table 2, then on the solution schemes for the discrete elastoplastic problem.

4 Integration Schemes

The present section provides a discussion that can be useful to the reader in deciding the integration scheme to adopt for the implementation of an elastoplastic model.

In general, an integration scheme should satisfy three requirements to be acceptable [52]: (i) *consistency* at least of order one, i.e., first-order *accuracy*; (ii) numerical *stability*; (iii) *incremental plastic consistency*. Conditions (i) and (ii) are necessary and sufficient conditions for attaining *convergence* of the numerical solution as the time increment tends to zero. To improve accuracy, higher-order approximations of the time derivative are needed. Condition (iii) is the algorithmic counterpart of the plastic consistency condition (58).

Integration schemes can be classically classified within the categories of *implicit* and *explicit* algorithms. Moreover, they can be classified depending on the previous *number of steps* used for computing the solution. Precisely, the method is one-step if, $\forall n \geq 0$, the solution at current time t_{n+1} depends on the solution at previous time t_n; otherwise the scheme is multi-step [53].

In *implicit* integration algorithms the solution at t_{n+1} depends implicitly on itself through a function defining the differential system [53]. On the one hand, these schemes generally provide great accuracy and stability as well as the satisfaction of the plastic consistency condition at the current time [54]; on the other hand, they require an iterative process to solve the obtained system of equations, which implies a considerable computational effort. In this category we find: (i) a first group that integrates the constitutive equations via an implicit linear multi-step scheme [52] and (ii) a second group that integrates the constitutive equations via an implicit one-step Runge–Kutta technique [44]. Further discussions can be found in [54–58].

In *explicit* integration algorithms the solution at t_{n+1} is computed directly in terms of (some of) the previous values at t_k with $k \leq n$ [53]. On the one hand, the methods are iterative-free, straightforward, and fast compared to the implicit ones, and can be used for any elastoplastic model [59–61]; on the other hand, they may present less accuracy than implicit methods and lack of stability and may not satisfy the incremental plastic consistency. In this category we find: (i) a first group that integrates the constitutive equations via an explicit linear multistep scheme [52] and (ii) a

second group that integrates the constitutive equations via an explicit one-step Runge–Kutta technique [62–67].

Few comparisons between implicit and explicit integration algorithms have been made in the literature for elastoplasticity, e.g., [66–68]. In [69, 70] the implementation of the forward- and the backward-Euler scheme are combined to obtain an accurate solution of the elastoplastic problem.

In addition to the above schemes, other *less-conventional* integration methods have been applied to elastoplasticity. Particularly, we recall the *group-preserving integration*, which exploits the internal symmetry of elastoplastic models [71, 72], and the *exponential-map integration*, converting the constitutive equations to an equivalent system of differential equations in the augmented stress space [73–82]. Exponential-map integration is sometimes classified as explicit integration, since the solution process is explicit, and as group-preserving integration, since it exploits internal symmetry properties. There are however some semi-implicit exponential schemes such as [78, 79, 83], where the idea is to improve the explicit scheme by finding the values of the control matrix at the middle of the elastoplastic part of the load step rather than at the beginning (see Sect. 4.4). A last group of methods is based on *exact* or *angle-based integration* that reduces the constitutive equations to a reduced number of ODEs by defining angles between plasticity variables and solving them analytically or through explicit Runge–Kutta techniques [84–92].

From the preceding discussion, we can summarize the integration schemes for elastoplasticity, as follows:

1. *Linear multi-step methods*
2. *One-step Runge–Kutta methods*
3. *Group-preserving methods*
4. *Exponential-map integration*
5. *Exact or angle-based integration*

Our analysis concerns the formulation of both conventional and *less-conventional* integration schemes in a uniform framework. First, we will review the general method and, then, we will report the plasticity models to which the method has been applied in the literature. For each method we will discuss on the fulfillment of the above three requirements. Classical schemes, as the linear multi-step and Runge–Kutta methods, are largely discussed in several textbooks and journal papers [9, 10, 93, 94].

4.1 Linear Multi-Step Methods

For notational convenience, we set $\mathbf{y} := (\boldsymbol{\varepsilon}^p, \boldsymbol{\xi})$ and $\mathbf{F} := (\mathbf{n}, \mathbf{h})$ and we write system (128) in the following form:

$$\begin{cases} \dot{\mathbf{y}} = \dot{\gamma}\mathbf{F}(\mathbf{y}) \\ f(\mathbf{y}) = 0 \end{cases} \tag{129}$$

subject to initial conditions:

$$\mathbf{y}(0) = \mathbf{y}_0 \tag{130}$$

at the time of initiation of plastic deformation, i.e., $t = t_0 = 0$.

The standard definition of a *multi-step* method with $p+1$ steps ($p \geq 0$) applied to a semi-explicit DAE system of index 2 is described as follows. The solution at current time, i.e., $\mathbf{y}_{n+1}$, depends on the previous $p+1$ values $\mathbf{y}_{n-j}$, with $j = 0, ..., p$. More precisely, a linear $(p+1)$-step method defines the algorithmic approximation $\mathbf{y}_{n+1}$ to the solution $\mathbf{y}(t_{n+1})$ by the following formula [95, 96]:

$$\begin{cases} \mathbf{y}_{n+1} = \sum_{j=0}^{p} a_{n,j}\mathbf{y}_{n-j} + \Delta\gamma_n \sum_{j=0}^{p} b_{n,j}\mathbf{F}_{n-j} + \Delta\gamma_n b_{n,-1}\mathbf{F}_{n+1} \\ f\left(\mathbf{y}_{n+1}\right) = 0 \end{cases} \tag{131}$$

given $\mathbf{y}_0$,...,$\mathbf{y}_p$ and $n = p, p+1, \ldots$. Here, $\Delta\gamma_n = \int_{t_n}^{t_{n+1}} \dot{\gamma} dt$ is the discrete consistency parameter. The non-negative coefficients $a_{n,j}$ and $b_{n,j}$ ($j = 0, ..., p$) are functions of the previous $p+1$ time step sizes and define the specific method: if $b_{n,-1} = 0$, the method is explicit, otherwise implicit. If $p = 0$, the method is one-step. From now on, for the sake of notation simplicity, we will use a_j, b_j, and $\Delta\gamma$, instead of $a_{n,j}$, $b_{n,j}$, and $\Delta\gamma_n$.

In the following, we first consider two important families of one-step algorithms for elastoplasticity; then, we consider backward difference formulas which are multi-step methods allowing to construct higher-order approximations.

4.1.1 Generalized Trapezoidal Integration

The *generalized trapezoidal integration* is a family of one-step algorithms that generalize the well-known trapezoidal rule and was introduced by Ortiz and Popov [52] in the elastoplastic context.

The scheme is obtained from system (130) by setting:

$$\begin{cases} a_0 = 1 \\ a_j = 0 \quad \text{for } j = 1, .., p \\ b_0 = 1 - \theta \\ b_j = 0 \quad \text{for } j = 1, .., p \\ b_{-1} = \theta \end{cases} \tag{132}$$

In an expanded form, system (130) is written as follows:

$$\begin{cases} \boldsymbol{\varepsilon}^p_{n+1} = \boldsymbol{\varepsilon}^p_n + \Delta\,\gamma\,[(1-\theta)\,\mathbf{n}_n + \theta\,\mathbf{n}_{n+1}] \\ \boldsymbol{\xi}_{n+1} = \boldsymbol{\xi}_n + \Delta\,\gamma\,[(1-\theta)\,\mathbf{h}_n + \theta\,\mathbf{h}_{n+1}] \\ f_{n+1} = 0 \end{cases} \tag{133}$$

where:

$$\mathbf{n}_n = \mathbf{n}(\boldsymbol{\sigma}_n, \boldsymbol{\chi}_n) \tag{134}$$

$$\mathbf{n}_{n+1} = \mathbf{n}(\boldsymbol{\sigma}_{n+1}, \boldsymbol{\chi}_{n+1}) \tag{135}$$

$$\mathbf{h}_n = \mathbf{h}(\boldsymbol{\sigma}_n, \boldsymbol{\chi}_n) \tag{136}$$

$$\mathbf{h}_{n+1} = \mathbf{h}(\boldsymbol{\sigma}_{n+1}, \boldsymbol{\chi}_{n+1}) \tag{137}$$

$$f_{n+1} = f(\boldsymbol{\sigma}_{n+1}, \boldsymbol{\chi}_{n+1}) \tag{138}$$

θ being an algorithmic parameter ranging from 0 to 1. The choice $\theta = 0$ corresponds to a fully explicit (forward-Euler) scheme, $\theta > 0$ leads to an implicit scheme, and $\theta = 1$ recovers the fully implicit (backward-Euler) scheme.

A detailed study on the accuracy and stability of this scheme (requirements (i) and (ii) discussed in Sect. 4) was presented by Ortiz and Popov [52] for perfect plasticity and possible non-associative flow rules. The scheme was shown to be first-order accurate for any θ and second-order accurate for $\theta = 1/2$. Stability was shown to depend on the shape of the yield surface: for surfaces with constant curvature in the stress space (e.g., von Mises surface), unconditional stability is obtained for $\theta \geq 1/2$; with increasing curvature, unconditional stability is guaranteed for values of θ around 1; for surfaces with infinite curvature (e.g., Tresca and Mohr–Coulomb surfaces), the algorithm is unconditionally stable for $\theta = 1$. Incremental plastic consistency (requirement (iii) discussed in Sect. 4) follows automatically from the enforcement of Eq. $(132)_3$. As it can be noted, the incremental plastic parameter $\Delta\gamma$ is determined with the aid of Eq. $(132)_3$.

4.1.2 Generalized Midpoint Integration

The *generalized midpoint integration* is a family of one-step algorithms that generalize the well-known midpoint rule and was introduced by Ortiz and Popov [52] in the elastoplastic context.

The scheme is obtained from system (130) by setting:

$$\begin{cases} a_0 = 1 \\ a_j = 0 \quad \text{for } j = 1, .., p \\ b_0 \neq 0 \\ b_j = 0 \quad \text{for } j = 1, .., p \\ b_{-1} \neq 0 \end{cases} \tag{139}$$

In an expanded form, system (130) is written as follows:

$$\begin{cases} \boldsymbol{\varepsilon}^p_{n+1} = \boldsymbol{\varepsilon}^p_n + \Delta\gamma\ \mathbf{n}_{n+\theta} \\ \boldsymbol{\xi}_{n+1} = \boldsymbol{\xi}_n + \Delta\gamma\ \mathbf{h}_{n+\theta} \\ f_{n+1} = 0 \end{cases} \tag{140}$$

where:

$$\mathbf{n}_{n+\theta} = \mathbf{n}(\boldsymbol{\sigma}_{n+\theta}, \boldsymbol{\chi}_{n+\theta}) \tag{141}$$

$$\mathbf{h}_{n+\theta} = \mathbf{h}(\boldsymbol{\sigma}_{n+\theta}, \boldsymbol{\chi}_{n+\theta}) \tag{142}$$

$$f_{n+1} = f(\boldsymbol{\sigma}_{n+1}, \boldsymbol{\chi}_{n+1}) \tag{143}$$

and

$$\begin{aligned} \boldsymbol{\sigma}_{n+\theta} &= (1-\theta)\ \boldsymbol{\sigma}_n + \theta\ \boldsymbol{\sigma}_{n+1} \\ \boldsymbol{\chi}_{n+\theta} &= (1-\theta)\ \boldsymbol{\chi}_n + \theta\ \boldsymbol{\chi}_{n+1} \end{aligned} \tag{144}$$

Again, parameter θ ranges between 0 to 1: $\theta = 0$ corresponds to a fully explicit (forward-Euler) scheme, $\theta > 0$ leads to an implicit scheme, and $\theta = 1$ recovers the fully implicit (backward-Euler) scheme. The generalized midpoint rule coincides with the generalized trapezoidal rule for $\theta = 1$, $\theta = 0$, and in case of von Mises yield criterion with associated linear hardening plasticity.

Also for this scheme, the work by Ortiz and Popov [52] provides a detailed study on the accuracy and stability characteristics. The scheme is first-order accurate for any θ and second-order accurate for $\theta = 1/2$. The generalized midpoint rule was shown to have better stability properties than the generalized trapezoidal rule, since it is unconditionally stable for $\theta \geq 1/2$, regardless of the choice of the yield surface. The considerations on the incremental plastic consistency, done for the generalized trapezoidal rule, are still valid for this scheme.

The analysis by Ortiz and Popov [52] concentrates on perfect plasticity and possible non-associative flow rules. Investigations for a von Mises model with isotropic hardening were performed in [97] and with a combination of linear isotropic hardening and nonlinear Armstrong–Frederick kinematic hardening in [73]. A study on the application of a midpoint method to models with nonlinear kinematic hardening was presented in [98]. The stability and accuracy analysis by Simo and Govindjee [99] focuses on materials with an associative hardening and flow rules and it is restricted to the case of linear elastic behaviour. Their results are in accordance with those by Ortiz and Popov [52].

A possible variation of the above generalized midpoint rule is obtained by replacing f_{n+1} in system (139) with [100]:

$$f_{n+\theta} = f(\boldsymbol{\sigma}_{n+\theta}, \boldsymbol{\chi}_{n+\theta}) \tag{145}$$

In this case, plastic consistency is enforced upon the generalized midpoint state, rather than the updated one. This alternative was discussed by Simo and Govindjee [99] who highlighted that the symmetry of the associated consistent tangent operators is ensured for fully associative models (a property not generally preserved by the family of algorithms based on the above consistency condition [101]).

In the literature, four integration schemes of this family have been investigated by Artioli et al. [102] for the von Mises plasticity model with linear isotropic and kinematic hardening. Specifically, the first two schemes are based on a traditional generalized midpoint integration rule (see Eqs. (139) and (145)) [52, 100], while the last two schemes are based on a two-stage algorithm, dividing each time

step into two subintervals, in which equations are solved sequentially (refer to [6] for details). Particularly, the fourth scheme, labelled with DMPT2 and constituting a generalization of the scheme proposed by Simo [6] for the case of von Mises perfect plasticity, seems the best performing generalized midpoint method: it is is the only scheme both B-stable and yield consistent, it performs better than the other investigated schemes in all the considered tests, and it is based on the combination of radial return maps, which is an advantage for the extension to more complex models.

Remark 5 (Solution) Both generalized trapezoidal and midpoint algorithms require the solution of a (generally nonlinear) system of equations for any θ [9]. An efficient scheme is generally obtained by adopting the Newton–Raphson method, as discussed in Sect. 5.1.1. For the fully explicit case, the equations can be simplified: all the variables become functions of $\Delta\gamma$ and the equations are reduced to a single scalar (generally nonlinear) equation. For specific models, simplifications are also possible for $\theta \neq 0$ (see, e.g., [9]).

4.1.3 Backward Difference Formulas

Backward difference formulas (BDF) are a family of linear multistep methods widely used in the numerical integration of stiff ordinary differential equation systems [103].

The scheme is obtained from system (130) by setting:

$$\begin{cases} a_j \neq 0 \quad \text{for } j = 0, .., p \\ b_j = 0 \quad \text{for } j = 0, .., p \\ b_{-1} \neq 0 \end{cases} \tag{146}$$

In an expanded form, system (130) is approximated as follows:

$$\begin{cases} \boldsymbol{\varepsilon}^p_{n+1} = \sum_{j=0}^{p} a_j \, \boldsymbol{\varepsilon}^p_{n-j} + \Delta\gamma \; b_{-1} \, \mathbf{n}_{n+1} \\ \boldsymbol{\xi}_{n+1} = \sum_{j=0}^{p} a_j \, \boldsymbol{\xi}_{n-j} + \Delta\gamma \; b_{-1} \, \mathbf{h}_{n+1} \\ f_{n+1} = 0 \end{cases} \tag{147}$$

Coefficients a_j and b_{-1} define the order $s = p + 1$ of the BDF (hence, the label BDFs). The lowest hierarchy of BDF methods (i.e., $s = 1$ and $p = 0$) coincides with the fully implicit (backward-Euler) method.

Accuracy and stability analyses (requirements (i) and (ii) discussed in Sect. 4) for BDF methods in plasticity have been performed in [6, 44]; for a general discussion, see [95]. The accuracy analysis of the BDF2 method, reported in [44, 104], leads to the following coefficients:

$$\begin{cases} a_0 = \dfrac{\left(\Delta t_{n-1} + \Delta t_n\right)^2}{\Delta t_{n-1}\left(\Delta t_{n-1} + 2\Delta t_n\right)} \\ a_1 = \dfrac{\Delta t_n^2}{\Delta t_{n-1}\left(\Delta t_{n-1} + 2\Delta t_n\right)} \\ b_{-1} = \dfrac{\left(\Delta t_{n-1} + \Delta t_n\right)}{\Delta t_{n-1} + 2\Delta t_n} \end{cases} \tag{148}$$

where $\Delta t_{n-1} = t_n - t_{n-1}$ and $\Delta t_n = t_{n+1} - t_n$. In case of constant step sizes, this leads to $a_0 = 4/3$, $a_1 = -1/3$, and $b_{-1} = 2/3$ [95].

As regards requirement (iii) discussed in Sect. 4, incremental plastic consistency follows from the enforcement of Eq. $(147)_3$. As it can be noted, the incremental plastic parameter $\Delta\gamma$ is determined with the aid of Eq. $(147)_3$. Differently from the generalized midpoint rule, the yield condition is consistently enforced at the end of each time interval.

Recall, also, that multi-step integration methods require a starting procedure. Moreover, such approaches usually lead to complex implicit nonlinear systems of algebraic equations, exhibiting difficulties in the iterative solution.

The BDF2 method has been tested on von Mises plasticity with linear [44] and nonlinear [104] isotropic hardening. In [44], the BDF2 method is automatically identical to the BDF1 method, which is first-order accurate, during the first plastic step. In [104] a unified approach is applied, where all unknowns (i.e., displacements and internal variables) are treated as global quantities. Then, the obtained DAE system is integrated by using a BDF2 method with automatic time step size control.

4.2 Runge–Kutta Methods

Now, for notational convenience, we set $\mathbf{y} := (\boldsymbol{\varepsilon}^p, \boldsymbol{\xi})$ and $\mathbf{F} := (\dot\gamma\mathbf{n}, \dot\gamma\mathbf{h})$ and we write system (119) in the following form:

$$\begin{cases} \dot{\mathbf{y}} = \mathbf{F}(\mathbf{y}, \dot\gamma) \\ f(\mathbf{y}) = 0 \end{cases} \tag{149}$$

subject to initial conditions:

$$\mathbf{y}(0) = \mathbf{y}_0 \tag{150}$$

at the time $t = t_0 = 0$ of initiation of plastic deformation.

The standard definition of an s-stage Runge–Kutta method with $s \geq 1$ applied to a semi-explicit DAE system of index 2 is described as follows [105]. We consider one step with step size Δt_n starting from $\mathbf{y}_n$ at time t_n. The numerical solution $\mathbf{y}_{n+1}$, which approximates the exact solution $\mathbf{y}(t_{n+1})$ at time t_{n+1}, is given by [105]:

$$\mathbf{y}_{n+1} = \mathbf{y}_n + \Delta t_n \sum_{i=1}^{s} b_i \mathbf{F}(\mathbf{Y}_{ni}, \dot{\mathbf{\Gamma}}_{ni}) \tag{151}$$

where $\dot{\mathbf{\Gamma}}_{ni}$ $(i = 1, ..., s)$ is the vector of algebraic variables $\dot{\gamma}$. The s internal stages $\mathbf{Y}_{ni}$ and $\dot{\mathbf{\Gamma}}_{ni}$ $(i = 1, ..., s)$ are the solutions of the system of nonlinear equations:

$$\begin{cases} \mathbf{Y}_{ni} = \mathbf{y}_n + \Delta t_n \sum_{j=1}^{s} a_{ij} \mathbf{F}(\mathbf{Y}_{nj}, \dot{\mathbf{\Gamma}}_{nj}) \quad i = 1, ..., s \\ f\left(\mathbf{Y}_{ni}\right) = 0 \quad i = 1, ..., s \end{cases} \tag{152}$$

Coefficients a_{ij}, b_i, and c_i define the specific method [105]; if $a_{ij} = 0$ for $j \geq i$, the method is explicit, otherwise implicit.

Runge–Kutta methods for DAEs of index 2 are very competitive and well-understood schemes and therefore have been applied to elastoplasticity [106]. They have the structure of one-step methods, but offer a higher order and superior stability properties (requirements (i) and (ii) discussed in Sect. 4) [106]. Compared to multistep methods (see Sect. 4.1.3), one-step methods have no Dahlquist barriers on the stability, which limit to two the order of accuracy of linear multistep methods, and they do not need history data [6, 106]. The increased accuracy in Runge–Kutta methods is however at the price of an increase of functional evaluations at each level, which is expensive from a computational point of view [53, 104]. A consequence is that they are more suitable than multi-step methods at adapting the step size, while estimating the local error for Runge–Kutta methods is more difficult [53]. Also, the complex implicit nonlinear systems of algebraic equations often exhibit difficulties in the iterative solution.

The plastic consistency condition (requirement (iii) discussed in Sect. 4) may be not satisfied in Runge–Kutta methods. The error depends on the step size and it is cumulative during the whole integration procedure. Therefore, *substepping methods*, which divide the increment into subincrements when the error in the increment exceeds a limit, have been introduced to limit the error in the computed stress and stress-like variables and have been generally employed in conjunction with a correction to restore the stress and stress-like variables to the yield surface during the integration process [60–62, 64, 107–110]. The procedure increases the CPU time for the increment, but it is preferable than taking small increments over the entire history. Another solution involves a correction of the stress and stress-like variable back to the yield surface at the end of each time increment and ensures that the error at the end of each step is smaller than a limit [111, 112]. However, the correction requests an iteration procedure at the end of each step, so it also increases the CPU time.

Runge–Kutta methods for plasticity have been proposed in [6, 106, 113–115]. Sloan and Booker [63], Solowski and Gallipoli [65] applied explicit Runge–Kutta methods to integrate the elastoplastic constitutive equations. Sloan et al. [64] discussed explicit substepping methods with a modified Euler scheme or a Runge–Kutta–Dormand–Prince scheme for the Tresca, Mohr–Coulomb, modified Cam-clay, and generalized Cam-clay models. For a given load path, Sloan et al. showed that the modified Euler scheme is able to control the integration error to lie near a prescribed tolerance. In case of explicit Runge–Kutta methods, the final stress has to be corrected by placing it on the yield surface, because the consistency condition is not automatically held during the stress updating process. In [106] implicit Runge–Kutta methods are used to solve the evolution equations for the von Mises model with nonlinear hardening. The convergence order depends on the switching point detection, i.e., the order holds only if the integration starts with consistent initial values at the switching point. Furthermore, it is shown that algebraically stable Runge–Kutta methods preserve the contractivity of the elastoplastic flow. Step size control is possible by means of embedded lower order methods. Yamaguchi [68] compared explicit Runge–Kutta and forward-Euler techniques with the implicit algorithm of Ortiz and Simo [54] and found that the Runge–Kutta scheme is superior for problems with complicated constitutive laws or high accuracy demands. In [115] a modular implementation of explicit Runge–Kutta methods with error control is presented, that is suitable for any rate-type constitutive model. The difficulties caused by the algebraic constraint of conventional plasticity are resolved through a simple subloading modification, i.e., the constraint $f = 0$ is replaced by $\dot{f} = 0$. This reduces the differentiation index of the DAE system from two to one, while preserving its rate-independence, by introducing into the material description a gradual transition from elastic to plastic behaviour. Conventional behaviour is recovered in the limit of normal yielding. Moreover, the conventional response may be closely approximated throughout by a suitable choice of the subloading function. With this approach, no special treatment is required to locate the position of the yield surface or to correct for drift away from it [64, 116]. Pedroso et al. [117] extended the explicit schemes presented by Sloan [62], Sloan et al. [64], and Sheng et al. [118] to the case where a nonconvex yield surface is adopted. The scheme is based on the Runge–Kutta-embedded method of second order and has the convenient feature of automatic substep and error control. The scheme is presented in a general form that can be applied to the solution of equations for both saturated and unsaturated soils.

4.3 Group-Preserving Integration

The class of methods based on the so-called *group-preserving integration* exploits the internal symmetries of the

elastoplastic models and Lie group properties [71, 72, 119, 120, 120]. Lie group methods share the geometric structure and invariants of ODEs and are accurate, stable and effective [121].

Integration schemes of this type have been developed for elasto-perfect plasticity [72], models with linear/nonlinear kinematic hardening/softening [122–124], degradation models with isotropic and linear kinematic hardening/softening [125, 126], and elasto-perfect models with Drucker–Prager yield surface [120], and an anisotropic quadratic yield surface [127]. Recently, Liu et al. [121] extended the group-preserving integration to models with non-quadratic yield surface by proposing a return-free integration scheme that keeps the stress points on the yield surfaces without any extra enforcement.

4.4 Exponential-Map Integration

The class of methods based on the so-called *exponential-map integration* has been first introduced by Hong and Liu [72, 119] and later investigated by Auricchio et al. [73–77] in the context of elastoplasticity.

The method is based on a quasi-linear formulation of the model equations, combined with an exponential-based time integration method to solve the obtained system of equations. Specifically, constitutive equations $(119)_1$ and $(119)_2$ are first converted to the equivalent system of linear, constant coefficients, ordinary, differential equations in the augmented stress space, as:

$$\dot{\mathbf{X}}(t) = \mathbb{A}(\mathbf{X})\mathbf{X}(t) \tag{153}$$

where $\mathbf{X}$ denotes the augmented stress vector and $\mathbb{A}$ the control matrix. In a general case, the matrix $\mathbb{A}$ depends on $\mathbf{X}$ and in this sense the problem is said to be quasi-linear.

The solution of system (152) with initial condition $\mathbf{X}(0)$ can be expressed through the following relation:

$$\dot{\mathbf{X}}(t) = exp(\mathbb{A}t)\mathbf{X}(0) \tag{154}$$

which has a closed-form exponential solution when $\mathbb{A}$ is constant. In reality, $\mathbb{A}$ is not constant in the plastic phase, but one may assume that $\mathbb{A}$ is constant during each time step Δt. The known value of $\mathbb{A}$ at the beginning of each time step, $\mathbb{A}_n$, is the value considered throughout the time interval. Thus, this can be expressed as:

$$\dot{\mathbf{X}}_{n+1} = exp\left(\mathbb{A}_n \Delta t\right)\mathbf{X}_n \tag{155}$$

The method is inspired by the works of internal symmetries which are explored individually in the augmented stress spaces. The internal symmetry group of the constitutive equations ensures that the plastic consistency condition is completely satisfied at each time step, if the numerical procedure can consider it [72].

This class has been applied to von Mises and Drucker–Prager models [72–83] and, recently, to the Bigoni–Piccolroaz model [74]. Auricchio and Beirao da Veiga [77] presented an exponential-based integration algorithm by employing an exponential map for the von Mises linear mixed hardening constitutive equations, but their technique is not consistent with the yield condition. Later, Artioli et al. [75] derived two different exponential schemes for the von Mises plasticity model with linear mixed hardening, to cure the lack of yield consistency. Then, the integration method was extended to second-order accuracy algorithms [76, 78]. Artioli et al. [128] presented a second-order algorithm based on exponential maps for the von Mises model with linear isotropic and Armstrong–Frederick kinematic hardening. Liu [120] investigated internal symmetries for the Drucker–Prager model and developed two consistent schemes based on exponential-maps in an explicit manner for the elasto-perfectly plastic Drucker–Prager criterion. Finally, Rezaiee-Pajand and Nasirai [79] presented two stress updating schemes in a semi-implicit manner for the Drucker–Prager plasticity with no hardening. This approach has a great accuracy and a quadratic rate of convergence.

4.5 Exact or Angle-Based Integration

An alternative approach to the integration methods discussed above consists in reducing the number of differential equations by defining some angles between the variables and, then, by applying explicit integration (e.g., explicit Runge–Kutta methods) or by deriving closed-form solutions. Therefore, we refer to these methodologies as *exact* or *angle-based integration* methods. These techniques are usually consistent.

Analytical solutions have been found for few plasticity models. To derive closed-form solutions, the strain increments are chosen to be constant in time. Briefly, the angle defined between the strain rate tensor and the so-called relative stress deviator is introduced as a variable: if the solution for this angle is known, then the exact expression for the deviatoric stress can be obtained in a linear combination. The governing equations lead to an integral, which defines the variation of the angle [129]. Krieg and Krieg [84] proposed an exact solution for the elasto-perfectly plastic von Mises model. The approach reduces the number of variables from six to one and the yield condition is always satisfied. The authors used the analytical solution to compare the accuracy and efficiency of different approximation schemes and found that approximations used in FE calculations could produce considerable errors even with small strain increments. Yoder and Whirley [130] extended the solution to the von Mises model with linear isotropic and kinematic hardening. Lee [131] derived exact solutions

Table 3 Incremental elastoplastic problem

Given the incremental strain $\Delta\boldsymbol{\varepsilon}$ for the considered time interval $[t_n, t_{n+1}]$ and the values $\boldsymbol{\varepsilon}^p_n$ and $\boldsymbol{\xi}_n$ at time t_n, find $\boldsymbol{\varepsilon}^p_{n+1}$, $\boldsymbol{\xi}_{n+1}$, and $\Delta\gamma$ at time t_{n+1}, which solve the following system of algebraic equations:

$$\begin{cases} \boldsymbol{\varepsilon}^p_{n+1} = \boldsymbol{\varepsilon}^p_n + \Delta\gamma \mathbf{n}(\boldsymbol{\sigma}_{n+1}, \boldsymbol{\chi}_{n+1}) \\ \boldsymbol{\xi}_{n+1} = \boldsymbol{\xi}_n + \Delta\gamma \mathbf{h}(\boldsymbol{\sigma}_{n+1}, \boldsymbol{\chi}_{n+1}) \\ \Delta\gamma \geq 0, f(\boldsymbol{\sigma}_{n+1}, \boldsymbol{\chi}_{n+1}) \leq 0, \Delta\gamma f(\boldsymbol{\sigma}_{n+1}, \boldsymbol{\chi}_{n+1}) = 0 \end{cases} \tag{156}$$

where:

$$\boldsymbol{\sigma}_{n+1} = \left.\frac{\partial \Psi}{\partial \boldsymbol{\varepsilon}^e}\right|_{n+1} \tag{157}$$

$$\boldsymbol{\chi}_{n+1} = -\left.\frac{\partial \Psi}{\partial \boldsymbol{\xi}}\right|_{n+1} \tag{158}$$

for the modified von Mises model. Loret and Prevost [85] obtained an exact solution for the Drucker–Prager criterion with non-associative linear isotropic hardening by solving the obtained scalar differential equation with an accurate Runge–Kutta procedure. Ristinmaa and Tryding [86] developed a unified approach which included all the previous exact integration methods and obtained closed-form solutions for the von Mises, Mohr–Coulomb, and Tresca models with non-associative isotropic and kinematic hardening. Szabo [89] utilized the incomplete beta functions to find an implicit solution for the von Mises plasticity model with linear isotropic hardening; therefore, the solution is semi-analytical. Kossa and Szabo [90] presented two semi-analytical solutions for the von Mises elastoplasticity model with linear isotropic and kinematic hardening. The first solution corresponds to strain-driven problems with constant strain rate assumption, whereas the second one is proposed for stress-driven problems using constant stress rate assumption. Results show that the new scheme requires more computational time than the radial return map algorithm discussed in Sect. 5. However, if considering the computational time in terms of the required accuracy, then the new method can be faster than the radial return map algorithm. Szabo and Kossa proposed an exact integration for the Drucker–Prager model with linear isotropic hardening [132] and Rezaiee-Pajand and Sharifian [91] for the Drucker–Prager's model with Armstrong–Frederick kinematic and linear isotropic hardening. The third-order Bogacki-Shampine Runge–Kutta method and the fifth-order Dormand-Prince Runge–Kutta scheme were used for medium and high accuracy, respectively. Wei et al. [87] presented a consistent scheme combining the advantages of the exact solution for the Prandtl-Reuss non-hardening elastoplastic models and the asymptotic convergence of the Newton–Raphson iteration tactics. Wallin and Ristinmaa [88] employed the assumption of constant strain rate to derive a set of ODEs, solved with the Dormand–Prince-Runge–Kutta method. The tests were performed on models with isotropic hardening, mixed isotropic and kinematic hardening, and damage evolution. The results provided by the Runge–Kutta method resulted accurate and almost independent of the global increment size. The standard fully implicit generalized trapezoidal rule was also applied and resulted inaccurate for the models with mixed isotropic and kinematic hardening and damage evolution. The angles-based integration had been also employed to solve the elastoplastic damage model [133] and the Drucker–Prager's model with the Chaboche isotropic and kinematic hardening [134].

5 Solution Schemes

We now focus on state-update procedures employed to derive the updated state in terms of strain- and stress-like internal variables. An example of *incremental elastoplastic problem* is reported in Table 3, where a fully implicit (backward-Euler) integration scheme has been applied to the rate formulation of Table 2. As it can be noted, the application of conventional procedures for standard IVPs is not possible, due to the presence of the discrete KT complementary conditions $(167)_3$.

In general, numerical algorithms should be: (i) *accurate*, (ii) *robust*, and (iii) *efficient*. Several solution schemes have been proposed in the literature for the treatment of the plasticity equations. Specifically, we can distinguish between the following approaches:

1. *Elastic predictor-plastic corrector algorithms*
2. *Complementary problem function-based algorithms*
3. *Mathematical programming algorithms*
4. *Incremental energy minimization algorithms*

The so-called *elastic predictor-plastic corrector* scheme is a classical approach, based on a two-step algorithm, which includes strategies as the radial-return, mean-normal, closest-point projection, and cutting-plane algorithm. These procedures represent the most used solution schemes thanks to their simple implementation and good numerical performances. The literature is very rich on this topic and discussions in terms of efficiency, robustness, and convergence are available, e.g., [9, 10, 135, 136].

Complementary problem function-based algorithms represent a *less-conventional* approach consisting in the equivalent formulation of the KT complementarity conditions as a CP function (see Sect. 2.2.10). The advantage is the possibility of dealing with only equalities. Few works

have been proposed along this line, and mostly for crystal plasticity [137, 138].

Algorithms from *mathematical programming* represent a *less-conventional* approach. These methods exploit the potential structure of many elastoplasticity models and concepts of convex analysis (see Sect. 2.2.12) to reduce the complete IBVP or the local elastoplastic IVP to a mathematical programming problem. The advantage is given by the possibility of easily treating (nonsmooth) singularities on the yield surface. However, the efficiency of these algorithms has not been assessed so far and detailed analyses are actually lacking.

Algorithms based on an *incremental energy minimization* formulation equally exploit the potential structure of elastoplasticity models and concepts of convex analysis (see Sect. 2.2.12). Advantages of this method are that the incremental plastic consistency is satisfied and yield surfaces with singularities can be treated in a simpler way. Also for this approach, detailed discussions are lacking and therefore they may be grouped into the *less-classical* group.

This section analyzes and discusses all the listed approaches.

5.1 Elastic Predictor-Plastic Corrector Algorithms

The class of elastic-predictor plastic-corrector algorithms is based on a two-step scheme: (i) an elastic trial state is first computed; (ii) then, if the onset of plasticity is detected, a plastic correction is computed using the trial state as initial condition to update all the internal variables[5]. This family is the most adopted thanks to the easy implementation, good numerical performances and properties (in terms of accuracy, robustness, and efficiency), and enforcement of the plastic consistency condition [10, 139].

The idea of such a scheme traces back to Wilkins [7] who proposed the *radial-return method* for the von Mises perfect plasticity. Extensions to linear isotropic and kinematic hardening [140], plane stress [141], nonlinear hardening [142], and smooth/nonsmooth yield conditions [143–145] have been also proposed. In the following, we describe two important classes of return mapping algorithms, namely, the closest-point projection and cutting-plane algorithms. The superiority of the radial-return method compared to other return schemes is established in [52, 84, 85, 130, 146].

An alternative justification for the elastic predictor-plastic corrector scheme was provided by Simo and Hughes [147], who interpreted this two-step scheme as a product formula algorithm arising from an elastoplastic *operator-split* of the constitutive equations. Such an interpretation is useful in analyzing and developing algorithms; as an example, the general notion of return mapping is exploited to develop the cutting-plane algorithm discussed in Sect. 5.1.3. An alternative plastic predictor-elastic corrector algorithm was proposed in [148].

Table 4 reports a well-known solution scheme belonging to this class, known as *backward-Euler elastic predictor/return mapping algorithm* [101]. It should be noted that a fully implicit integration scheme is used; however, other integration rules can be adopted, as discussed in Sect. 4. As an example, the generalized trapezoidal rule, described

Table 4 Backward-Euler elastic predictor/return mapping algorithm for the numerical solution of the incremental elastoplastic problem reported in 3

Given quantities: $\boldsymbol{\varepsilon}_{n+1}, \boldsymbol{\varepsilon}^p_n, \boldsymbol{\xi}_n, \gamma_n$

1. **Elastic predictor step**
   - Assume elastic behaviour in the time interval $[t_n, t_{n+1}]$
   - Compute trial state:

$$\begin{cases} \boldsymbol{\varepsilon}^{p,trial}_{n+1} = \boldsymbol{\varepsilon}^p_n \\ \boldsymbol{\xi}^{trial}_{n+1} = \boldsymbol{\xi}_n \\ \Delta\gamma^{trial} = 0 \\ \boldsymbol{\sigma}^{trial}_{n+1} = -\dfrac{\partial \Psi}{\partial \boldsymbol{\varepsilon}^p}\Big|^{trial}_{n+1} \\ \boldsymbol{\chi}^{trial}_{n+1} = -\dfrac{\partial \Psi}{\partial \boldsymbol{\xi}}\Big|^{trial}_{n+1} \end{cases}$$

2. Check plastic admissibility
   - IF $f\left(\boldsymbol{\sigma}^{trial}_{n+1}, \boldsymbol{\chi}^{trial}_{n+1}\right) \leq 0$ THEN
   - Elastic step

$$\begin{cases} \boldsymbol{\varepsilon}^p_{n+1} = \boldsymbol{\varepsilon}^{p,trial}_{n+1} \\ \boldsymbol{\xi}_{n+1} = \boldsymbol{\xi}^{trial}_{n+1} \\ \Delta\gamma = \Delta\gamma^{trial} \\ \boldsymbol{\sigma}_{n+1} = \boldsymbol{\sigma}^{trial}_{n+1} \\ \boldsymbol{\chi}_{n+1} = \boldsymbol{\chi}^{trial}_{n+1} \end{cases}$$

   - ELSE
3. **Plastic corrector step** (or return mapping algorithm)
   - Solve system:

$$\begin{cases} \boldsymbol{\varepsilon}^p_{n+1} - \boldsymbol{\varepsilon}^p_n - \Delta\gamma \mathbf{n}\left(\boldsymbol{\sigma}_{n+1}, \boldsymbol{\chi}_{n+1}\right) = \mathbf{0} \\ \boldsymbol{\xi}_{n+1} - \boldsymbol{\xi}_n - \Delta\gamma \mathbf{h}\left(\boldsymbol{\sigma}_{n+1}, \boldsymbol{\chi}_{n+1}\right) = \mathbf{0} \\ f\left(\boldsymbol{\sigma}_{n+1}, \boldsymbol{\chi}_{n+1}\right) = 0 \end{cases}$$

   where:

$$\boldsymbol{\sigma}_{n+1} = -\frac{\partial \Psi}{\partial \boldsymbol{\varepsilon}^p}\Big|_{n+1}$$

$$\boldsymbol{\chi}_{n+1} = -\frac{\partial \Psi}{\partial \boldsymbol{\xi}}\Big|_{n+1}$$

[5] Such a step is also known as *return mapping algorithm*.

in Sect. 4.1.1, generalizes the concept of return mapping, introduced by Wilkins [7] and refined in [149], for the von Mises yield criterion. For $\theta = 1/2$ and the case of a von Mises yield criterion with associated perfect plasticity, such a rule coincides in fact with the the midpoint return map proposed by Rice and Tracy [150]. For $\theta = 1$ and associated plasticity, the closest-point projection algorithm is obtained [151]. The generalized midpoint rule, described in Sect. 4.1.2, can be also adopted, as proposed in [52, 100]. For the von Mises plasticity this results in the return map proposed in [150], which is second-order accurate. A recent comparison between four integration schemes for associated and non-associated plasticity is provided in [152]. The integration schemes are a fully implicit (backward-Euler), semi-explicit convex cutting plane, fully explicit (forward-Euler), and fully explicit (forward-Euler) next increment corrects error. The backward-Euler scheme in implicit solver was shown to be 10 times faster than the same in explicit solver and faster than all the explicit schemes in explicit solver. The computation time and accuracy for both associated and non-associated flow rules were shown to be not much different when the same integration scheme was used. Moreover, in case of large-scale sheet metal forming simulations, the explicit type stress integration algorithm was shown to be a more practical choice, since it does not deteriorate the computational accuracy and efficiency compared to the fully implicit algorithm.

5.1.1 Solution of the Return Mapping Equations

As anticipated in Sect. 4.1.2, a closed-form solution of the plasticity equations can be found for simple cases [153], while most of the cases require an iterative algorithm for the solution of the nonlinear system of equations (see item 3 in Table 4).

A *Newton–Raphson scheme* is generally applied thanks to its asymptotic quadratic rate of convergence and linearization in closed-form, which leads to the consistent material tangent employed in the global IBVP (see Sect. 5.5) [52, 142]. However, some drawbacks of this scheme have to be taken into account [9].

First, the computation of the Jacobian and the inversion of a positive-definite fourth-order tensor to construct the algorithmic consistent material tangent are needed at each local iteration. This may increase the computational time and may be prone to errors, especially in case of complex constitutive equations. A possible overcome is to employ symbolic software such as Mathematica [154].

Second, a strategy to ensure that the converged incremental plastic multiplier is positive, i.e., $\Delta\gamma \geq 0$, should be considered, especially in case of complex material models.

Third, the limited local convergence properties of Newton–Raphson schemes do not guarantee global convergence and make this approach difficult to apply to complex constitutive models [9] or in case of elastic trial states close to the neighborhood of high-curvature points of the yield surface [155, 156]. Various techniques have been proposed to avoid this drawback, such as *line-search* methods [155, 157, 158], *sub-stepping* schemes [45, 62–64, 116, 159–164], *quasi-Newton procedures* [9], ad-hoc integration algorithms [62, 157–159, 165], alternative trial predictors initializing the iterative process [15, 166, 167]. Solutions for the Bigoni–Piccolroaz yield function have been proposed in [168, 169].

Fourth, the return schemes generally require huge computational times in (three-dimensional) large-scale computations. Each point of the structure requires, in fact, the update of all the internal variables at each loading step. An expected result is an increased computational cost which is $O(n^3/3)$ for the factorization, where n is the matrix order [53].

Recall that return mapping algorithms can be then simplified by exploiting the coaxiality of trial stress, increment of plastic strain, and updated stress [170, 171]. As a consequence, the elastoplastic evolution equations can be solved with respect to three unknowns, instead of the six, since the linear space of second-order symmetric tensors sharing the same principal directions is of dimension three. Different choices are possible for the coaxial second-order tensor basis, see, e.g., [153, 165, 172–178].

5.1.2 Closest-Point Projection

We now recall the closest-point projection algorithm, since it is a common strategy in practical applications. It was proposed by Ortiz et al. [151] as a generalization of the radial-return algorithm.

The algorithm applies a classical implicit backward-Euler integration of Eqs. (167), obtaining the following system:

$$\begin{cases} \boldsymbol{\varepsilon}^e_{n+1} - \boldsymbol{\varepsilon}^{e,trial}_{n+1} + \Delta\gamma\, \mathbf{n}\left(\boldsymbol{\sigma}_{n+1}, \boldsymbol{\chi}_{n+1}\right) = \mathbf{0} \\ -\boldsymbol{\xi}_{n+1} + \boldsymbol{\xi}^{trial}_{n+1} + \Delta\gamma\, \mathbf{h}\left(\boldsymbol{\sigma}_{n+1}, \boldsymbol{\chi}_{n+1}\right) = \mathbf{0} \\ \Delta\gamma \geq 0,\ f\left(\boldsymbol{\sigma}_{n+1}, \boldsymbol{\chi}_{n+1}\right) \leq 0,\ \Delta\gamma\, f\left(\boldsymbol{\sigma}_{n+1}, \boldsymbol{\chi}_{n+1}\right) = 0 \end{cases} \tag{159}$$

with:

$$\boldsymbol{\sigma}_{n+1} = \left.\frac{\partial \Psi}{\partial \boldsymbol{\varepsilon}^e}\right|_{n+1} \tag{160}$$

$$\boldsymbol{\chi}_{n+1} = -\left.\frac{\partial \Psi}{\partial \boldsymbol{\xi}}\right|_{n+1} \tag{161}$$

$$\boldsymbol{\varepsilon}^e_{n+1} = \boldsymbol{\varepsilon}_{n+1} - \boldsymbol{\varepsilon}^p_{n+1} \tag{162}$$

$$\boldsymbol{\varepsilon}^{e,trial}_{n+1} = \boldsymbol{\varepsilon}_{n+1} - \boldsymbol{\varepsilon}^p_n \tag{163}$$

Table 5 Closest-point projection equations (155) and related variational structures, as proposed in [155]

Variational formulationm	Associated functional
PRIMAL	
Proposition 1	Lagrangian in Eq. (165)
Proposition 3	Augmented Lagrangian in Eq. (167)
DUAL	
Proposition 2	Lagrangian in Eq. (165)
Proposition 4	Augmented Lagrangian in Eq. (167)

$$\boldsymbol{\xi}_{n+1}^{trial} = \boldsymbol{\xi}_n \tag{164}$$

Accordingly, the algorithm is first-order accurate and unconditionally stable provided that the elastic region is convex. The algorithm is also referred to as the *Newton closest-point projection* approximation, since the solution is generally obtained with a Newton–Raphson scheme [10].

We now focus on the variational structure behind these equations by briefly reporting the noteworthy results presented in [155]. This brief review allows us to discuss the algorithms based on such variational formulations, as proposed in [155, 158]. As detailed in the following, the closest-point projection equations define a discrete *unilaterally constrained problem* of evolution, governed by the discrete KT conditions $(155)_3$. In fact, this problem reduces to the problem of finding the closest distance (in the energy norm) of a point (the trial state) to a convex set (the elastic domain). From the computational point of view, its solution reduces to the (iterative) solution of a convex mathematical programming problem (see Sect. 5.3).

Following [155], the formulation of the variational structure requires two assumptions:

1. The Helmholtz free-energy is a strictly convex function in $(\boldsymbol{\varepsilon}^p, \boldsymbol{\xi})$ and is twice-differentiable with positive-definite Hessian matrix. This implies the positive definiteness of $\mathbb{C}$ and $\mathbb{D}$. The convexity of the Gibbs free-energy derives from the convexity of the Helmholtz free-energy.
2. The evolution equations are assumed to be associated for a convex yield function that is, the normality rules apply for plastic flow vectors in case of a differentiable yield function.

Simo and Hughes [10] discussed the algorithm for the case of constant elasticity tensor and linear strain hardening. The treatment of the equations reported in this section and taken from [155] can be considered in a more general setting, not involving the convexity and associativity assumptions.

We first report *primal* variational formulations for the unilaterally constrained problem, which involve stresses and stress-like internal variables, and then, *dual* variational formulations which incorporate explicitly the plastic multiplier[6]. The formulations in [155] involve both Lagrangian and augmented Lagrangian approaches (see Table 5). The use of augmented Lagrangians allows the regularization of the original constrained problem and leads to the proper framework for the formulation of new and improved numerical algorithms.

We first report the *primal variational principle* for problem (155) as in [155], as follows.

Proposition 1 *(Primal variational principle* [155]*) Under the two reported assumptions, the discrete equations (155) can be obtained as the first-order necessary conditions of the unilaterally constrained variational problem:*

$$\begin{aligned} &\min_{(\boldsymbol{\sigma},\chi)} \quad \left[G(\boldsymbol{\sigma},\chi) - \boldsymbol{\varepsilon}_{n+1}^{e,trial}{:}\boldsymbol{\sigma} + \boldsymbol{\xi}_{n+1}^{trial} * \chi\right] \\ &f(\boldsymbol{\sigma},\chi) \le 0 \end{aligned} \tag{165}$$

If the solution of problem (164) exists, it is unique and gives the solution of the closest-point projection equations [155]; for the proof, refer to [155].

Following classical results of constrained optimization theory [179, 180], the Lagrangian associated to problem (164) is defined as [155]:

$$\mathcal{L} = G(\boldsymbol{\sigma},\chi) - \boldsymbol{\varepsilon}_{n+1}^{e,trial}{:}\boldsymbol{\sigma} + \boldsymbol{\xi}_{n+1}^{trial} * \chi + \overline{\gamma} f(\boldsymbol{\sigma},\chi) \tag{166}$$

where $\overline{\gamma} \ge 0$ is the Lagrange multiplier.

We now report the *dual variational principle* for problem (155) as in [155], as follows.

Proposition 2 *(Dual variational principle* [155]*) Under the above assumptions, the plastic multiplier$\Delta\gamma$ in the closest-point projection approximation defined by Eq. (155) can be characterized as the argument of the variational problem:*

$$\max_{\overline{\gamma}\ge 0}\left[\min_{(\boldsymbol{\sigma},\chi)}\left[\mathcal{L}\left(\boldsymbol{\sigma},\chi,\overline{\gamma}\right)\right]\right] \tag{167}$$

where$\left(\boldsymbol{\sigma}_{n+1},\chi_{n+1}\right)$ are given by the arguments of the unconstrained minimization problem$\min_{(\boldsymbol{\sigma},\chi)}\left[\mathcal{L}\left(\boldsymbol{\sigma},\chi,\overline{\gamma}\right)\right]$ for $\overline{\gamma} = \Delta\gamma$.

[6] We here adopt the terminology used in [155]: "primal" is intended in the classical sense of constrained optimization theory [179] and it is not the terminology used when considering the global IBVP. In this context, the variational problem in terms of displacements and strains is referred to as primal form, while the problem in terms of stresses and stress-like internal variables to as dual form [155].

For the proof, refer to [155]. Here, the unconstrained minimization problem is well-defined given the convexity of $\mathcal{L}$ in $(\boldsymbol{\sigma}, \boldsymbol{\chi})$. Moreover, the minimization problem is not constrained, since $\overline{\gamma}$ is fixed [155].

Following classical results of constrained optimization theory [179, 180], the augmented Lagrangian associated to problem (164) is given by:

$$\begin{aligned}\mathcal{L}_a =& G(\boldsymbol{\sigma}, \boldsymbol{\chi}) - \boldsymbol{\varepsilon}^{e,trial}_{n+1} : \boldsymbol{\sigma} + \boldsymbol{\xi}^{trial}_{n+1} * \boldsymbol{\chi} \\ &+ \frac{c}{2}\left[\left\langle \frac{\overline{\lambda}}{c} + f(\boldsymbol{\sigma}, \boldsymbol{\chi})\right\rangle^2 - \left(\frac{\overline{\lambda}}{c}\right)^2\right]\end{aligned} \tag{168}$$

c being a constant positive penalty parameter and $\overline{\lambda}$ a scalar unconstrained variable. After setting the gradient of $\mathcal{L}_a$ to zero and denoting the final solution by $\left(\boldsymbol{\sigma}_{n+1}, \boldsymbol{\chi}_{n+1}, \Delta\lambda\right)$, we obtain:

$$\begin{cases} \left.\dfrac{\partial \mathcal{L}_a}{\partial \boldsymbol{\sigma}}\right|_{(\boldsymbol{\sigma}_{n+1}, \boldsymbol{\chi}_{n+1}, \Delta\lambda)} = \mathbf{0} \\ \left.\dfrac{\partial \mathcal{L}_a}{\partial \boldsymbol{\chi}}\right|_{(\boldsymbol{\sigma}_{n+1}, \boldsymbol{\chi}_{n+1}, \Delta\lambda)} = \mathbf{0} \\ \left.\dfrac{\partial \mathcal{L}_a}{\partial \overline{\lambda}}\right|_{(\boldsymbol{\sigma}_{n+1}, \boldsymbol{\chi}_{n+1}, \Delta\lambda)} = 0 \end{cases} \tag{169}$$

which corresponds to:

$$\begin{cases} \boldsymbol{\varepsilon}^{e}_{n+1} - \boldsymbol{\varepsilon}^{e,trial}_{n+1} + \left\langle \Delta\lambda + c f_{n+1}\right\rangle \mathbf{n}_{n+1} = \mathbf{0} \\ -\boldsymbol{\xi}_{n+1} + \boldsymbol{\xi}^{trial}_{n+1} + \left\langle \Delta\lambda + c f_{n+1}\right\rangle \mathbf{h}_{n+1} = \mathbf{0} \\ \dfrac{1}{c}\left[\left\langle \Delta\lambda + c f_{n+1}\right\rangle - \Delta\lambda\right] = 0 \end{cases} \tag{170}$$

The solution $\left(\boldsymbol{\sigma}_{n+1}, \boldsymbol{\chi}_{n+1}, \Delta\lambda\right)$ of system (168) corresponds to the solution of the closest-point projection equations [155]. In fact, identifying the relation:

$$\Delta\gamma = \langle \Delta\lambda + c f_{n+1}\rangle \tag{171}$$

leads to:

$$\Delta\lambda + c f_{n+1} \leq 0 \quad \Rightarrow \quad \Delta\lambda = 0 \quad \Rightarrow \quad \Delta\gamma = 0 \tag{172}$$

and

$$\Delta\lambda + c f_{n+1} > 0 \quad \Rightarrow \quad f_{n+1} = 0 \quad \Rightarrow \quad \Delta\gamma = \langle \Delta\lambda\rangle > 0 \tag{173}$$

which recover the discrete KT conditions (57).

We now report the *augmented Lagrangian primal principle* for problem (155) as in [155], as follows.

Proposition 3 *(Augmented Lagrangian primal principle [155]) Under the above assumptions, the discrete equations (1) can be obtained from the variational problem:47*

$$\min_{(\boldsymbol{\sigma}, \boldsymbol{\chi})}\left[\max_{\overline{\lambda}}\left[\mathcal{L}_a\left(\boldsymbol{\sigma}, \boldsymbol{\chi}, \overline{\lambda}\right)\right]\right] \tag{174}$$

forc > 0*.The solution* $\left(\boldsymbol{\sigma}_{n+1}, \boldsymbol{\chi}_{n+1}\right)$ *is obtained as the argument of the solution of problem (173), with the plastic multiplier*$\Delta\gamma$ *obtained as*$\Delta\gamma = \langle \Delta\lambda\rangle$ *for the last argument*$\Delta\lambda$ *of the solution of problem (173).*

Similarly, we report the augmented Lagrangian dual principle for problem (155) as in [155], as follows.

Proposition 4 *(Augmented Lagrangian dual principle [155]) Under the above assumptions, the plastic multiplier* $\Delta\gamma$ *in the closest-point projection approximation defined by Eqs. (155) can be characterized as:*

$$\Delta\gamma = \langle \Delta\lambda + c\bar{f}_c(\Delta\lambda)\rangle \tag{175}$$

for the unique non-negative root$\Delta\lambda$*of equation:*

$$\bar{f}_c(\Delta\lambda) = 0 \quad \text{if} \quad f^{trial}_{n+1} > 0 \tag{176}$$

or

$$\Delta\lambda = 0 \quad \text{if} \quad f^{trial}_{n+1} \leq 0 \tag{177}$$

for the function$\bar{f}_c\left(\boldsymbol{\sigma}_c(\overline{\lambda}), \boldsymbol{\chi}_c(\overline{\lambda})\right)$*with*$\left(\boldsymbol{\sigma}_c(\overline{\lambda}), \boldsymbol{\chi}_c(\overline{\lambda})\right)$*corresponding to the argument of the unconstrained minimization problem:*

$$\begin{aligned}\min_{(\boldsymbol{\sigma}, \boldsymbol{\chi})}\Bigg[& G(\boldsymbol{\sigma}, \boldsymbol{\chi}) - \boldsymbol{\varepsilon}^{e,trial}_{n+1} : \boldsymbol{\sigma} + \boldsymbol{\xi}^{trial}_{n+1} * \boldsymbol{\chi} \\ &+ \frac{c}{2}\left[\left\langle \frac{\overline{\lambda}}{c} + f(\boldsymbol{\sigma}, \boldsymbol{\chi})\right\rangle^2 - \left(\frac{\overline{\lambda}}{c}\right)^2\right]\Bigg]\end{aligned} \tag{178}$$

forc > 0*.The other components of the solution are then simply obtained as*$\left(\boldsymbol{\sigma}_{n+1}, \boldsymbol{\chi}_{n+1}\right) = \left(\boldsymbol{\sigma}_c(\overline{\lambda}), \boldsymbol{\chi}_c(\overline{\lambda})\right)$.

Armero and Pérez-Foguet [155] and Pérez-Foguet and Armero [158] developed globally convergent root-finding algorithms based on the reported primal and dual formulations, which are considered in a general setting without requiring the above convexity assumption. These algorithms consist in Newton–Raphson schemes in conjuction with line-search strategies and lead to two-level schemes: (i) the upper level consisting of the enforcement of the plastic consistency condition through an iteration in the plastic multiplier and (ii) the lower level consisting of the solution of the closest-point projection equations for a fixed plastic multiplier. The line-search scheme was shown to account for the positiveness of the plastic multiplier and to lead to the global convergent primal algorithm. The dual method was shown to not be computationally competitive in situations where the primal algorithm show no difficulties. Major advantages are clear in cases where the primal

Table 6 Newton–Raphson algorithm to solve problem (179) in strain-space [10]

1. Define the residual at iteration (k) by:
$$\nabla\mathcal{L}^{(k)} = \left[\partial_{\boldsymbol{\varepsilon}^e}\mathcal{L}^{(k)} \;\; \partial_{\Delta\delta}\mathcal{L}^{(k)}\right]^T$$
2. IF $\left\|\nabla\mathcal{L}^{(k)}\right\| < tol$ THEN
   - Exit
3. ELSE
   - Compute the Hessian $\nabla^2\mathcal{L}^{(k)}$
   - Solve the linearized system:
   $$\nabla^2\mathcal{L}^{(k)}\left[\Delta\boldsymbol{\varepsilon}^{e(k)} \;\; \Delta^2\delta^{(k)}\right]^T = -\nabla\mathcal{L}^{(k)}$$
   - Update the solution:
   $$\begin{cases}\Delta\delta^{(k+1)} = \Delta\delta^{(k)} + \Delta^2\delta^{(k)}\\ \boldsymbol{\varepsilon}^{e(k+1)} = \boldsymbol{\varepsilon}^{e(k)} + \Delta\boldsymbol{\varepsilon}^{e(k)}\end{cases}$$
   - Update $k = k+1$
   - GO to step 2

algorithm requires a large number of iterations to converge. The augmented Lagrangian-based algorithms show improved properties with respect to the non-augmented ones, since they do not need to enforce explicitly the constraint of nonnegative plastic multipliers, leading to unconstrained problems which are easily to treat analytically and avoid line-search strategies. Moreover, they were shown to reduce the computational cost when the penalty parameter is chosen in a given range.

Augmented Lagrangian approaches to plasticity have been also introduced in [181, 182]. In [181] the constitutive laws of elastoplasticity with internal variables are described through the definition of suitable dual potentials, including various hardening models. A family of variational principles for inelastic problems is so obtained using convex analysis tools and the structural problem is analyzed using the complementary energy functional.

Remark 6 (Example) As an example, we examine the geometric interpretation for the simple case of perfect plasticity in strain-space. Following [10], the state $\boldsymbol{\varepsilon}^e_{n+1}$ is the solution of the optimization problem:

$$\begin{aligned}\min_{\boldsymbol{\varepsilon}^e} \quad & \frac{1}{2}\left\|\boldsymbol{\varepsilon}^{e,trial} - \boldsymbol{\varepsilon}^e\right\|^2_{\mathbb{C}}\\ f(\nabla\Psi(\boldsymbol{\varepsilon}^e)) \le 0 \quad &\end{aligned} \tag{179}$$

where $\|\cdot\|_{\mathbb{C}} := \sqrt{\cdot:\mathbb{C}\cdot}$ is the energy norm induced by $\mathbb{C}$. Such a problem reduces to the standard problem of finding the closest distance (in the energy norm) of a point (the trial state) to a convex set (the elastic domain), thus the common name of closest-point projection. Such a geometric interpretation follows by noting that the associated Lagrangian is expressed as:

$$\mathcal{L} = \frac{1}{2}\left\|\boldsymbol{\varepsilon}^{e,trial} - \boldsymbol{\varepsilon}^e\right\|^2_{\mathbb{C}} + \Delta\delta f(\nabla\Psi(\boldsymbol{\varepsilon}^e)) \tag{180}$$

and the corresponding KT optimality conditions are:

$$\begin{cases}-\boldsymbol{\varepsilon}^{e,trial} + \boldsymbol{\varepsilon}^e_{n+1} + \Delta\gamma\left.\dfrac{\partial f}{\partial\boldsymbol{\sigma}}\right|_{n+1} = \mathbf{0}\\ \Delta\gamma \ge 0,\; f\left(\nabla\Psi(\boldsymbol{\varepsilon}^e_{n+1})\right) \le 0,\; \Delta\gamma f\left(\nabla\Psi(\boldsymbol{\varepsilon}^e_{n+1})\right) = 0\end{cases} \tag{181}$$

Here, $\boldsymbol{\varepsilon}^e$ and $\Delta\delta$ are the generic elastic strain and Lagrange multiplier, respectively; $\boldsymbol{\varepsilon}^e_{n+1}$ and $\Delta\gamma$ denote the elastic strain and the Lagrange multiplier at the solution.

We now formulate on the algorithmic scheme for problem (178) (see Table 6), as reported in [10]. Since E_{σ} is convex, the algorithm is unconditionally convergent, regardless of the initial starting point $(\boldsymbol{\varepsilon}^{e,trial}_{n+1}, \boldsymbol{\xi}^{trial}_{n+1})$ [10].

A similar interpretation holds in stress-space [10]. For an associative flow rule, $\boldsymbol{\sigma}_{n+1}$ is the closest-point projection in the energy norm of the trial elastic stress $\boldsymbol{\sigma}^{trial}$ onto the yield surface, i.e., $\boldsymbol{\sigma}_{n+1}$ is solution of the following problem:

$$\min_{\boldsymbol{\sigma}\in E_{\sigma}} \frac{1}{2}\left\|\boldsymbol{\sigma}^{trial} - \boldsymbol{\sigma}\right\|^2_{\mathbb{C}^{-1}} \tag{182}$$

where $\|\cdot\|: = \sqrt{\cdot:\mathbb{C}^{-1}\cdot}$. Such a geometric interpretation follows by noting that the associated Lagrangian is expressed as:

$$\mathcal{L} = \frac{1}{2}\left\|\boldsymbol{\sigma}^{trial} - \boldsymbol{\sigma}\right\|^2_{\mathbb{C}^{-1}} + \Delta\delta f(\boldsymbol{\sigma}) \tag{183}$$

and the corresponding KT optimality conditions are given by:

$$\begin{cases}-\boldsymbol{\sigma}^{trial} + \boldsymbol{\sigma}_{n+1} + \Delta\gamma\left.\dfrac{\partial f}{\partial\boldsymbol{\sigma}_{n+1}}\right|_{n+1} = \mathbf{0}\\ \Delta\gamma \ge 0,\; f\left(\boldsymbol{\sigma}_{n+1}\right) \le 0,\; \Delta\gamma f\left(\boldsymbol{\sigma}_{n+1}\right) = 0\end{cases} \tag{184}$$

Here, $\boldsymbol{\sigma}$ and $\Delta\delta$ are the generic stress and Lagrange multiplier, respectively; $\boldsymbol{\sigma}_{n+1}$ and $\Delta\gamma$ denote the stress and the Lagrange multiplier at the solution, respectively.

The algorithmic scheme for problem (181) is similar to that presented in Table 6.

5.1.3 Cutting-Plane Algorithm

We now recall the *cutting-plane algorithm* [54, 142], since it avoids the computation of the gradients of the flow rules, which are required by the closest-point iterative procedure.

The algorithm is based on a steepest descent strategy which involves the following steps [10]:

1. Assume plastic loading $\Rightarrow f_{n+1}^{trial} > 0$ and $\Delta\gamma > 0$. Then, integrate the rate constitutive equations in terms of stress and stress-like variables using a forward-Euler scheme.
2. Linearize $f(\boldsymbol{\sigma}(\Delta\gamma), \boldsymbol{\xi}(\Delta\gamma)) = 0$ and solve for $\Delta\gamma$.
3. Update $\Delta\gamma$ and the other variables and check for the satisfaction of the consistency condition $f(\boldsymbol{\sigma}(\Delta\gamma), \boldsymbol{\xi}(\Delta\gamma)) = 0$. Return to step 1 if the constraint is violated.

As it can be observed, the procedure is explicit, since it involves only functional evaluations, and its convergence is obtained at a quadratic rate [10]. This makes the algorithm very attractive for complex models or explicit simulations. Normality is in fact enforced at the initial iterate and the incremental stress-strain relation is not suitable to the derivation of the consistent tangent modulus, needed in case of implicit analyses [9]. Moreover, such scheme has shown poorer accuracy properties when compared to the closest-point projection approximation [6].

5.2 Complementary Problem Function-Based Algorithms

The replacement of the KT conditions by equivalent complementary functions, as discussed in Sect. 2.2.10, allows to rewrite system (167), as follows[7]

$$\begin{cases} \boldsymbol{\epsilon}_{n+1}^{p} = \boldsymbol{\epsilon}_{n}^{p} + \Delta\gamma \mathbf{n}(\boldsymbol{\sigma}_{n+1}, \boldsymbol{\chi}_{n+1}) \\ \boldsymbol{\xi}_{n+1} = \boldsymbol{\xi}_{n} + \Delta\gamma \mathbf{h}(\boldsymbol{\sigma}_{n+1}, \boldsymbol{\chi}_{n+1}) \\ \Phi_{\delta}(f_{n+1}, \Delta\gamma) = 0 \end{cases} \tag{185}$$

where Φ_{δ} is the discrete smoothed complementarity function (see definition (88)).

In case of the FB smoothed function (87), Eq. $(184)_3$ takes the form:

$$\sqrt{f_{n+1}^2 + \Delta\gamma^2 + 2\delta} + f_{n+1} - \Delta\gamma = 0 \tag{186}$$

In case of the NN smoothed funtion (100), it becomes:

$$-f_{n+1} - \delta \ln\left[1 + \exp^{-\frac{\Delta\gamma + f_{n+1}}{\delta}}\right] = 0 \tag{187}$$

In case of the CHKS smoothing function (101), we have:

Table 7 Mathematical program definition [189, 190]

Let $\mathbf{x} = (x_1, ..., x_N) \in \Re^N$. A mathematical program consists in finding the values $\overline{\mathbf{x}} = (\overline{x}_1, ..., \overline{x}_N)$ of the variables $\mathbf{x}$, minimizing the objective function $z : \Re^N \rightarrow \Re$:

$$z = z(\mathbf{x}) \tag{189}$$

and satisfying:

- M_I inequality constraints $c_I : \Re^N \rightarrow \Re^{M_I}$

$$c_I \leq 0 \tag{190}$$

- M_E equality constraints $c_E : \Re^N \rightarrow \Re^{M_E}$

$$c_E = 0 \tag{191}$$

- box constraints

$$\mathbf{L} \leq \mathbf{x} \leq \mathbf{U} \tag{192}$$

where $\mathbf{L}, \mathbf{U} \in \Re^N$ such that $-\infty \leq L_i \leq U_i \leq +\infty$, $i = 1, ..., N$.

Functions z, c_I, and c_E are real functions of the N variables, but they are not necessarily differentiable nor continuous.

$$\frac{\Delta\gamma - f_{n+1}}{2} - \frac{\sqrt{\left(\Delta\gamma + f_{n+1}\right)^2 + 4\delta^2}}{2} = 0 \tag{188}$$

The procedure is no more based on a two-step algorithm and system of equations (167) can be solved by using classical numerical methods, e.g., a Newton–Raphson scheme. The procedure thus allows to avoid an active set search, which may become costly when dealing with many coupled evolution equations and constraints on internal variables. Numerical accuracy depends on the value of the regularization parameter δ, as discussed in Sect. 4. Possible numerical difficulties, especially for complex model problems, may be associated to the presence of δ and to a proper choice of the Newton–Raphson initial guess to guarantee a fast and correct convergence. To overcome potential difficulties, it is possible to apply a line-search strategy.

The applications of these algorithms to elastoplasticity are, however, limited. The effective and efficient procedure based on the FB smoothing function has been introduced in the context of crystal plasticity in in [137, 138] and applied to solve several engineering problems, e.g., [183, 184]. The NN smoothing function-based procedure has been applied to finite strain plasticity with elastic isotropy and arbitrary flow rules in [34], while the CHKS smoothing function has been used in several fields ranging from reactor networks and chemical processes to tray optimization [185–187].

[7] A fully implicit (backward-Euler) integration scheme is used; however, other integration rules can be adopted (see Sect. 4).

Table 8 Some mathematical program types [189]

The general mathematical program defined in Table 7 is:

- *Unconstrained* if:

  there are no inequality, equality, and box constraints

  otherwise it is *constrained*.
- *Quadratic* if:

  $\begin{cases} z \text{ quadratic function} \\ c_I,\ c_E \text{ linear functions} \end{cases}$
- *Convex* if:

  $\begin{cases} z \text{ convex function} \\ c_I \text{ concave functions} \\ c_E \text{ linear functions} \end{cases}$
- *Conic* if:

  $\begin{cases} z = < \mathbf{c}, \mathbf{x} > \\ \text{subject to constraint } \mathbf{A}\mathbf{x} = \mathbf{b} \\ \mathbf{x} \in K \subset \Re^N \text{ closed convex cone} \end{cases}$

  where $\mathbf{c} \in \Re^N$, $\mathbf{A} \in \Re^{M_E \times N}$, $\mathbf{b} \in \Re^{M_E}$, and $< \bullet, \bullet >$ represents the general scalar/inner product.
- *Linear* if:

  $\{z,\ c_I,\ c_E$ linear functions
- *Nonlinear* if:

  $\{z$ and/or c_I and/or c_E nonlinear functions
- *Program with equilibrium constraints* if:

  $\begin{cases} z : \Re^{N+P} \to \Re :\ z = z(\mathbf{x}, \mathbf{y}) \\ \text{subject to } G(\mathbf{x}, \mathbf{y}) \leq 0 \\ \mathbf{y} \in S \end{cases}$

  with $\mathbf{x} \in \Re^N$, $\mathbf{y} \in \Re^P$, $G : \Re^{N+P} \to \Re^{M_E + M_I}$, and S solution set of the equilibrium constraints depending on $\mathbf{x}$. Equilibrium constraints include variational inequalities or complementarities.

5.3 Mathematical Programming

A different approach consists in reducing the global IBVP (see Table 1) or the local IVP (see Table 2) to a *mathematical programming* (MP) problem that can be solved using optimization methods [180, 188].

MP is part of the theory of optimization [180, 188] and involves the minimization (or maximization) of a function of a finite number of real variables that can be subject to a finite number of constraints [189, 190]. The literature on MP theory and methods is very vast and the reader is referred to [188, 191, 192] for details. Table 7 reports the general definition of *mathematical program* that can be classified according to the nature and properties of the objective and constraint functions or number of variables. Some examples are reported in Table 8.

From the numerical point of view, the solution of MP problems highlighted important challenges between the eighties and nineties, since the simplex method was the only reliable and available algorithm. This algorithm is relatively robust, but it is characterized by a significant increase in computational effort as the problem size increases [193]. Later, a number of new methods of optimization have been proposed [194, 195] and MP started to be used in several fields, e.g., economics and finance. Several authors focused on MP in computational plasticity, e.g., [189, 196–200]. The use of MP for the state-update has several attractive features, especially when dealing with nonsmooth energy and dissipation potentials or variational inequalities. Compared to return mapping algorithms, the MP approach does not identify artificially the set of active constraints. Despite these advantages, the application of MP has been mostly limited to problems of plastic limit analysis [201] and the efficiency of MP algorithms, if compared to elastic predictor/plastic corrector schemes, has not been assessed [9]. In the following, we will review and propose some MP algorithms for the elastoplasticity problem.

5.3.1 Quadratic Programming

The approach based on *quadratic programming* (QP) was initiated by Maier [202–204] and Capurso and Maier [205], who employed a piecewise linear approximation of the yield surface to reduce the incremental problem to a *convex* QP (see Table 8). Due to the approximation, the application was limited to few examples on truss or frame structures [206].

Martin and coworkers [207–211] extended the contributions by Maier and coworkers [197, 212] by expressing the evolution equations in terms of the dissipation function and by exploiting the properties of convexity and positive homogeneity of this function to introduce a discretized version of the problem, with the aim of solving a succession of incremental problems. Martin et al. [210] discussed two solution strategies: the first based on a piecewise linear approximation leading to a QP problem [212], while the second employing a Newton–Raphson solution strategy [197]. The formulations and algorithms presented by Martin and coworkers [207–211] provide a viewpoint, dual to that proposed by Simo and Taylor [100]. The advantage is that QP can always be solved (or shown to be infeasible) in a finite amount of computation, however the effort required to find a solution depends on the properties of the objective function and on the number of inequality constraints [188].

The *sequential quadratic programming* (SQP) approach [188] is an effective method for nonlinear programming (see Table 8) and it is appropriate for small or large problems. We group this method in the present

section, since the basic idea is to model the mathematical problem of elastoplasticity in Table 7 by a QP subproblem at each iterate and to define the search direction to be the solution of this subproblem. Wieners [213, 214] introduced a SQP method for the case of perfect plasticity and plasticity with hardening. The algorithm is derived by a linearization of the flow rule which then leads to a sequence of linear variational subproblems with linear inequality constraints. Each subproblem was shown to be equivalent to a quadratic minimization problem and thus the method is equivalent to the SQP method. In case of hardening, Wieners proved global convergence for the semi-smooth Newton method used to solve the derived quadratic minimization problem. Wieners [213] reported the advantages in using SQP methods: the large flexibility allows to enhance and stabilize the method to general (and even nonconvex) plasticity models (e.g., multi-yield plasticity or finite plasticity), where the realization of the projection method is not straightforward. Recently, Bilotta et al. [215] proposed a novel method based on SQP with equality constraints. The idea was to improve the efficiency and the robustness of the solution method by maintaining all the variables of the problem at the same level and by performing a consistent linearization of all the equations, allowing the iterations to evolve towards the solution. The algorithm was shown to possess good accuracy, robustness, and convergence.

5.3.2 *Convex Programming*

As discussed in Sect. (2.2.11), the principle of maximum plastic dissipation provides an interpretation of the plasticity flow theory as optimality conditions of a convex minimization problem and allows to apply algorithms for convex MP.

Among the others, interior-point methods have proved to be successful either for linear and nonlinear programming [188]. The basic idea is to solve the optimality conditions associated to the minimization problem with a suitably penalized mathematical program.

Krabbenhoft et al. [193] treated the problem of infinitesimal rate-independent elastoplasticity using convex programming algorithms. Following the interior-point methodology, Krabbenhoft et al. rewrote the principle of maximum plastic dissipation (112), as follows:

$$\max_{(\boldsymbol{\sigma},\boldsymbol{\chi},s)} \boldsymbol{\sigma}:\dot{\boldsymbol{\varepsilon}}^p + \boldsymbol{\chi} * \dot{\boldsymbol{\xi}} + \mu_b \log s \tag{193}$$

subject to:

$$f(\boldsymbol{\sigma},\boldsymbol{\chi}) + s = 0 \tag{194}$$

where $s > 0$ is the slack variable and $\mu_b \log s$ is the so-called logarithmic barrier function, μ_b being an arbitrarily small positive constant. Recall that if the yield function is convex, this is a convex program.

The associated Lagrangian is:

$$\mathcal{L} = \boldsymbol{\sigma}:\dot{\boldsymbol{\varepsilon}}^p + \boldsymbol{\chi} * \dot{\boldsymbol{\xi}} + \mu_b \log s - \dot{\gamma}\left[f(\boldsymbol{\sigma},\boldsymbol{\chi}) + s\right] \tag{195}$$

where $\dot{\gamma}$ is a Lagrange multiplier. The first-order necessary and sufficient KKT optimality conditions associated with problem (188) follow from the Lagrangian (194), as:

$$\begin{cases} \partial_{\boldsymbol{\sigma}}\mathcal{L} = \dot{\boldsymbol{\varepsilon}}^p - \dot{\gamma}\partial_{\boldsymbol{\sigma}} f(\boldsymbol{\sigma},\boldsymbol{\chi}) = \mathbf{0} \\ \partial_{\boldsymbol{\chi}}\mathcal{L} = \dot{\boldsymbol{\xi}} - \dot{\gamma}\partial_{\boldsymbol{\chi}} f(\boldsymbol{\sigma},\boldsymbol{\chi}) = \mathbf{0} \\ \partial_{\dot{\gamma}}\mathcal{L} = -f(\boldsymbol{\sigma},\boldsymbol{\chi}) - s = 0 \\ \partial_s\mathcal{L} = \mu_b s^{-1} - \dot{\gamma} = 0 \quad \Rightarrow \quad s\dot{\gamma} = \mu_b \end{cases} \tag{196}$$

which correspond, respectively, to the associated flow rules, yield condition, and plastic consistency condition, $\dot{\gamma}$ being the plastic multiplier. It should be noted that since $s > 0$ and $\mu_b > 0$, we have $\dot{\gamma} > 0$. These conditions, together with the two last optimality conditions, define the loading/unloading conditions (57). Note, however, that only strict inequality is satisfied for the first two equations of the KT conditions (57), since $\mu_b > 0$, whereas the last condition is fulfilled to within some arbitrarily small positive constant proportional to μ_b [193].

After integrating system (195) by using a backward-Euler scheme, Krabbenhoft et al. [193] solved the (global) primal problem by using a Newton's method with a reduced step length to ensure that all points remained in the interior of the feasible solution space. As the solution converges, the barrier parameter μ_b is reduced according to a certain law. The main difficulty in applying a Newton's method to sets of optimality conditions is that usually little knowledge about the optimal solution is available [193]; thus, choosing an initial point within the convergence radius of Newton's method is generally difficult. Therefore, an important point is a rule for how the barrier parameter should be decreased during the iterations: if it is reduced too much, the iterations will diverge; if it is not reduced enough, the iterations may be too high. Krabbenhoft et al. [193] observed that the number of iterations is about 20-50 in each load step, independent of the size of the problem, if the reduction rule for μ_b is well chosen. In elastoplastic computations, however, the authors showed that a good estimate of the optimal solution is usually available (usually the last converged solution) and the number of iterations is about 10.

The resulting algorithm shares several features with that by Simo and Taylor [100]. For example, a quantity which is similar to the consistent tangent modulus derived in [100] plays an important role in the algorithm. Regarding the efficiency, the method in [193] is competitive with the Simo and Taylor method: the cost of each iteration and the iteration counts are comparable. Moreover, a quadratic rate of convergence is attained as the

solution is approached. The algorithmic robustness also appears excellent and can be further enhanced by a line-search strategy. Finally, the algorithm can be extended to multi-surface plasticity without any difficulty or additional computational effort and can be implemented in other FE formulations than those based on standard displacement elements [193]. Recall however that, since Ψ^p is a function of χ only, there is a natural limitation to the type of hardening laws that can be considered within this framework, see [193] for details.

Lotfian and Sivaselvan [216] focused on the dual problem, associated to the primal problem treated by Krabbenhoft et al. [193]. The authors considered material behaviors described by convex energy and dissipation functions and cast the incremental state update into a convex minimization problem in terms of stresses. They proposed a projected Newton method to solve the dual of this problem which does not require a return-mapping scheme. Moreover, the local quadratic model of the objective function, used to determine a search direction, is based on a reduced Hessian and the step length in each iteration is determined by searching along a piecewise linear path (rather than along a straight line) obtained by projecting the search direction on the feasible region. The methodology can be extended to finite deformation or non-convex cases, because they can be approached using a succession of convex subproblems, as well as to multi-surface plasticity.

5.3.3 Conic Programming

As discussed in Sect. 2.2.6, plasticity with nonsmooth potentials is generally treated with the methodology by Koiter (see [10, 217] and references therein). However, singularities as in the Drucker–Prager cone, where only one surface can be identified, need special attention [217]. In such cases, the theory is usually formulated in a more rigorous way using the concept of subgradient [39].

In the last years, research has been dedicated to *conic programming* (CP), where the problem can be written as a linear program with one or more cone constraints (see Table 8). In CP, the definition of a cone is quite broad and often non-conic constraints can be reformulated. Robust algorithms, also applicable to large-scale problems, have been developed for a certain number of cones, e.g., [218]; the most commons are the second-order and positive semidefinite cones.

In elastoplasticity, the methodology exploited in CP is similar to the one introduced by Moreau for plasticity and its use is advantageous since the existence of singularities does not involve any problem [217]. Despite this, its application to elastoplastic problems has been limited to few cases. We recall the work by Makrodimopoulos and Martin [219], employing second-order cone programming (SOCP) for the upper bound limit analysis of cohesive-frictional continua. Krabbenhoft et al. [217] presented standard forms for CP (second-order and semidefinite programs) of both limit and incremental elastoplastic analysis and discussed the types of yield criteria that can be treated by CP. The results presented for the Mohr–Coulomb criterion appears the most satisfactory and various mixed FE are considered. The authors concluded stating that the performance of suitable CP algorithms still has to be evaluated. Three-dimensional Mohr–Coulomb limit analysis was solved by semidefinite programming [220]. The realization of the cone representation of some plasticity failure criteria have been proposed in [221]. Applications also to smooth problems have been presented in [222, 223].

Recently, attention has been paid to *second-order cone complementarity problems* (SOCCP), which is a class of MP problems that can be regarded as the extension of linear complementarity problems by allowing for nonlinear inequality constraints in the form of a convex cone [224]. Various methods have been proposed for solving the SOCCPs, e.g., interior-point methods [190], non-interior smoothing Newton methods [225], smoothing-regularization method [226], merit function methods [227], and semismooth Newton methods [228].

The use of SOCCP is advantageous for non-associative plasticity, where the principle of maximum plastic dissipation is not applicable and the problem can be formulated in terms of complementary problems or variational inequalities. Zhang et al. employed SOCCPs to solve the von Mises model with combined linear kinematic and isotropic hardening and the Drucker–Prager perfect model. A semi-smooth Newton algorithm is used to solve the obtained SOCCPs, integrated with a backward-Euler scheme. The main idea of the semi-smooth Newton method for SOCCPs is to replace the second-order cone complementarity condition by a complementarity function (see Sect. 2.2.10) and to solve the obtained nonlinear equations by semi-smooth Newton algorithm [228]. This method has been also used to solve the nonlinear complementary formulation of elastoplasticity in [229] and the SOCCPs of three-dimensional frictional contact problems in [230]. In [231] the von Mises yield criterion with linear strain hardening is formulated as a SOCCP condition. The minimization problems of the potential and complementary energy are formulated as a primal-dual pair of SOCP problems and solved by using a polynomial-time primal-dual interior-point method. To enhance the numerical performance in tracing the equilibrium path, the authors proposed a warm-start strategy for a primal-dual interior-point method for SOCP. On the one hand, an advantage is that the number of iterations required for finding an equilibrium solution does not depend on the size of the loading step, differently from many existing

methods which often spend more iterations if a larger loading step is chosen [100]. On the other hand, since the elastic and plastic strain tensors at each Gauss point are considered as independent variables, a potential disadvantage in terms of computational time and storage may arise for large-scale problems. Linear complementarity problems have been also used to solve elastoplastic problems [232]; however, a drawback is that an explicit linearization procedure is required to make the approach applicable for problems with nonlinear yield functions [233].

5.3.4 Least-Squares Approach

An alternative approach in the MP field is to consider a *bound-constrained least-squares* problem, defined as follows:

$$\min_{\mathbf{L}\le\mathbf{x}\le\mathbf{U}} \left\{ \frac{1}{2}||r(\mathbf{x})||^2 \right\} \tag{197}$$

where $r{:}\Re^N \rightarrow \Re^{M_E+M_I}$ is a continuously differentiable function.

The advantages in the above formulation are twofold: (i) problem (196) is unconstrained, except for the bounds on $\mathbf{x}$; (ii) the evaluation of the gradient and Hessian of $1/2||r(\mathbf{x})||^2$ is easier [188].

Applying the above definition to the elastoplastic IVP of Table 3, we obtain:

$$\min_{\substack{(\boldsymbol{\varepsilon}^p,\,\xi,\,\Delta\gamma)\\ \Delta\gamma\,\ge\,0}} \left\{ \frac{1}{2}||r(\boldsymbol{\varepsilon}^p,\xi,\Delta\gamma)||^2 \right\} \tag{198}$$

with:

$$r = \begin{Bmatrix} \boldsymbol{\varepsilon}^p_{n+1} - \boldsymbol{\varepsilon}^p_n - \Delta\gamma\mathbf{n}(\boldsymbol{\sigma}_{n+1},\chi_{n+1}) \\ \xi_{n+1} - \xi_n - \Delta\gamma\mathbf{h}(\boldsymbol{\sigma}_{n+1},\chi_{n+1}) \\ \Delta\gamma f(\boldsymbol{\sigma}_{n+1},\chi_{n+1}) \\ \frac{1}{2}\left\langle 0, f(\boldsymbol{\sigma}_{n+1},\chi_{n+1})\right\rangle^2 \end{Bmatrix} \tag{199}$$

To obtain problem (196), the inequalities in the general form $t(\mathbf{x}) \le 0$ have been replaced by equalities, by using the continuously differentiable function $1/2 < 0, t >^2$. A fully implicit (backward-Euler) scheme is adopted in problem (197), however other integration schemes may be investigated.

Classical algorithms for solving least-square problems fit into the line-search and trust-region frameworks [188]. These methods are based on Newton and quasi-Newton approaches, with modifications that exploit the specific structure of the function r. A trust-region Gauss-Newton method for small and zero residual bound-constrained nonlinear least-squares problems (see Eq. (196)) has been proposed in [234–236]. The algorithm solves overdeterminated and undeterminated problems, generates feasible iterates, and relies on matrix factorization. Moreover, it is globally and fast locally convergent under standard assumptions. A discussion of the accuracy, computational cost, and robustness is also provided in [234]. The algorithm presented in [234] offers the additional advantage of an internal reformulation of systems of nonlinear equalities and inequalities as problem (196), preserving the smoothness required by the trust-region algorithm. The Matlab code, called TRESNEI, is available on the web [237] and uses a finite difference approximation of the Jacobian of r, if not provided.

5.4 Incremental Energy Minimization

We now focus on the class of variational methods known as *variational constitutive updates*, which relies on an *incremental energy minimization* approach.

Using standard results in convex analysis [39], the incremental boundary-value problem, together with the incremental elastoplastic problem (see Table 2), is formally equivalent to the following minimization problem:

$$\inf_{(\mathbf{u},\boldsymbol{\varepsilon}^p,\xi)} \{e(\mathbf{u},\boldsymbol{\varepsilon}^p,\xi)\} \tag{200}$$

where:

$$e = \int_\Omega (\Psi + D^p)\, dV - \int_\Omega \mathbf{b}\cdot\mathbf{u}\, dV - \int_{\Gamma^N} \bar{\mathbf{t}}\cdot\mathbf{u}\, d\Gamma \tag{201}$$

$\mathbf{u}$ being subject to boundary conditions (123) $_1$.

Several algorithms have been proposed to solve problem (199) at a global or global/local level, e.g., [238–249]. If we apply spatial discretization, e.g., in an FE environment, problem (199) may be split into two subproblems: (i) the first one corresponds to the minimization with respect to $\mathbf{u}$ and may be solved by employing the FE software (global level); (ii) the second one corresponds to problem (199) with fixed $\mathbf{u}$, i.e., minimization only with respect to internal variables (local level), and represents the constitutive relations implicitly included in problem (199). This is equivalent to the following problem:

$$\inf_{\mathbf{u}} \left\{ \inf_{\boldsymbol{\varepsilon}^p,\xi} \{e(\mathbf{u},\boldsymbol{\varepsilon}^p,\xi)\} \right\} \tag{202}$$

Both problems must be solved consecutively and the resulting solution is equivalent to the solution of problem (199) for infinitesimally refined time discretization. Therefore, the second subproblem leads to a reduced incremental energy minimization problem in the form:

$$\inf_{\boldsymbol{\varepsilon}^p,\xi} \{e(\boldsymbol{\varepsilon}(\mathbf{u}),\boldsymbol{\varepsilon}^p,\xi)\} \tag{203}$$

We now apply a backward-Euler integration scheme to problem (202) and we assume that plastic strain and strain-like internal variables vary linearly in each time step Δt_n, such that:

$$\Psi = \Psi\left(\boldsymbol{\varepsilon}_{n+1} - \boldsymbol{\varepsilon}_n^p - \Delta\boldsymbol{\varepsilon}_n^p, \boldsymbol{\xi}_n + \Delta\boldsymbol{\xi}_n\right) \tag{204}$$

and

$$D^p = D^p\left(\Delta\boldsymbol{\varepsilon}_n^p, \Delta\boldsymbol{\xi}_n\right) \tag{205}$$

This means that the evolution of internal variables in a finite time step incrementally minimizes a suitable convex functional, given by the sum of the internal energy and dissipation function. The incremental form of the Biot's equations (118) represents in fact the Euler-Lagrange first-order conditions associated to this incremental minimization problem and are expressed as:

$$\begin{cases} \partial_{\Delta\boldsymbol{\varepsilon}_n^p}\Psi\left(\boldsymbol{\varepsilon}_{n+1} - \boldsymbol{\varepsilon}_n^p - \Delta\boldsymbol{\varepsilon}_n^p, \boldsymbol{\xi}_n + \Delta\boldsymbol{\xi}_n\right) + \partial_{\Delta\boldsymbol{\varepsilon}_n^p} D^p\left(\Delta\boldsymbol{\varepsilon}_n^p, \Delta\boldsymbol{\xi}_n\right) \ni \mathbf{0} \\ \partial_{\Delta\boldsymbol{\xi}_n}\Psi\left(\boldsymbol{\varepsilon}_{n+1} - \boldsymbol{\varepsilon}_n^p - \Delta\boldsymbol{\varepsilon}_n^p, \boldsymbol{\xi}_n + \Delta\boldsymbol{\xi}_n\right) + \partial_{\Delta\boldsymbol{\xi}_n} D^p\left(\Delta\boldsymbol{\varepsilon}_n^p, \Delta\boldsymbol{\xi}_n\right) \ni \mathbf{0} \end{cases} \tag{206}$$

An advantage of this method is that it provides a criterion of choice if non-unique solutions exist [248].

Problem (202) takes the form of an unconstrained program (see Sect. 5.3) and standard optimization algorithms can be applied [188]. As an example, derivative-based optimization methods (e.g., gradient descent method) can be applied, but they can be less efficient in the presence of several nonsmooth cases, although generally faster. An alternative is the derivative-free optimization algorithm by Nelder and Mead [250] which is suitable in case of nonsmooth functions.

Variational constitutive updates are relatively well developed for associative evolution equations [251], while the general non-associative case still need investigations [252]. The paper by Nodargi et al. [239] focuses on the incremental energy formulation for elastoplastic hardening materials characterized by isotropic deviatoric yield function and associative flow laws. A two-step algorithm is proposed to perform the state update: (i) an elastic prediction of the updated material state is first carried out; (ii) if it is not plastically admissible, a Newton–Raphson scheme is adopted to solve the constitutive variational problem (205). The authors adopted the Haigh-Westergaard representation and reduced the problem to a nonlinear scalar equation. Their numerical approach appears to be complementary to the classical return map strategy, because no convergence difficulties arise when the stress is close to points of the yield surface with high curvature. The state-update algorithm proposed in [240] is used in case of associative hardening plasticity (with arbitrary isotropic and linear kinematic hardening) and nonlinear elastic constitutive law. The algorithm does not require matrix inversion and exhibits global convergence even for yield functions with high-curvature points or not defined on the whole stress space.

Remark 7 (Example) As an example, we specify problem (202) for the case of the von Mises elasto-perfectly plastic model, as:

$$\inf_{\boldsymbol{\varepsilon}^p}\left\{e\left(\boldsymbol{\varepsilon}_{n+1}(\mathbf{u}_{n+1}), \boldsymbol{\varepsilon}^p\right)\right\} \tag{207}$$

with:

$$e = \frac{1}{2}K\theta_{n+1}^2 + \mu||\mathbf{e}_{n+1} - \boldsymbol{\varepsilon}^p||^2 + \sqrt{\frac{2}{3}}\sigma_{y,0}||\boldsymbol{\varepsilon}^p - \boldsymbol{\varepsilon}_n^p|| \tag{208}$$

After applying a backward-Euler integration scheme to problem (206) and assuming that plastic strain and strain-like internal variables vary linearly in each time step Δt_n, we obtain the corresponding incremental form of the Biot's equations, as follows:

$$0 \in -2\mu(\mathbf{e}_{n+1} - \boldsymbol{\varepsilon}_n^p - \Delta\boldsymbol{\varepsilon}_n^p) + \sqrt{\frac{2}{3}}\sigma_{y,0}\partial||\Delta\boldsymbol{\varepsilon}_n^p|| \tag{209}$$

5.5 Consistent Tangent Matrix

In an implicit FE framework, the equilibrium equations are solved at the end of each increment and the so-called *tangent modulus* is needed if a Newton–Raphson scheme is applied. The use of the *continuum tangent modulus*, defined in Eq. (66), is however not consistent with the Newton–Raphson method, since it is based on instantaneous values of the rate constitutive equations before numerical integration [142]. Therefore, the so-called *consistent tangent matrix*, which depends on the local integration, has to be used to obtain a quadratic convergence rate. Specifically, its computation consists in differentiating the stress with respect to the strain, taking into account all the variables appearing in the update algorithm. Defining such variables with $\mathbf{q}$, we obtain:

$$\frac{d\boldsymbol{\sigma}(\mathbf{q}(\boldsymbol{\varepsilon}), \boldsymbol{\varepsilon})}{d\boldsymbol{\varepsilon}} = \frac{\partial\boldsymbol{\sigma}}{\partial\boldsymbol{\varepsilon}} + \frac{\partial\boldsymbol{\sigma}}{\partial\mathbf{q}}\frac{\partial\mathbf{q}}{\partial\boldsymbol{\varepsilon}} \tag{210}$$

where $\partial\mathbf{q}/\partial\boldsymbol{\varepsilon}$ is derived from:

$$\frac{d\mathbf{R}}{d\boldsymbol{\varepsilon}} = \frac{\partial\mathbf{R}}{\partial\boldsymbol{\varepsilon}} + \frac{\partial\mathbf{R}}{\partial\mathbf{q}}\frac{\partial\mathbf{q}}{\partial\boldsymbol{\varepsilon}} = \mathbf{0} \tag{211}$$

$\mathbf{R}$ being the residual vector of local discrete elastoplastic equations. The current availability of symbolic software notably simplifies the computation of the tangent matrix, especially for complex material models. Other solutions may consist in the approximated computation of the consistent tangent matrix using, for instance, finite differences.

The literature is very rich on this topic and a detailed discussion is out of the present scope. The reader is referred to the works previously discussed for the derivation and

Table 9 Model parameters adopted in the numerical simulations

Symbol	Description	Set 1	Set 2	Unit
E	Young's modulus	30000	21000	MPa
ν	Poisson's ratio	0.3	0.3	-
$\sigma_{y,0}$	Initial yield stress	3	24	MPa
H_{iso}	Isotropic hardening constant	0	100	MPa
H_{kin}	Kinematic hardening constant	0	1	MPa

computation of the consistent tangent matrix. Recall, however, that the origin of such a notion can be found in [253–255]. Nagtegaal [254] and Runesson and Booker [255] linearized the time discretized constitutive equations with and without linear isotropic hardening, respectively, to derive a proper Jacobian. Simo and Taylor [142] extended the study to nonlinear kinematic and isotropic hardening. In [256] a complex nonlinear kinematic hardening model is studied, while in [257] the Newton's method is combined with a secant approach to further improve the efficiency. A Newton–Schur alternative to the consistent tangent approach is proposed in [258]. An attempt to propose a general method to derive the plastic corrections and the consistent tangent modulus for a wide class of nonlinear hardening models is available in [259].

6 Numerical Simulations

This section presents a comparison between several solution schemes to study the accuracy, robustness, and efficiency granted by the numerical algorithms on standard tests and practical engineering problems.

To our purpose, from each classical and *less-classical* category reviewed in Sect. 5, we analyze the following solution schemes:

- RM: Return Map algorithm (see Sect. 5.1)
- FB: Fischer–Burmeister smoothing function-based algorithm (see Sect. 5.2)
- NN: Neural Networks smoothing function-based algorithm (see Sect. 5.2)
- LS: bound-constrained least-squares problem solved with the TRESNEI algorithm (see Sect. 5.3.4)
- NM: incremental energy minimization problem solved with the Nelder-Mead algorithm (see Sect. 5.4)

All the algorithms are tested on strain loading histories for a material point, implemented in the Matlab environment, for which optimization functions are available, included the TRESNEI code [237] and the built-in *fminsearch* function. The RM and FB algorithms are then tested on two

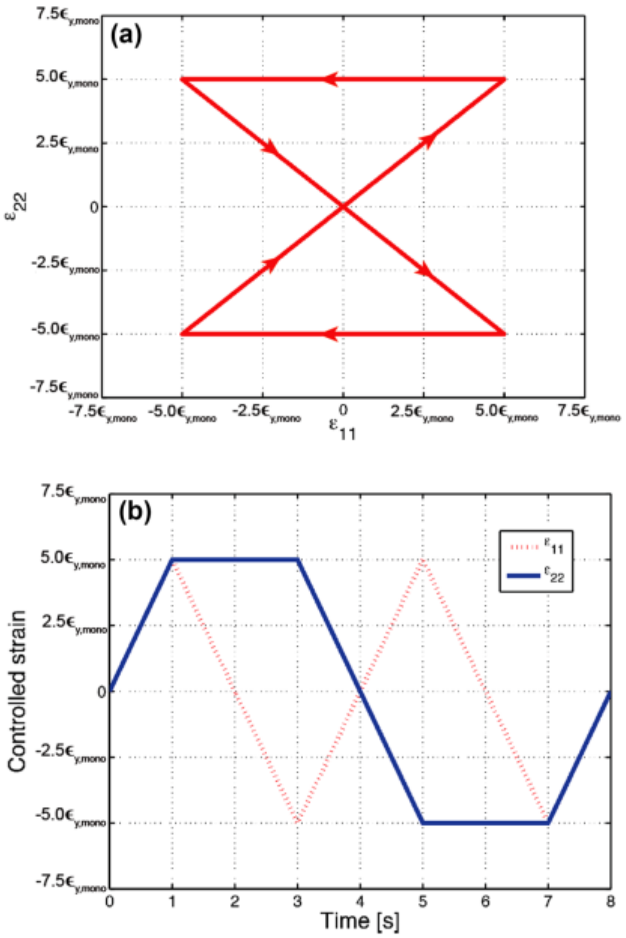

Fig. 6 **a** Butterfly-shaped loading history. **b** Loading histories varying in time in the range $\pm 5\epsilon_{y,mono}$, where $\epsilon_{y,mono} = \sqrt{3/2}\sigma_{y,0}/E$

FE boundary-value problems. The FE implementation is carried out using the symbolic code generation system AceGen/AceFEM [260], for which exact linearization and analytic derivation of the consistent tangent matrix are possible (refer to our discussion in Sect. 5.5).

We adopt the two set of material parameters listed in Table 9. Set 1 corresponds to the von Mises elasto-perfectly plastic model and it is used to perform the tests based on strain loading histories for a material point. Set 2 corresponds to the von Mises model with linear isotropic kinematic hardening and it is adopted for the FE simulations. The model is governed by the following system of equations in a time-continuous framework:

$$\begin{cases} \dot{\boldsymbol{\epsilon}}^p = \dot{\gamma}\dfrac{\partial f}{\partial \boldsymbol{\sigma}} \\ \dot{\boldsymbol{\alpha}} = H_{kin}\dot{\gamma}\dfrac{\partial f}{\partial \boldsymbol{\sigma}} \\ \dot{\gamma} \geq 0,\ f \leq 0,\ \dot{\gamma} f = 0 \end{cases} \tag{212}$$

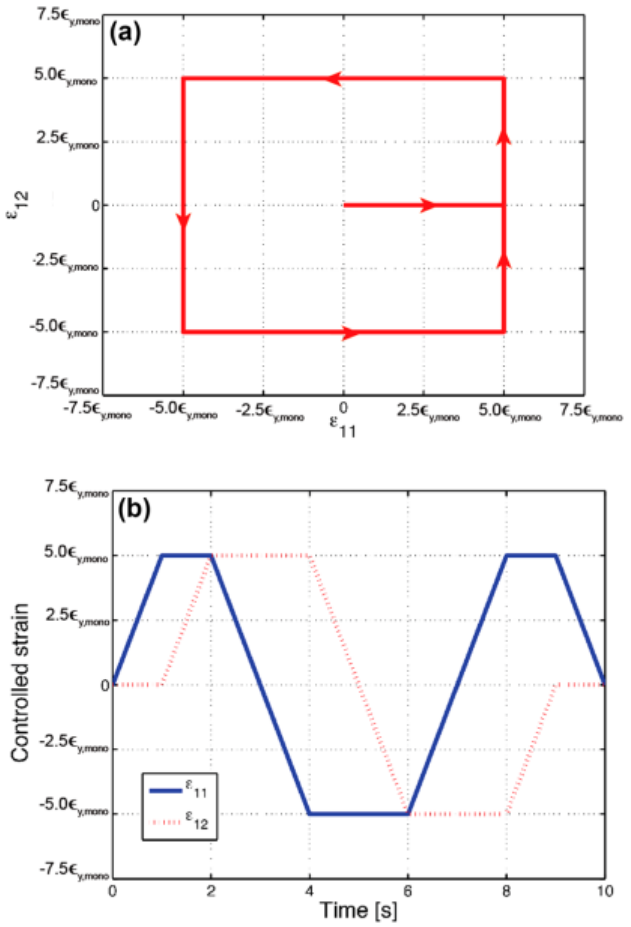

Fig. 7 **a** Square-shaped loading history. **b** Loading histories varying in time in the range $\pm 5\epsilon_{y,mono}$, where $\epsilon_{y,mono} = \sqrt{3/2}\sigma_{y,0}/E$

where the yield function f is defined as:

$$f = \|\mathbf{s} - \boldsymbol{\alpha}\| - \sigma_{y,0} - H_{iso}\bar{e}^p \tag{213}$$

Here, H_{kin}, $\sigma_{y,0}$ and H_{iso} are, respectively, a material constant accounting for kinematic hardening, the initial yield stress, and a material constant accounting for isotropic hardening. These equations are integrated in time using a fully implicit (backward-Euler) method.

6.1 Strain Loading Histories

We consider two nonproportional strain loading histories, obtained by assuming to control the six strain components, i.e., $\{\epsilon_{11}, \epsilon_{22}, \epsilon_{33}, \epsilon_{12}, \epsilon_{13}, \epsilon_{23}\}$. For each loading we vary two strain components, respectively $(\epsilon_{11}, \epsilon_{22})$ and $(\epsilon_{11}, \epsilon_{12})$, according to a chosen history, while the remaining are kept equal to zero. The loading histories consist, respectively, of a hourglass- and square-shaped input (see Figs. 6a and 7a), defined on the time interval $[0, T]$, with T equal to 8 and 10 s, respectively. The strain components vary in the range

Table 10 Butterfly-shaped loading history. Comparison between the algorithmic schemes in terms of total computational time

Algorithm	Time step	Computational time [s]
RM	0.1	0.60
	0.05	0.87
	0.025	1.48
FB	0.1	0.61
	0.05	1.12
	0.025	2.19
NN	0.1	0.61
	0.05	1.22
	0.025	2.50
NM	0.1	2.17
	0.05	4.20
	0.025	8.51
LS	0.1	0.77
	0.05	1.35
	0.025	2.48

$\pm 5\epsilon_{y,mono}$, where $\epsilon_{y,mono} = \sqrt{3/2}\sigma_{y,0}/E$. Figures 6(b) and 7(b) show the history input for each component in case of the hourglass- and square-shaped loading, respectively. The tests are performed using time step increments Δt of 0.1, 0.05, and 0.025 s.

All the results have been obtained by considering a regularized parameter $2\delta = 10^{-9}$ and $\delta = 0.003$ for the FB and NN algorithms, respectively.

To assess accuracy and robustness, we introduce the following stress relative error:

$$E_R^n = \frac{\left\|\boldsymbol{\sigma}_n^{num} - \boldsymbol{\sigma}_n^{anal}\right\|_2}{\sigma_{y,0}} \tag{214}$$

and total error:

$$E_T = \sum_{i=1}^{N} \Delta t \left\|\boldsymbol{\sigma}_n^{num} - \boldsymbol{\sigma}_n^{anal}\right\|_1 \tag{215}$$

where $\boldsymbol{\sigma}_n^{anal}$ and $\boldsymbol{\sigma}_n^{num}$ are, respectively, the 'analytic' and the 'numerical' stresses at time t_n. Lacking the analytical solution of the loading histories under investigation, we compute the 'exact' solution using the RM algorithm with a very fine time discretization, corresponding to $\Delta t = 0.0001$ s. Then, we compare the 'analytic' solutions to the 'numerical' ones, computed respectively with Δt of 0.1, 0.05, and 0.025 s. Figures 8 and 9 show the stress relative errors for the butterfly- and square-shaped history, respectively, while Figs. 10 and 11 present the stress total errors versus the number of steps per second for the butterfly- and square-shaped history, respectively. All the schemes are

Table 11 Square-shaped loading history. Comparison between the algorithmic schemes in terms of total computational time

Algorithm	Time step	Computational time [s]
RM	0.1	0.64
	0.05	1.18
	0.025	2.20
FB	0.1	0.74
	0.05	1.55
	0.025	3.29
NN	0.1	0.87
	0.05	1.64
	0.025	3.54
NM	0.1	2.57
	0.05	5.27
	0.025	10.86
LS	0.1	0.97
	0.05	1.87
	0.025	3.55

first-order accurate. The error plots show similar results for all the algorithms, except for the NN scheme, whose accuracy is strongly influenced by δ. Lower values for δ in the NN algorithm have been tested; however, they determine ill-conditioning of the system.

To assess computational efficiency, Tables 10 and 11 report the computational time for the butterfly- and square-shaped histories, respectively. As observed, the RM algorithm presents the lowest computational times, while the less performing algorithm is the NM algorithm. The FB and NN algorithms present values comparable to those of the RM scheme for low time steps (0.1 s), while, for increasing time steps, the FB scheme necessitates slightly lower computational times than the NN. The LS scheme presents an overall good performance, comparable to that of the NN algorithm.

6.2 Boundary-Value Problems

We first consider a three-dimensional square plate with a hole. The plate has an edge of 50 mm, a thickness of 10 mm, and a central circular hole of radius 10 mm. According to the symmetry of the problem, we model only one quarter of the plate by applying appropriate boundary conditions. The mesh is composed of 3, 080 8-node brick elements and 4, 002 nodes (see Fig. 12). Mesh refinement has been performed to choose the appropriate mesh.

The plate is subject to a displacement-control extension along the z-direction (see Fig. 12), consisting of loading up to a maximum displacement of 0.1 mm and unloading back

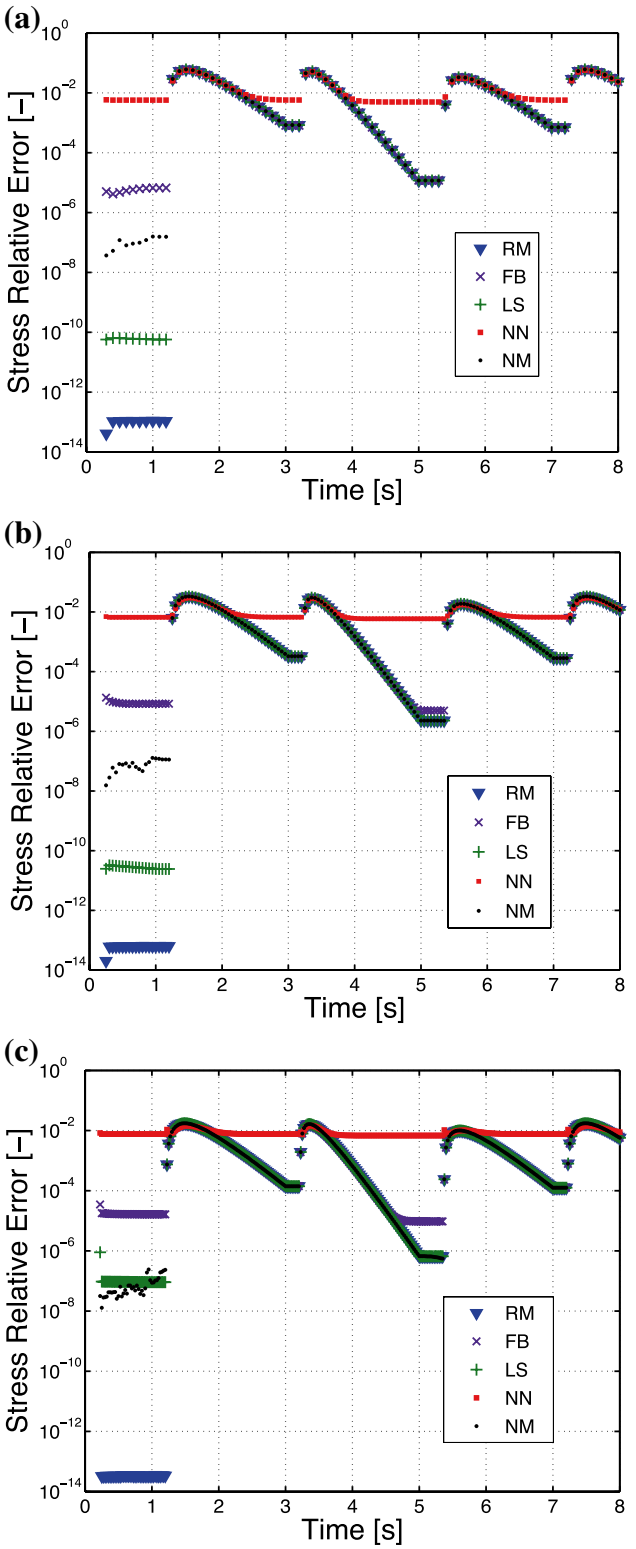

Fig. 8 Butterfly-shaped loading history. Stress relative error E_R^n for Δt of 0.1, 0.05 and 0.025 s for the algorithmic schemes

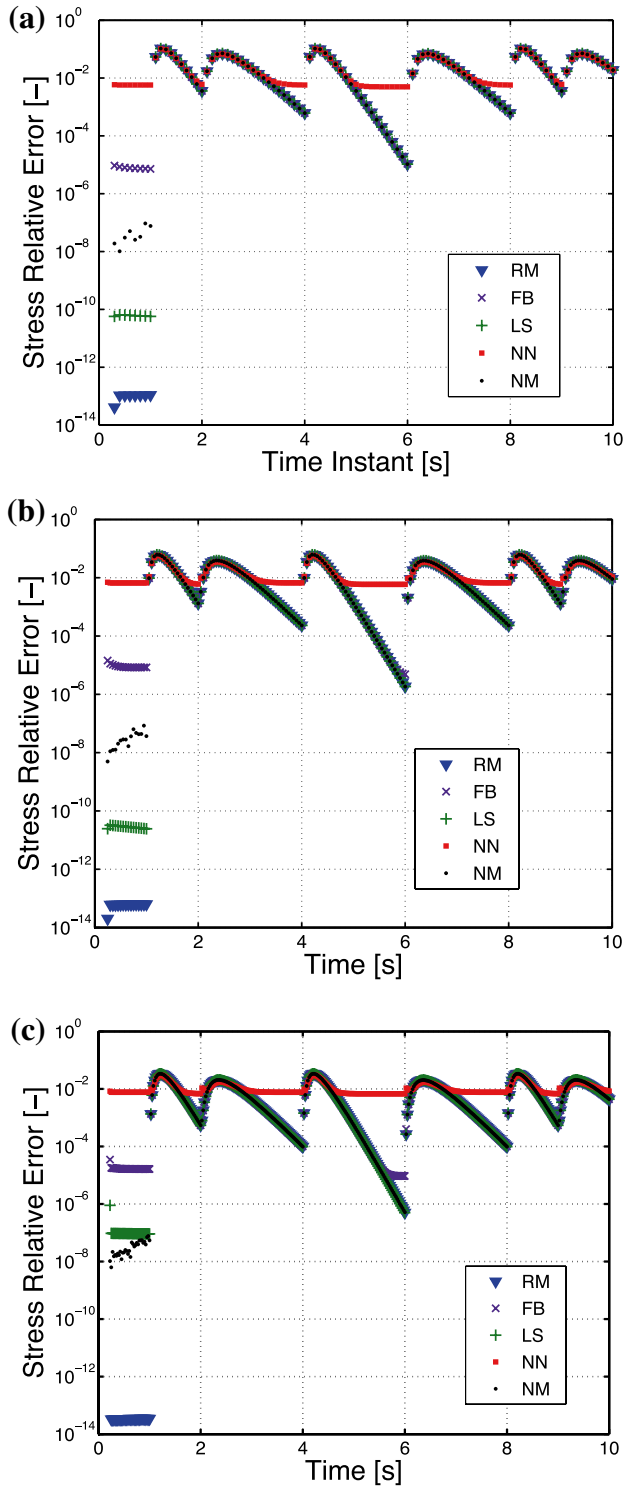

Fig. 9 Square-shaped loading history. Stress relative error E_R^n for Δt of 0.1, 0.05 and 0.025 s for the algorithmic schemes

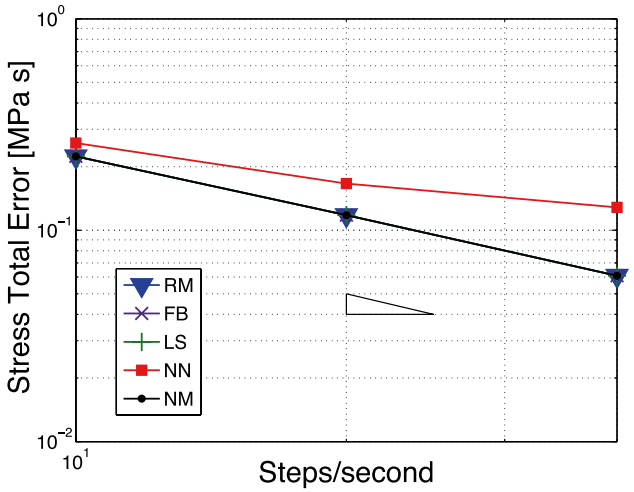

Fig. 10 Butterfly-shaped loading history. Stress total error E_T versus number of steps per second for the algorithmic schemes

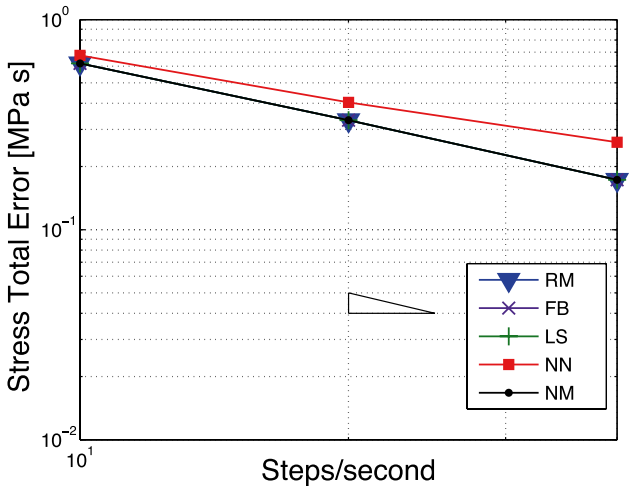

Fig. 11 Square-shaped loading history. Stress total error E_T versus number of steps per second for the algorithmic schemes

to zero. The total analysis time is 2 s. Tests are performed using time step increments Δt of 0.1 and 0.01 s, corresponding to 20 and 200 steps.

To compare the methods, we evaluate the following error on stresses and strains:

$$E^{\mathbf{v}} = \sqrt{\frac{\int_\Omega ||\mathbf{v}_n^{num} - \mathbf{v}_n^{anal}||^2}{\int_\Omega ||\mathbf{v}_n^{anal}||^2}} \tag{216}$$

The quantity $\mathbf{v}_n^{num}$ is the 'numerical' stress and strain tensor calculated adopting a prescribed time step Δt, while $\mathbf{v}_n^{anal}$ is the corresponding 'analytic' solution evaluated with the RM scheme using a time step $\Delta t = 0.0001$ s. In the following tests we use two different time steps, respectively of 0.1 and 0.01 s, and we evaluate the error at four different

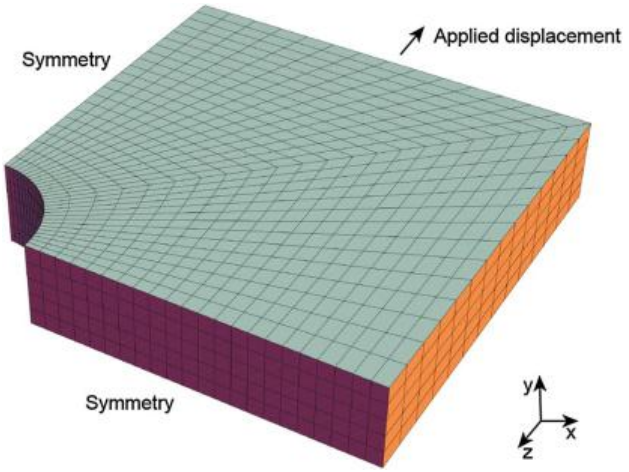

Fig. 12 Three-dimensional plate with hole. Adopted mesh and boundary conditions

Table 12 Three-dimensional plate with hole. Comparison between the RM and the FB algorithmic schemes in terms of average number of global Newton iterations and average computational time per time step

Algorithm	Number of steps	Average iterations/step	Average comp. time/step [s]
RM	20	5.55	1.83
	200	4.77	1.36
FB	20	5.55	2.13
	200	4.74	1.64

instants of the loading history, i.e., at 0.5, 1.0, 1.5, and 2.0 s. The results are summarized in Table 13.

To assess the computational efficiency of the RM and FB algorithms, Table 12 reports the average number of global Newton iterations and the average computational time per time step increment (Table 13).

We now consider a helical spring. The spring has 3.5 free coils, initial length of 24.59 mm, a wire diameter of 1.5 mm, a spring external and internal diameters of 13.3 and 10.3 mm, and a pitch size of 6.4 mm. Figure 13 shows the adopted mesh, consisting of 6, 912 8-node brick elements and 7, 497 nodes. Again, mesh refinement has been performed to choose the appropriate mesh.

The spring is fixed at one end and subject to an axial tensile force at the other end (see Fig. 13). The force is increased up to a value of 3 N and then unloaded back to zero. The total analysis time is 2 s. Tests are performed using time step increments Δt of 0.1 and 0.01 s, corresponding to 10 and 100 steps per second.

The results for the errors defined in Eq. (215) are summarized in Table 14.

Table 15 reports the average number of global Newton iterations and the average evaluation time per time step increment for the RM and FB algorithmic schemes.

All the report results are obtained by considering a regularized parameter $2\delta = 10^{-9}$ for the FB algorithm. As it can be observed, the RM and FB algorithms produce quite identical results in terms of stress and strain errors. Both the number of global Newton iterations and the computational time are comparable for the two algorithms and decrease as the number of steps per second increases. As expected, both are first-order accurate. The FB algorithm therefore offer an alternative solution to the RM scheme. We remark again that possible difficulties in the FB scheme could be linked to the numerical sensitiveness of such scheme, due to the presence of the regularization parameter, and to the proper choice of the Newton–Raphson initial guess to guarantee a fast and correct convergence. In fact, a potential disadvantage of this method is that when the initial point is far from a solution, the method might not converge or may converge very slowly. To resolve these shortcomings, we could apply a line-search strategy. In the present case, however, the presence of the regularization parameter in the FB algorithm does not affect the convergence. Therefore, the obtained results encourage a further investigation of the FB scheme and of its application to more complex constitutive models, e.g., involving nonlinear kinematic hardening or describing the behavior of smart materials.

7 Conclusions and Perspectives

This paper has proposed a theoretical and numerical review of the three-dimensional rate-independent plasticity equations in an infinitesimal framework. From the theoretical standpoint, we have recalled main concepts of time-continuous equations in a rate and variational formulation. From the numerical viewpoint, we have investigated the accuracy, stability, yield consistency, and the algorithm behaviour of several state-update procedures. Particularly, we have analyzed conventional and *less-conventional* solution schemes in a uniform context. The review has been completed by a comparison between several numerical schemes through the simulation of simple and complex problems. The analyzed algorithms can be extended to more complex models.

The literature has been shown to be very rich on the treated topic and the choice of the algorithm to use strongly depends on the problem under investigation. Despite this, *less-conventional* approaches need further investigations and several alternative are still possible, e.g., in the framework of mathematical programming. As an example, the possibility of recasting the plasticity problem as a convex QP may allow the application of algorithms as the alternating direction method of multipliers [261]. The method has

Table 13 Three-dimensional plate with hole. Error on stress and strain tensors, evaluated with the RM and the FB algorithmic schemes at 0.5, 1.0, 1.5, and 2.0 s

Error	Time step [s]	RM	FB
t = 0.5 s			
E^{σ}	0.1	$2.31 \cdot 10^{-3}$	$2.31 \cdot 10^{-3}$
	0.01	$0.30 \cdot 10^{-3}$	$0.30 \cdot 10^{-3}$
t = 1.0 s			
E^{σ}	0.1	$4.69 \cdot 10^{-3}$	$4.69 \cdot 10^{-3}$
	0.01	$0.49 \cdot 10^{-3}$	$0.49 \cdot 10^{-3}$
t = 1.5 s			
E^{σ}	0.1	$18.51 \cdot 10^{-3}$	$18.51 \cdot 10^{-3}$
	0.01	$1.95 \cdot 10^{-3}$	$1.96 \cdot 10^{-3}$
t = 2.0 s			
E^{σ}	0.1	$5.39 \cdot 10^{-3}$	$5.39 \cdot 10^{-3}$
	0.01	$0.60 \cdot 10^{-3}$	$0.60 \cdot 10^{-3}$
t = 0.5 s			
E^{ϵ}	0.1	$4.75 \cdot 10^{-3}$	$4.75 \cdot 10^{-3}$
	0.01	$0.69 \cdot 10^{-3}$	$0.68 \cdot 10^{-3}$
t = 1.0 s			
E^{ϵ}	0.1	$5.01 \cdot 10^{-3}$	$5.01 \cdot 10^{-3}$
	0.01	$0.53 \cdot 10^{-3}$	$0.53 \cdot 10^{-3}$
t = 1.5 s			
E^{ϵ}	0.1	$6.46 \cdot 10^{-3}$	$6.45 \cdot 10^{-3}$
	0.01	$0.68 \cdot 10^{-3}$	$0.68 \cdot 10^{-3}$
t = 2.0 s			
E^{ϵ}	0.1	$10.80 \cdot 10^{-3}$	$10.79 \cdot 10^{-3}$
	0.01	$1.14 \cdot 10^{-3}$	$1.14 \cdot 10^{-3}$

Table 14 Three-dimensional helical spring. Error on stress and strain evaluated with the RM and the FB algorithmic schemes at 0.5, 1.0, 1.5 and 2.0 s

Error	Time step [s]	RM	FB
t = 0.5 s			
E^{σ}	0.1	$0.39 \cdot 10^{-3}$	$0.39 \cdot 10^{-3}$
	0.01	$0.05 \cdot 10^{-3}$	$0.05 \cdot 10^{-3}$
t = 1.0 s			
E^{σ}	0.1	$42.95 \cdot 10^{-3}$	$42.95 \cdot 10^{-3}$
	0.01	$4.88 \cdot 10^{-3}$	$4.88 \cdot 10^{-3}$
t = 1.5 s			
E^{σ}	0.1	$44.92 \cdot 10^{-3}$	$44.92 \cdot 10^{-3}$
	0.01	$5.10 \cdot 10^{-3}$	$5.10 \cdot 10^{-3}$
t = 2.0 s			
E^{σ}	0.1	$45.22 \cdot 10^{-3}$	$45.22 \cdot 10^{-3}$
	0.01	$5.11 \cdot 10^{-3}$	$5.11 \cdot 10^{-3}$
t = 0.5 s			
E^{ϵ}	0.1	$0.27 \cdot 10^{-3}$	$0.27 \cdot 10^{-3}$
	0.01	$0.04 \cdot 10^{-3}$	$0.04 \cdot 10^{-3}$
t = 1.0 s			
E^{ϵ}	0.1	$45.46 \cdot 10^{-3}$	$45.46 \cdot 10^{-3}$
	0.01	$4.99 \cdot 10^{-3}$	$4.99 \cdot 10^{-3}$
t = 1.5 s			
E^{ϵ}	0.1	$46.16 \cdot 10^{-3}$	$46.16 \cdot 10^{-3}$
	0.01	$5.06 \cdot 10^{-3}$	$5.06 \cdot 10^{-3}$
t = 2.0 s			
E^{ϵ}	0.1	$46.65 \cdot 10^{-3}$	$46.65 \cdot 10^{-3}$
	0.01	$5.11 \cdot 10^{-3}$	$5.11 \cdot 10^{-3}$

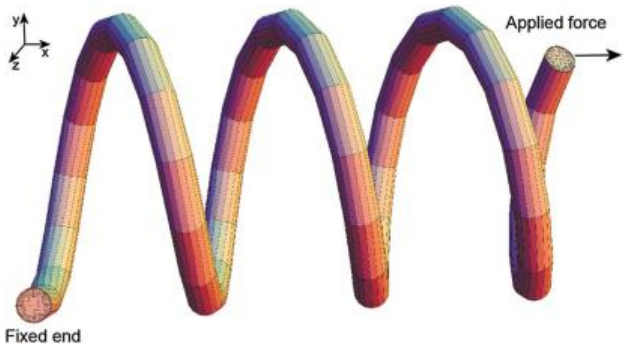

Fig. 13 Three-dimensional helical spring. Adopted mesh and applied boundary conditions

Table 15 Three-dimensional helical spring. Comparison of computational efficiency between the RM and the FB algorithmic schemes in terms of average number of global Newton iterations and average computational time per time step

Algorithm	Number of steps	Average iterations/step	Average comp. time/step [s]
RM	10	5.65	11.67
	100	5.04	7.94
FB	10	5.70	8.45
	100	4.70	7.82

an iterative solution scheme based on an operator splitting algorithm, which is suitable to efficiently solve large-scale variational problems. An application to the field of limit analysis has been recently proposed in [262].

The reported analysis can be used for finding effective algorithms for a wide range of applications (e.g., involving contact or damage), plastic materials (e.g., rate-independent, anisotropic, or crystal plasticity), and framework (e.g., finite strain) and can be a reference or offer novel ideas for the developments of numerical schemes for more complex constitutive models describing, e.g., the behaviour of smart materials.

Compliance with Ethical Standards

Conflict of interest The authors declare that they have no conflict of interest.

Ethical approval This article does not contain any studies with human participants or animals performed by any of the authors.

Informed consent Informed consent was obtained from all individual participants included in the study.

References

1. Tresca H (1868) Mémoire sur l'écoulement des corps solides. Mém Prés par Div Savants 18:733–799
2. von Mises V (1913) Mechanik der festen korper im plastischedeformablen zustand. nachr. d. gesellsch d. wissensch. zu göttingen. Math Phys Klasse 1913:582–592
3. Hill R (1950) The mathematical theory of plasticity. Clarendon Press, Oxford
4. Prager W, Hodge PG (1951) Theory of perfectly plastic solids. Wiley, New York
5. Koiter WT (1953) Stress-strain relations, uniqueness and variational theorems for elasto-plastic materials with singular yield surface. Q Appl Math 11:350–354
6. Simo JC (1999) Topics on the numerical analysis and simulation of plasticity. In: Ciarlet PG Lions JL (eds) Handbook of numerical analysis, vol 4. Elsevier, Amsterdam
7. Wilkins ML (1964) Calculation of elastic-plastic flow. In: Methods in computational physics, vol. 3, Academic Press, New York, pp 211–263
8. Mendelson A (1968) Plasticity: theory and application. Macmillan, New York
9. de Souza Neto EA, Perić D, Owen DRJ (2008) Computational methods for plasticity: theory and applications. Wiley, New York
10. Simo JC, Hughes TJR (1998) Computational Inelasticity. Springer, New York, 1998
11. Lubliner J (1990) Plasticity theory. MacMillan, New York
12. Lemaitre J, Chaboche JL (1994) Mechanics of Solid Materials. Cambridge University Press, Cambridge
13. Chaboche JL (2008) A review of some plasticity and viscoplasticity constitutive theories. Int. J. Plasticity 24:1642–1693
14. Besson J, Cailletaud G, Chaboche JL, Forest S (2010) Non-linear mechanics of materials. Springer, Netherlands
15. Han W, Reddy BD (1999) Plasticity: mathematical theory and numerical analysis. Springer, New York
16. Gurtin ME, Fried E, Anand L (2010) The mechanics and thermodynamics of continua, volume 158. Cambridge University Press, Cambridge
17. Coulomb CA (1776) Essai sur une application des règles des maximis et minimis à quelquels problèmes de statique relatifs, à la architecture. Mem Acad R Div Sav 7:343–387
18. Drucker DC, Prager W (1952) Soil mechanics and plasticity analysis of limit design. Q J Appl Math 10:157–162
19. Bigoni D, Piccolroaz A (2004) Yield criteria for quasibrittle and frictional materials. Int. J. Solids Struct. 41(11–12):2855–2878
20. Eve RA, Reddy BD, Rockafellar RT (1990) An internal variable theory of plasticity based on the maximum plastic work inequality. Q. Appl. Math. 48:59–83
21. Duvaut G, Lions JL (1976) Inequalities in Mechanics and Physics. Springer, Berlin Heidelberg
22. Lei X, Lissenden CJ (2007) Pressure sensitive non-assocaitive plasticity model for DRA composites. J. Eng. Mater-T. ASME 129:255–264
23. Armstrong PJ, Frederick CO (1966) A mathematical representation of the multiaxial bauschinger effect. Technical report, CEGB: Report RD/B/N 731
24. Kuhn HW, Tucker AW (1951) Nonlinear programming. In: Proceedings of the 2nd Berkeley symposium, University of California Press, Berkeley, pp 481–492
25. Karush W (1939) Minima of functions of several variables with inequalities as side constraints. Master's thesis, Department of Mathematics, University of Chicago, Chicago
26. Hjiaj M, Fortin J, de Saxcé G (2003) A complete stress update algorithm for the non-associated Drucker-Prager model including treatment of the apex. Int J Eng Sci 41:1109–1143
27. Fischer A (1997) Solution of monotone complementarity problems with locally lipschitzian functions. Math Program 76:513–532
28. Leyffer S (2006) Complementarity constraints as nonlinear equations: theory and numerical experience. In Optimization with multivalued mappings. Springer, Dordrecht
29. Luo ZQ, Pang JS, Ralph D (1996) Mathematical programs with equilibrium constraints. Cambridge University Press, Cambridge
30. Bolzon G (2015) Complementarity problems in structural engineering: an overview. Archives of computational methods in engineering. Springer, Dordrecht, pp 1–14
31. Fischer A (1992) A special Newton-type optimization method. Optimization 24:269–284
32. Kanzow C (1996) Some non-interior continuation methods for linear complementarity problems. SIAM J. Matrix Anal A 17:851–868
33. Chen C, Mangasarian OL (1996) A class of smoothing functions for nonlinear and mixed complementarity problems. Comput Optim Appl 5:97–138
34. Areias P, Dias-da-Costa D, Pires EB, Infante Barbosa J (2012) A new semi-implicit formulation for multiple-surface flow rules in multiplicative plasticity. Comput. Mech. 49:545–564
35. Mandel J (1964) Contribution Theorique a l'Etude de l'Ecrouissage et des Lois de l'Ecoulement Plastique. In: Proceedings of the eleventh international congress on applied mechanics, pp 502–509
36. Lubliner J (1984) A maximum-dissipation principle in generalized plasticity. ACTA Mech 52:225–237
37. Lubliner J (1986) Normality rules in large-deformation plasticity. Mech Mater 5:29–34
38. Rockafellar RT (1970) Convex analysis. Princeton University Press, Princeton
39. Moreau J (1976) Application of convex analysis to the treatment of elastoplastic systems. In Applications of methods of functional analysis to problems in mechanics. Springer Berlin
40. Romano G, Rosati L, Marotti de Sciarra F (1993) Variational principles for a class of finite step elastoplastic problems with non-linear mixed hardening. Comput Method Appl Mech Eng 109:293–314
41. Nguyen QS, Halphen B (1975) Sur les matériaux standard généralisés. J Mecanique 14:39–63
42. Rockafellar RT, Wets JB (1998) Variational analysis. Springer, Berlin
43. Biot MA (1965) Mechanics of incremental deformations. Wiley, New York
44. Papapadopulos P, Taylor RL (1994) On the application of multi-step integration methods to infinitesimal elastoplasticity. Int J Numer Method E 37:3169–3184
45. Owen DRJ, Hinton E (1980) Finite elements in plasticity. Pineridge Press, Swansea
46. Owen DRJ, Salonen EM (1975) Three-dimensional elasto-plastic finite element analysis. Int J Numer Method E 9(1):209–218
47. Bathe KJ (1996) Finite element procedures, 1st edition. Prentice Hall, Englewood Cliff

48. Taylor RL (2005) A finite-element analysis program. University of California, Berkeley. http://www.ce.berkeley.edu/projects/feap/
49. Wriggers P (2008) Nonlinear finite element methods. Springer, Berlin
50. Hinton E, Owen DRJ (1977) Finite element programming. Academic Press, London
51. Zienkiewicz OC, Taylor RL, Zhu JZ (2013) The finite element method: its basis and fundamentals, 7th edition. Butterworth-Heinemann, Oxford
52. Ortiz M, Popov EP (1985) Accuracy and stability of integration algorithms for elastoplastic constitutive relations. Int J Numer Method E 21(9):1561–1576
53. Quarteroni A, Sacco R, Saleri F (2007) Numerical mathematics. Springer, Berlin
54. Ortiz M, Simo J (1986) An analysis of a new class of integration algorithms for elastoplastic constitutive relations. Int J Numer Method E 23:353–366
55. Crisfield MA (1991) Non-linear finite element analysis of solids and structures, vol 1. Wiley, Chichester
56. Crisfield MA (1997) Non-linear finite element analysis of solids and structures, vol 2. Wiley, Chichester
57. Borja RI, Lee SR (1990) (1990) Cam-Clay plasticity, Part 1: implicit integration of elasto-plastic constitutive relations. Comput Method Appl Mech Eng 78:49–72
58. Borja RI (1991) Cam-clay plasticity. Part II: implicit integration of constitutive equations based on a non-linear elastic stress predictor. Comput Method Appl Mech Eng 88:225–40
59. Amirkhizi AV, Nemat-Nasser S (2007) A framework for numerical integration of crystal elasto-plastic constitutive equations compatible with explicit finite element codes. Int J Plasticity 23:1918–1937
60. Ding KZ, Qin QH, Cardew-Hall M (2007) Substepping algorithms with stress correction for the simulation of sheet metal forming process. Int J Mech Sci 49(11):1289–1308
61. Polat MU, Dokainish MA (1989) An automatic subincrementation scheme for accurate integration of elasto-plastic constitutive relation. Comput Struct 31:339–347
62. Sloan SW (1987) Substepping schemes for the numerical integration of elastoplastic stress-strain relations. Int J Numer Method E 24:893–911
63. Sloan SW, Booker JR (1992) Integration of Tresca and Mohr-Coulomb constitutive relations in plane strain elastoplasticity. Int J Numer Method E 33:163–196
64. Sloan S, Abbo A, Sheng D (2001) Refined explicit integration of elastoplastic models with automatic error control. Eng Comput 18:121–194
65. Solowski WT, Gallipoli D (2010) Explicit stress integration with error control for the barcelona basic model part i: algorithms formulations. Comp Geotechnic 37:59–67
66. Potts DM, Ganendra D (1992) A comparison of solution strategies for non-linear finite element analysis of geotechnical problems. In: Proceedings of the 3rd international conference on computational plasticity, Barcelona, pp 803–14
67. Potts DM, Ganendra D (1994) An evaluation of substepping and implicit stress point algorithms. Comput Method Appl Mech Eng 119:341–54
68. Yamaguchi E (1993) A comparative study of numerical methods for computing stress increments in elastic-plastic materials. In: Proceedings of the Asia-Pacific symposium on advances in plasticity and its applications, Hong Kong, pp 625–30
69. Halilovic M, Vrha M, Stok B (2009) NICE-an explicit numerical scheme for efficient integration of nonlinear constitutive equations. Math Comput Simulat 80:294–313
70. Vrh M, Halilovic M, Stok B (2010) Improved explicit integration in plasticity. Int J Numer Method E 81:910–938
71. Hong H-K, Liu C-S (1999) Lorentz group SOo(5,1) for perfect elastoplasticity with large deformation and a consistency numerical scheme. Int J NonLinear Mech 34:1113–1130
72. Hong H-K, Liu C-S (2000) Internal symmetry in the constitutive model of perfect elasto-plasticity. Int J NonLinear Mech 35:447–466
73. Artioli E, Auricchio F, da Veiga L (2007) Second-order accurate integration algorithms for von-Mises plasticity with a nonlinear kinematic hardening mechanism. Comput Method Appl Mech Eng 196:1827–1846
74. Rezaiee-Pajand M, Auricchio F, Sharifian M, Sharifian M (2015) Exponential-based integration for Bigoni-Piccolroaz plasticity model. Eur J Mech A-Solid 51:107–122
75. Artioli E, Auricchio F, da Veiga L (2005) Integration schemes for von-Mises plasticity models based on exponential maps: numerical investigations and theoretical considerations. Int J Numer Method E 64:1133–1165
76. Artioli E, Auricchio F, Beirao da Veiga L (2006) A novel optimal exponential-based integration algorithm for von-Mises plasticity with linear hardening: theoretical analysis on yield consistency, accuracy, convergence and numerical investigations. Int J Numer Method E 67:449–498
77. Auricchio F, da Veiga LB (2003) On a new integration scheme for von-Mises plasticity with linear hardening. Int J Numer Method E 56:1375–1396
78. Rezaiee-Pajand M, Nasirai C (2007) Accurate integration scheme for von-Mises plasticity with mixed-hardening based on exponential maps. Eng Comput 24(6):608–635
79. Rezaiee-Pajand M, Nasirai C (2008) On the integration schemes for Drucker-Prager's elasto-plastic models based on exponential maps. Int J Numer Method E 74:799–826
80. Rezaiee-Pajand M, Nasirai C, Sharifian M (2010) Application of exponential-based methods in integrating the constitutive equations with multicomponent kinematic hardening. J Eng Mech-ASCE 136(12):1502–1518
81. Rezaiee-Pajand M, Sharifian M, Sharifian M (2011) Accurate and approximate integrations of Drucker-Prager plasticity with linear isotropic and kinematic hardening. Eur J Mech A Solids 30:345–361
82. Rezaiee-Pajand M, Nasirai C, Sharifian M (2011) Integration of nonlinear mixed hardening models. Multidiscip Model Mat Struct 7(3):266–305
83. Rezaiee-Pajand M, Auricchio F, Sharifian M, Sharifian M (2014) Computational plasticity of mixed hardening pressure-dependency constitutive equations. Acta Mech 225(6):1699–1733
84. Krieg RD, Krieg DB (1977) Accuracies of numerical solution methods for the elastic-perfectly plastic model. J Press Vess-T ASME 99:510–515
85. Loret B, Prevost JH (1986) Accurate numerical solutions for Drucker-Prager elastic-plastic models. Comput Method Appl Mech Eng 54:259–277
86. Ristinmaa M, Tryding J (1993) Exact integration of constitutive equations in elasto-plasticity. Int J Numer Method E 36:2525–2544
87. Wei Z, Peric D, Owen DRJ (1996) Consistent linearization for the exact stress update of Prandtl-Reuss non-hardening elastoplastic models. Int J Numer Method E 39:1219–1235
88. Wallin M, Ristinmaa M (2001) Accurate stress updating algorithm based on constant strain rate assumption. Comput Method Appl Mech Eng 190:5583–5601
89. Szabo L (2009) A semi-analytical integration method for J2 flow theory of plasticity with linear isotropic hardening. Comput Method Appl Mech Eng 198:2151–2166

90. Kossa A, Szabo L (2009) Exact integration of the von Mises elasto-plasticity model with combined linear isotropic-kinematic hardening. Int J Plasticity 25:1083–1106
91. Rezaiee-Pajand M, Sharifian M (2012) A novel formulation for integrating nonlinear kinematic hardening Drucker-Prager's yield condition. Eur J Mech A-Solid 31:163–178
92. Becker R (2011) An alternative approach to integrating plasticity relations. Int J Plasticity 27(8):1224–1238
93. Runesson K, Sture S, Willam K (1988) Integration in computational plasticity. Comput Struct 30(12):119–130
94. Kojic M (2002) Stress integration procedures for inelastic material models within the finite element method. Appl Mech Rev 55(4):389–414
95. Hairer E, Lubich C, Wanner G (2002) Geometric numerical integration. Springer, Berlin
96. Brennan K, Campbell S, Petzold L (1996) Numerical solution of initial value problems in ordinary differential-algebraic equations. SIAM, Philadelphia
97. Gratacos P, Montmitonnet P, Chenot JL (1992) An integration scheme for Prandtl-Reuss elastoplastic constitutive equations. Int J Numer Method E 33:943–961
98. Cailletaud G, Chaboche JL (1996) Integration methods for complex plastic constitutive equations. Comput Method Appl Mech Eng 133(1–2):125–155
99. Simo JC, Govindjee S (1991) Non-linear B-stability and symmetry preserving return mapping algorithms for plasticity and viscoplasticity. Int J Numer Method E 31:151–176
100. Simo JC, Taylor RL (1986) A return mapping algorithm for plane stress elastoplasticity. Int J Numer Method E 22:649–670
101. Ortiz M, Martin JB (1989) Symmetry-preserving return mapping algorithms and incrementally extremal paths: a unification of concepts. Int J Numer Method E 28:1839–1853
102. Artioli E, Auricchio F, da Veiga L (2007) Generalized midpoint integration algorithms for J2 plasticity with linear hardening. Int J Numer Method E 72:422–463
103. Gear CW (1971) Numerical Initial value problems in ordinary differential equations. Prentice-Hall PTR, Upper Saddle River
104. Eckert S, Baaser H, Gross D, Scherf O (2004) A BDF2 integration method with step size control for elasto-plasticity. Comput Mech 34:377–386
105. Jay LO (2006) Specialized runge-kutta methods for index 2 differential-algebraic equations. Math Comput 75(254):641–654
106. Buttner J, Simeon S (2002) Runge-Kutta methods in elastoplasticity. Appl Numer Math 41:443–458
107. Bushnell D (1973) Large deflection elastic-plastic creep analysis of axisymmetric shells. In: Hartung F (ed) Numerical solution of nonlinear structural problems. 6:103–138
108. Yamada Y, Yoshimura N, Sakurai T (1968) Plastic stress-strain matrix and its application for the solution of elastic-plastic problems by the finite element method. Int J Mech Sci 10(5):343–354
109. Stricklin JA, Haisler WE, von Riesemann WA (1972) Computation and solution procedures for nonlinear analysis by combined finite element-finite difference methods. Comput Struct 2(5–6):955–974
110. Wissmann JW, Hauck C (1983) Efficient elastic-plastic finite element analysis with higher order stress point algorithms. Comput Struct 17:89–95
111. Mattsson H, Axelsson K, Klisinski M (1998) A method to correct yield surface drift in soil plasticity under mixed control and explicit integration. Int J Numer Anal Met 21:175–197
112. Potts DM, Gens A (1985) A critical assessment of methods of correcting for drift from the yield surface in elasto-plastic finite element analysis. Int J Numer Method E 9(2):149–159
113. Hartmann S (2002) Computation in finite-strain viscoelasticity: finite elements based on the interpretation as differential-algebraic equations. Comput Method Appl Mech Eng 191:1439–1470
114. Ellsiepen P, Hartmann S (2001) Remarks on the interpretation of current non-linear finite element analyses as differential algebraic equations. Int J Numer Method E 51:679–707
115. Hiley RA, Rouainia M (2008) Explicit Runge-Kutta methods for the integration of rate-type constitutive equations. Comput Mech 42:53–66
116. Luccioni LX, Pestana JM, Taylor RL (2001) Finite element implementation of non-linear elastoplastic constitutive laws using local and global explicit algorithms with automatic error control. Int J Numer Method E 50:1191–1212
117. Pedroso DM, Sheng D, Sloan SW (2008) Stress update algorithm for elastoplastic models with nonconvex yield surfaces. Int J Numer Method E 76:2029–2062
118. Sheng D, Sloan SW, Gens A, Smith DW (2003) Finite element formulation and algorithms for unsaturated soils. part i: theory. Int J Numer Anal Met 27:745–765
119. Hong H-K, Liu C-S (2001) Lorentz group on Minkowski spacetime for construction of the two basic principles of plasticity. Int J NonLinear Mech 36:679–686
120. Liu C-S (2004) Internal symmetry groups for the Drucker-Prager material model of plasticity and numerical integrating methods. Int J Solids Struct 41:3771–3791
121. Liu C-S, Liu L-W, Hong H-K (2016) A scheme of automatic stress-updating on yield surfaces for a class of elastoplastic models. Int J NonLinear Mech 85:6–22
122. Hong H-K, Liu C-S (1999) Internal symmetry in bilinear elastoplasticity. Int J NonLinear Mech 34:279–288
123. Liu C-S, Li C-F (2005) Geometrical numerical algorithms for a plasticity model with Armstrong-Frederick kinematic hardening rule under strain and stress controls. Int J Numer Method E 63:1396–1423
124. Liu C-S (2005) Computational applications of the Poincaré group on the elastoplasticity with kinematic hardening. CMES-Comp Model Eng 8:231–258
125. Liu C-S (2003) Symmetry groups and the pseudo-Riemann spacetimes for mixed hardening elastoplasticity. Int J Solids Struct 40:251–269
126. Liu C-S (2004) A consistent numerical scheme for the von Mises mixed-hardening constitutive equations. Int J Plasticity 20:663–704
127. Liu C-S, Chang C-W (2005) Non-canonical Minkowski and pseudo-Riemann frames of plasticity models with anisotropic quadratic yield criteria. Int J Solids Struct 42:2851–2882
128. Artioli E, Auricchio F, Beirao da Veiga L (2007) Generalized midpoint integration algorithms for J2 plasticity with linear hardening. Int J Numer Method E 72:422–463
129. Marques JMMC, Owen DRJ (1984) Some reflections on elastoplastic stress calculation in finite element analysis. Comput Struct 18(6):1135–1139
130. Yoder PJ, Whirley RG (1984) On the numerical implementation of elastoplastic models. J Appl Mech-T ASME 51:283–288
131. Lee JH (1988) Accuracies of numerical solution method for the pressure-modified von Mises model. Int J Numer Method E 26:453–465
132. Szabo L, Kossa A (2012) A new exact integration method for the Drucker-Prager elastoplastic model with linear isotropic hardening. Int J Solids Struct 49:170–190
133. Wallin M, Ristinmaa M (2008) An alternative method for the integration of continuum damage evolution laws. Comput Mech 41:347–359

134. Rezaiee-Pajand M, Sharifian M, Sharifian M (2014) Angles based integration for generalized non-linear plasticity model. Int J Mech Sci 87:241–257
135. Borja RI (2013) Plasticity: modeling & computation. Springer, Berlin
136. Onate E, Owen R (2010) Computational Plasticity. Springer, Netherlands
137. Schmidt-Baldassari M (2003) Numerical concepts for rate-independent single crystal plasticity. Comput Method Appl Mech Eng 192:1261–1280
138. Akpama HK, Ben Bettaieb M, Abed-Meraim F (2016) Numerical integration of rate-independent BCC single crystal plasticity models: comparative study of two classes of numerical algorithms. Int J Numer Method Eng. doi:10.1002/nme.5215
139. De Angelis F, Taylor RL (2015) An efficient return mapping algorithm for elastoplasticity with exact closed form solution of the local constitutive problem. Eng Comput 32(8):2259–2291
140. Krieg RD, Key SW Implementation of a time dependent plasticity theory into structural computer programs. In: Stricklin JA, Saczalski KJ (eds) Constitutive equations in viscoplasticity: computational and engineering aspects, AMD-20. ASME, New York
141. Dodds RH Jr (1987) Numerical techniques for plasticity computations in finite element analysis. Comput Struct 26(5):767–779
142. Simo JC, Taylor RL (1985) Consistent tangent operators for rate-independent elastoplasticity. Comput Method Appl Mech Eng 48(1):101–118
143. Clausen J, Damkilde L, Andersen L (2006) Efficient return algorithms for associated plasticity with multiple yield planes. Int J Numer Method Eng 66:1036–1059
144. Tu X, Andrade JE, Chen Q (2009) Return mapping for nonsmooth and multiscale elastoplasticity. Comput Method Appl Mech Eng 198:2286–2296
145. Hopperstad OS, Remseth S (1995) A return mapping algorithm for a class of cyclic plasticity models. Int J Numer Method Eng 38:549–564
146. Schreyer HL, Kuhk RF, Kramer MM (1979) Accurate numerical solutions for elastic-plastic models. J Press Vess-T ASME 101:226–234
147. Simo JC, Hughes TRJ (2006) General return mapping algorithms for rate-independent plasticity. In: Desai CS et al (eds) Constitutive laws for engineering materials: theory and applications. Elsevier, New York, pp 221–231
148. Nemat-Nasser S (1991) Rate-independent finite-deformation elastoplasticity: a new explicit constitutive algorithm. Mech Mater 11:235–249
149. Ortiz M, Pinsky PM, Taylor RL (1983) Operator split methods for the numerical solution of the elastoplastic dynamic problem. Comput Struct 17(3):345–359
150. Rice JR, Tracy DM (1973) Computational fracture mechanics. In: Fenves SJ (ed) Proceedings of symposium numerical and computer methods in structural mechanics, page 585, Urbana. Academic Press, New York
151. Ortiz M, Pinsky PM (1981) Global analysis methods for the solution of elastoplastic and viscoplastic dynamic problems. Report UCB/SESM 81/08, University of California, Berkeley
152. Safaei M, Lee M-G, De Waele W (2015) Evaluation of stress integration algorithms for elastic-plastic constitutive models based on associated and non-associated flow rules. Comput Method Appl Mech Eng 295:414–445
153. Asensio G, Moreno C (2003) Linearization and return mapping algorithms for elastoplasticity models. Int J Numer Method Eng 57(7):991–1014
154. Wolfram (2013) Mathematica Documentation, http://www.wolfram.com
155. Armero F, Pérez-Foguet A (2002) On the formulation of closest-point projection algorithms in elastoplasticity-Part I: the variational structure. Int J Numer Method Eng 53:297–329
156. Brannon RM, Leelavanichkul S (2012) A multi-stage return algorithm for solving the classical damage component of constitutive models for rocks, ceramics, and other rock-like media. Int J Fracture 163(1–2):133–149
157. Dutko M, Péric D, Owen DRJ (1993) Universal anisotropic yield criterion based on superquadratic functional representation: Part I. Algorithmic issues and accuracy analysis. Comput Method Appl Mech Eng 109:73–93
158. Pérez-Foguet A, Armero F (2002) On the formulation of closest-point projection algorithms in elastoplasticity-Part II: globally convergent schemes. Int J Numer Method Eng 53:331–374
159. Abbo AJ, Sloan SW (1996) An automatic load stepping algorithm with error control. Int J Numer Method Eng 39:1737–1759
160. Pérez-Foguet A, Rodríguez-Ferran A, Huerta A (2001) Consistent tangent matrices for substepping schemes. Comput Method Appl Mech Eng 190:4627–4647
161. Genna F, Pandolfi A (1994) Accurate numerical integration of drucker-prager's constitutive equations. Meccanica 29:239–260
162. Sheng D, Sloan SW, Yu HS (2000) Aspects of finite element implementation of critical state models. Comput Mech 26:185–196
163. Hashiguchi K, Saitoh K, Okayasu T, Tsutsumi S (2002) Evaluation of typical conventional and unconventional plasticity models for prediction of softening behaviour of soils. Geotechnique 52(8):561–578
164. Sheng D, Sloan SW, Abbo AJ (2002) An automatic Newton-Raphson scheme. Int J Geomech 2:471–502
165. Rosati L, Valoroso N (2004) A return map algorithm for general isotropic elasto/visco-plastic materials in principal space. Int J Numer Method E 60(2):461–498
166. de Souza Neto EA, Perić D, Owen DRJ (1994) A model for elastoplastic damage at finite strains. Eng Comput 11:257–281
167. Bićanić N, Pearce CJ (1996) Computational aspects of a softening plasticity model for plain concrete. Mech Cohes Frict Mat 1:75–94
168. Stupkiewicz S, Denzer R, Piccolroaz D, Bigoni A (2014) Implicit yield function formulation for granular and rock-like materials. Comput Mech 54(5):1163–1173
169. Penasa M, Piccolroaz A, Argani L, Bigoni D (2014) Integration algorithms of elastoplasticity for ceramica powder compaction. J Eur Ceram Soc 34(11):2775–2788
170. Simo JC (1992) Algorithms for static and dynamic multiplicative plasticity that preserve the classical return mapping schemes of the infinitesimal theory. Comput Method Appl Mech Eng 99(1):61–112
171. Matzenmiller A, Taylor RL (1994) A return mapping algorithm for isotropic elastoplasticity. Int J Numer Method Eng 37(5):813–826
172. Tamagnini C, Castellanza R, Nova R (2002) A generalized backward Euler algorithm for the numerical integration of an isotropic harderning elastoplastic model for mechanical and chemical degradation of bonded geomaterials. Int J Numer Anal Met 26(10):963–1004
173. Borja RI, Sama KM, Sanza PF (2003) On the numerical integration of three-invariant elastoplastic constitutive models. Comput Method Appl Mech Eng 192(9–10):1227–1258
174. Foster CD, Regueiro RA, Fossum AF, Borja RI (2005) Implicit numerical integration of a three invariant, isotropic/kinematic hardening cap plasticity model for geomaterials. Comput Method Appl Mech Eng 194(50–52):5109–5138

175. Peng Q, Chen MX (2012) An efficient return mapping algorithm for general isotropic elastoplasticity in principal space. Comput Struct 92–93:173–184
176. Chen JS, Pan SH (2012) A survey on SOC complementarity functions and solution methods for SOCPs and SOCCPs. Pac J Optim 8:33–74
177. Chen MX, Peng Q, Huang J (2014) On the representation and implicit integration of general isotropic elastoplasticity based on a set of mutually orthogonal unit basis tensors. Int J Numer Method Eng 99(9):654–681
178. Cecilio DL, Devloo PRB, Gomes SM, dos Santos ERS, Shauer N (2015) An improved numerical integration algorithm for elastoplastic constitutive equations. Comput Geotech 64:1–9
179. Bertsekas DP (1982) Constrained optimization and lagrange multiplier methods. Academic Press, New York
180. Luenberger DG, Ye Y (1984) Linear and nonlinear programming. Springer, Berlin
181. Cuomo M, Contrafatto L (2000) Stress rate formulation for elastoplastic models with internal variables based on augmented Lagrangian regularization. Int J Solids Struct 37:3935–3964
182. Contrafatto L, Ventura G (2004) Numerical analysis of Augmented Lagrangian algorithms in complementary elastoplasticity. Int J Numer Method Eng60:2263–2287
183. Ahn J (2007) A vibrating string with dynamic frictionless impact. Appl Numer Math 57:861–884
184. Tin-Loi F (1999) A smoothing scheme for a minimum weight problem in structural plasticity. Struct Optim 17:279–285
185. Balakrishna S, Biegler LT (1992) Targeting strategies for the synthesis and energy integration of nonisothermal reactor networks. Ind Eng Chem Res 31:2152–2164
186. Gopal V, Biegler LT (1999) Smoothing methods for complementarity problems in process engineering. AICHE J 45(7):1535–1547
187. Lang YD, Biegler LT (2002) Distributed stream method for tray optimization. AICHE J 48(3):582–595
188. Nocedal J, Wright S (1999) Numerical optimization. Springer, New York
189. Lloyd Smith D (ed) (1990) Mathematical programming methods in structural plasticity. CISM International Centre for Mechanical Sciences. Springer, Berlin
190. Ben-Tal A, Nemirovski A (2001) Lectures on modern convex optimization. Society for Industrial and Applied Mathematics
191. Fletcher R (2000) Practical methods of optimization. Wiley, New York
192. Boyd S, Vandenberghe L (2004) Convex optimization. Cambridge University Press, Cambridge
193. Krabbenhoft K, Lyamin AV, Sloan SW, Wriggers P (2007) An interior point algorithm for elastoplasticity. Int J Numer Method Eng 69:592–626
194. Karmarkar N (1984) A new polynomial-time algorithm for linear programming. Combinatorica 4:373–395
195. Nash SG, Sofer A (1996) Linear and nonlinear programming. McGraw-Hill, New York
196. Maier G (1984) Mathematical programming applications to structural mechanics: some introductory thoughts. Eng Struct 6(1):2–6
197. Maier G, Munro J (1982) Mathematical programming applications to engineering plastic analysis. Appl Mech Rev 35:1631–1643
198. Maier G, Grierson D (1979) Engineering plasticity by mathematical programming. Pergamon Press, New York
199. Christensen PW (2002) A non-smooth Newton method for elastoplastic problems. Comput Method Appl Mech Eng 191:1189–1219
200. Feijoo RA, Zouain N (1988) Formulations in rates and increments for elastic-plastic analysis. Int J Numer Method Eng 26:2031–2048
201. Garcea G, Leonetti L (2011) A unified mathematical programming formulation of strain driven and interior point algorithms for shakedown and limit analysis. Int J Numer Method Eng 88(11):1085–1111
202. Maier G (1968) Quadratic programming theory for elastic perfectly plastic structures. Meccanica 3:31–39
203. Maier G (1968) A quadratic programming approach for certain classes on nonlinear structural problems. Meccanica 3:121–130
204. Maier G (1970) A matrix structural theory of piece-wise linear plasticity with interacting yield planes. Meccanica 6:55–66
205. Capurso M, Maier G (1970) Incremental elastoplastic analysis and quadratic optimization. Meccanica 5:107–116
206. Spiliopoulos KV, Patsios TN (2010) An efficient mathematical programming method for the elastoplastic analysis of frames. Eng Struct 32(5):1199–1214
207. Martin JB (1987) A complementary work bounding principle for forward integration along the path of loading for elasto-plastic bodies. J Appl Mech 109:341–345
208. Bird WW, Martin JB (1990) Consistent predictors and the solution of the piecewise holonomic incremental problem in elastoplasticity. Eng Struct 12:9–14
209. Martin JB (1981) An internal variable approach to the formulation of finite element problems in plasticity. In: Hult J, Lemaitre J (eds) Physical nonlinearities in structural analysis. Springer, Berlin, pp 165–176
210. Martin JB, Reddy BD, Griffin TB, Bird WW (1987) Applications of mathematical programming concepts to incremental elastic-plastic analysis. Eng Struct 9:171–176
211. Martin JB, Nappi A (1990) An internal variable formulation for perfectly plastic and linear hardening relations in plasticity. Eur J Mech A-Solid 9:107–131
212. Maier G, Nappi A (1983) Mechanics of material behaviour, chapter on the unified framework provided by mathematical programming to plasticity. Elsevier, Amsterdam, pp 253–273
213. Wieners C (2007) Nonlinear solution methods for infinitesimal perfect plasticity. ZAMM-Z Angew Math Mech 87:643–660
214. Wieners C (2008) SQP methods for incremental plasticity with kinematic hardening. In: IUTAM symposium on theoretical computational and modeling aspects of inelastic media. Springer, volume 11(4), pp 143–153
215. Bilotta A, Leonetti L, Garcea G (2012) An algorithm for incremental elastoplastic analysis using equality constrained sequential quadratic programming. Comput Struct 102–103:97–107
216. Lotfian Z, Sivaselvan MV (2014) A projected Newton algorithm for the dual convex program of elastoplasticity. Int J Numer Method Eng 97:903–936
217. Krabbenhoft K, Lyamin AV, Sloan SW (2007) Formulation and solution of some plasticity problems as conic programs. Int J Solids Struct 44:1533–1549
218. Tütüncü RH, Toh KC, Todd MJ (2003) Solving semidefinite-quadratic-linear programs using SDPT3. Math Program 95(2):189–217
219. Makrodimopoulos A, Martin CM (2005) A novel formulation of upper bound limit analysis as a second-order programming problem. In: Onate E, Owen D (eds) Proceedings of Complas, Barcelona
220. Krabbenhoft K, Lyamin AV, Sloan SW (2008) Three-dimensional Mohr-Coulomb limit analysis using semidefinite programming. Commun Numer Meth Eng 24:1107–1119, 2008
221. Bisbos CD, Pardalos PM (2007) Second-order cone and semidefinite representations of material failure criteria. J Optim Theory Appl 134:275–301

222. Bisbos CD, Makrodimopoulos A, Pardalos PM (2005) Second-order cone programming approaches to static shakedown analysis in steel plasticity. Optim Method Soft 20:25–52
223. Makrodimopoulos A (2006) Computational formulation of shakedown analysis as a conic quadratic optimization problem. Mech Res Commun 33:72–83
224. Zhang LL, Li JY, Zhang HW, Pan SH (2013) A second order cone complementarity approach for the numerical solution of elastoplasticity problems. Comput Mech 51(1):1–18
225. Fukushima M, Luo ZQ, Tseng P (2002) Smoothing functions for second-order cone complementarity problems. SIAM J Optim 12:436–460
226. Hayashi S, Yamashita N, Fukushima M (2005) A combined smoothing and regularization method for monotone second-order cone complementarity problems. SIAM J Optimiz 15:593–615
227. Chen JS, Tseng P (2005) An unconstrained smooth minimization reformulation of the second-order cone complementarity problem. Math Program 104:293–327
228. Pan SH, Chen JS (2010) A semi-smooth newton method for SOCCPs based on a one-parametric class of complementarity functions. Comput Optim Appl 45:59–88
229. Hager C, Wohlmuth B (2009) Nonlinear complementarity functions for plasticity problems with frictional contact. Comput Method Appl Mech Eng 198:3411–3427
230. Zhang HW, Li JY, Pan SH (2011) New second-order cone linear complementarity formulation and semi-smooth Newton algorithm for finite element analysis of 3D frictional contact problem. Comput Method Appl Mech Eng 200:77–88
231. Yonekura K, Kanno Y (2012) Second-order cone programming with warm start for elastoplastic analysis with von mises yield criterion. Optim Eng 13:181–218
232. Zhu C (1995) A finite element-mathematical programming method for elastoplastic contact problems with friction. Finite Elem Anal Des 20:273–282
233. Zhang HW, He SY, Li XS, Wriggers P (2004) A new algorithm for numerical solution of 3D elastoplastic contact problems with orthotropic friction law. Comput Mech 34:1–14
234. Morini B, Porcelli M (2012) TRESNEI, a Matlab trust-region solver for systems of nonlinear equalities and inequalities. Comput Optim Appl 51(1):27–49
235. Macconi M, Morini B, Porcelli M (2009) Trust-region quadratic methods for nonlinear systems of mixed equalities and inequalities. Appl Numer Math 9(5):859–876
236. Macconi M, Morini B, Porcelli M (2009) A Gauss-Newton method for solving bound-constrained underdetermined nonlinear systems. Optim Method Soft 24(2):219–235
237. Morini B, Porcelli M http://tresnei.de.unifi.it/?p=home
238. Mosler J (2010) Variationally consistent modeling of finite strain plasticity theory with non-linear kinematic hardening. Comput Method Appl Mech Eng 199:2753–2764
239. Nodargi NA, Artioli E, Caselli F, Bisegna P (2014) State update algorithm for associative elastic-plastic pressure-insensitive materials by incremental energy minimization. Frattura ed Integrità Strutturale 29:111–127
240. Nodargi NA, Bisegna P (2016) State update algorithm for isotropic elastoplasticity by incremental energy minimization. Int J Numer Method Eng 105(3):163–196
241. Radovitzky R, Ortiz M (1999) Error estimation and adaptive meshing in strongly nonlinear dynamic problems. Comput Method Appl Mech Eng 172:203–240
242. Ortiz M, Stainier L (1999) The variational formulation of viscoplastic constitutive updates. Comput Method Appl Mech Eng 171:419–444
243. Comi C, Corigliano A, Maier G (1991) Extremum properties of finite-step solutions in elastoplasticity with nonlinear mixed hardening. Int J Solids Struct 27(8):965–981
244. Comi C, Perego U (1995) A unified approach for variationally consistent finite elements in elastoplasticity. Comput Method Appl Mech Eng 121:323–344
245. Comi C, Maier G, Perego U (1992) Generalized variable finite element modeling and extremum theorems in stepwise holonomic elastoplasticity with internal variables. Comput Method Appl Mech Eng 96:213–237
246. Miehe C, Schotte J, Lambrecht M (2002) Homogenization of inelastic solid materials at finite strains based on incremental minimization principles. application to texture analysis of polycrystals. J Mech Phys Solids 50:2123–2167
247. Carstensen C, Hackl K, Mielke A (2002) Non-convex potentials and microstructures in finite-strain plasticity. Proc R Soc Ser A 458:299–317
248. Petryk H (2003) Incremental energy minimization in dissipative solids. CR Mecanique 331:469–474
249. Reddy BD, Martin JB (1991) Algorithms for the solution of internal variable problems in plasticity. Comput Method Appl Mech Eng 93:253–273
250. Nelder JA, Mead R (1965) A simplex method for function minimization. Comput J 7:308–313
251. Mosler J, Bruhns OT (2010) On the implementation of rate-independent standard dissipative solids at finite strain-variational constitutive updates. Comput Method Appl Mech Eng 199:417–429
252. Mosler J, Bruhns OT (2009) Towards variational constitutive updates for non-associative plasticity models at finite strain: models based on a volumetric-deviatoric split. Int J Solids Struct 46:1676–1684
253. Hughes T, Taylor RL (1978) Unconditionally stable algorithms for quasi-static elasto/viscoplastic finite element analysis. Comput Struct 8:169–173
254. Nagtegaal JC (1982) On the implementation of inelastic constitutive equations with special reference to large deformation problems. Comput Method Appl Mech 33:469–484
255. Runesson K, Booker JR (1982) On mixed and displacement finite element methods in perfect elasto-plasticity. In: Proceedings of the fourth international conference on finite element methods, Melbourne, pp 85–89
256. Doghri I (1993) Fully implicit integration and consistent tangent modulus in elasto-plasticity. Int J Numer Method Eng 36:3915–3932
257. Alfano G, Rosati L, Valoroso N (1999) A tangent-secant approach to rate-independent elastoplasticity: formulations and computational issues. Comput Method Appl Mech 179:379–405
258. Kulkarni DV, Tortorelli DA, Wallin M (2007) A newton-schur alternative to the consistent tangent approach in computational plasticity. Comput Method Appl Mech Eng 196:1169–1177
259. Le Van A, de Saxcé G, Le Grognec P (2003) General formulation for local integration in standard elastoplasticity with an arbitrary hardening model. Comput Struct 81:2099–2109
260. Korelc J (2002) Multi-language and multi-environment generation of nonlinear finite element codes. Eng Comput 18(4):312–327
261. Boyd S, Parikh N, Chu E, Peleato B, Eckstein J (2011) Distributed optimization and statistical learning via the alternating direction method of multipliers. Found Trends Mach Learn 3(1):1–122
262. Deusdado NM, Da Silva MV, Antao AN (2015) Parallel 3D limit analysis via the alternating direction method of multipliers. In: Proceedings of the XIII international conference on computational plasticity: fundamentals and applications (COMPLAS XIII)